Title
Crossed Beams Studies of Nonadiabatic Collision Dynamics

Author
Suits, Arthur G.

Publication Date
1991-06-01

LBL-30901

Lawrence Berkeley Laboratory
UNIVERSITY OF CALIFORNIA

Materials & Chemical Sciences Division

Crossed Beams Studies of Nonadiabatic Collision Dynamics

A.G. Suits
(Ph.D. Thesis)

June 1991

Prepared for the U.S. Department of Energy under Contract Number DE-AC03-76SF00098

DISCLAIMER

LBL-30901

CROSSED BEAMS STUDIES OF NONADIABATIC COLLISION DYNAMICS

Arthur Gilmore Suits

Department of Chemistry
University of California

and

Chemical Sciences Division
Lawrence Berkeley Laboratory
Berkeley, CA 94720 USA

June 1991

This work was supported by the Director, Office of Energy Research, Office of Basic Energy Sciences, Chemical Sciences Division, of the U.S. Department of Energy under Contract No. DE-AC03-76SF00098.

Crossed Beams Studies of Nonadiabatic Collision Dynamics

by

Arthur G. Suits

ABSTRACT

Nonadiabatic product channels have been studied for a variety of collision processes using crossed molecular beams under single collision conditions. Laboratory angular distributions, translational energy distributions and collision energy dependence have been measured for several chemiionization reactions in an effort to gain an understanding of the underlying collision dynamics. In addition, reactivity has been studied as a function of excited state orbital alignment in a number of these chemiionization reactions, and very strong alignment effects are observed. This alignment dependence provides insight into the features of the reactive encounter at the critical configuration at which electron transfer occurs.

Chemiions Ba^+ and $BaBr^+$ produced in reaction of $Ba(^1S_0,^1P_1)$ with Br_2 were studied as a function of laboratory scattering angle, translational energy release, barium electronic state and alignment of the barium p orbital at collision energies of

1.1 and 1.5 eV. The contour map obtained for the $BaBr^+$ product indicates a close near-collinear collision is required to gain access to the region in which the second electron transfer may occur. Orbital alignment dependence of Ba^+ recorded for in-plane and out-of-plane rotation of the barium p orbital was used in conjunction with angular distributions to gain insight into the full geometry of the collision process.

Chemiions Ba^+, BaO^+, BaO_2^+ and BaO_3^+ from reaction of ground state and electronically excited Ba with O_3 were studied in an effort to extend the insights obtained in the Br_2 studies to an atom-triatom system. A profound dependence of reactive signal on orbital alignment was observed at some scattering angles, despite the reduced symmetry of these systems compared to Br_2. Energy dependence of the relative cross sections was used in addition to angular distributions and orbital alignment effects to reveal relatively simple reactive behavior despite the complexity of the system.

Contour maps of scattered $Ba(^3P_2)$ flux from collision of $Ba(^1P_1)$ with O_2 and N_2 were obtained from simulations of measured $Ba(^3P_2)$ Doppler spectra taken at a variety of probe laser angles in a crossed beams experiment. Collision with O_2 was dominated by a near-resonant process in which initial electronic energy was efficiently coupled into O_2 vibration with little momentum transfer. The contour map obtained for N_2 showed the collision was dominated by the production of sideways scattered $Ba(^3P_2)$ corresponding to N_2 (v=0), but a near-resonant process was also observed as a minor contribution.

For my family.

And the end of all our exploring

Will be to arrive where we started

And know the place for the first time.

-T. S. Eliot

Table of Contents

Acknowledgements

It is with honor and pleasure that I thank Yuan T. Lee for his encouragement, inspiration and support during my time at Berkeley. His insight and intuition have been awe-inspiring, and the freedom he afforded us to pursue our own wild ideas allowed us to get our mistakes out of the way quickly and without prejudice.

My family has been a constant source of inspiration and encouragement through many lean years. My parents and siblings, all, have contributed importantly to my progress here, and the thanks I offer them I know is inadequate. I spare them the embarrassment of a detailed enumeration of their gifts to me, but thank them with all my heart. Saltpeter, sulfur and charcoal in the Christmas stockings: its been a linear path in curved space ever since. Jay Heinecke has been a close friend whose careless remark at a party helped launch me on this trajectory. Jay has shown me that excitement and joy are the rewards of science, and creativity, passion and madness sure paths to those rewards. Katie Vignery has been a dear friend whose candid observations and patient ear have helped me keep some perspective all these years.

The A machine has been a high intensity data source in recent years largely owing to the celebrated oven designed by Floyd Davis. It was exciting being involved in its development, and participating in the harvest has been great fun. Floyd

generously shared his experimental acumen with a first-year more familiar with lipoproteins than lasers, and his apparently boundless energy and stamina have left me nodding many mornings around 4:30 a.m. I am very grateful for our productive collaboration. Mike Covinsky was a valuable source of information and ideas who was always willing to engage in debate with an ill-informed but enthusiastic novice in the molecular beams business. Hongtao Hou, the newest member of the A-team, has always been a pleasure to work with (and argue with), and his contributions appear on virtually every page of this dissertation.

Countless others in the Lee Group have smoothed the way here: Anne-Marie Schmoltner answered many naive questions about the GM program; Bob Continetti shared his extensive beam experience when we were stuck; John Price always had helpful suggestions on PC programming and ion optics; Pam Chu kept the microvax going in the early days; Marc Vrakking has taught me that pride has a comic dimension, and I've tried to teach him this in turn. It was fun working with Albert Stolow on the long-shot NaCl experiment (sometimes they do come in) and I've enjoyed our wide-ranging conversations. James Chesko has kept the microvaxes going admirably, and his enthusiasm is amazing in its intensity and its high dimensionality. Laura Smoliar has brought a new infusion of energy to the surface experiment, and I'm sorry I won't be here to see the data start to flow. Ann Weightman was very helpful keeping me in touch with Yuan, wherever he was, and sending endless faxes to France. Countless other Lee Group members have contributed to making the lab a pleasant home away from home, and to all those unnamed I say thanks as well.

Down the hall on D level were my cappuccino companions Penny Teal and Roger Van Zee. Penny is one of the wisest and funniest scientists I know, I will deeply miss our conversations over coffee. Roger's convictions about the vanity of all experiments not involving formaldehyde or the measurement of fundamental constants were a valuable reminder: all the data flows to the journals, but the journals are never full.

A close group of friends outside the world of science have kept me sane in Berkeley, and I owe them more than I can say. Margaret Malamud was always encouraging and supportive, and showed me by example that it is all possible. Dan Suffian gave me the magic number which has been of crucial importance the last year or so. Melanie and Julian rescued me my first month in Berkeley, and were always there even though I was not.

It was a great pleasure to work with Jean-Michel Mestdagh and the group at Saclay. Jean-Michel's creativity and vision show up in several chapters here, and it was always very stimulating to work with him. Saclay was a wonderful place to do science and I am deeply indebted to everyone there for making it so pleasant for me. Jean-Paul Visticot took much time to help me with the computers, and he and Jean Berlande provided additional useful criticisms through many revisions of the manuscript for the paper. Christian Alcaraz helped with many discussions in Berkeley and in Paris, with the loan of a few figures and with a strong suggestion that I learn a little french. I'm sure he regrets that now. Thomas Gustavsson introduced me to many of the methods in use, provided insightful discussions and helped me to improve my

english. Pierre Meynadier kept the lasers on line and Olivier Sublemontier kept the machine running during all the experiments, an amazing feat, while Patrick de Pujo and Jean Cuvellier helped out whenever necessary. I look forward to a continuing pleasant collaboration, and I am very grateful to Jean-Michel for making it all possible.

I thank the National Science Foundation for a graduate fellowship which was very helpful my first years here, and NATO for sponsoring the Saclay collaboration. This work was supported by the Director, Office of Basic Energy Sciences, Chemical Sciences Division of the U. S. Department of Energy under contract No. DE-AC03-76SF00098.

Chapter I: Introduction

The experiments described herein cover a broad range of chemically relevant collision processes, but in their very diversity they proclaim the power and versatility of crossed beams techniques. In the study of reactive processes, crossed beams experiments performed under single collision conditions have raised the experimental standard to the point that newly developed "ab initio" quantum mechanical scattering calculations may be directly and meaningfully compared with experiment.[1,2] The universal crossed beam machine[3-5] allows the complete picture of the collisional encounter to emerge; there are no dark states containing unknown or unsuspected product channels. The differential cross sections often reveal the nature of the reactive encounter directly. This may be by means of the forward-backward symmetry which is the signature of the long-lived (several rotational periods) collision complex;[6] in the backscattering characteristic of a low-impact parameter, rebound collisions;[7] or through the low translational energy, forward scattering which signals the classic spectator stripping.[8]

The development of narrow band, tunable dye lasers has added a new dimension to the study of reaction dynamics in crossed beams experiments.[9-11] With the availability of electronically excited reagents we now may choose not only the

initial energy available to the system (translational or electronic), but we can select the initial potential energy surface. Furthermore, excited states prepared by means of polarized lasers possess well-defined symmetries, which may be aligned or oriented with respect to the symmetries inherent in the experiment. For crossed beams experiments, both the initial relative velocity vector and the detection plane represent important symmetry elements and in favorable cases these may be used to elucidate the actual reactive configuration at critical moments in the collision.[9]

Chemiionization reactions, when they occur at all in thermal energy collisions, are usually minor channels. Ground state reactions at modest collision energies, generally follow the adiabatic pathway.[12,13] Precisely for this reason, nonadiabatic reaction products, such as chemiions or chemiluminescent products, may show exquisite sensitivity to the factors which govern electron transfer probability at intersections of the potential energy surfaces. The theoretical[14] and experimental[15] foundations for an understanding of these factors are firmly established, so these nonadiabatic channels can become windows into the total reaction dynamics.

The ability of these nonadiabatic reaction products to illuminate the features of the reaction dynamics is even more compelling for excited state reactants. The coupling between "diabatic" surfaces may be strongly modulated by the alignment of the excited orbital with respect to the nuclear geometry. When used in conjunction with the angular distributions, this alignment dependence can provide unprecedented insight, even revealing the full geometry of the reaction.

Detection of ions and electronically excited products affords a luxury not routinely available to crossed beams detection of neutrals, viz., the measurement of relative cross sections. In highly exoergic reactions, particularly from excited state reactants, when there are a range of possible products the energy dependence of the cross sections may contain valuable clues to the underlying dynamics.

Chapters III-V present studies of positive ions produced in reaction of ground state and electronically excited barium with a variety of simple molecules. Chapter III describes the dynamics of $BaBr^+$ production in reaction of $Ba(^1S_0)$ and $Ba(^1P_1)$ with Br_2. The results for the ground state reaction indicate the importance of a strongly coupled collision in reaching the second crossing leading to chemiion products. Results for reaction of $Ba(^1P_1)$ show a strong threshold behavior, and the angular distributions are used to suggest a dynamic rather than energetic origin of this threshold.

Chapter IV reports solely on orbital alignment dependence and angular distributions of Ba^+ produced in reaction of electronically excited barium with Br_2. The observed alignment dependence was incredibly strong, reaching $(I_{max}-I_{min})/I_{min} = 4$, a value unprecedented in atom-molecule scattering. Different dependence observed for in-plane and out-of-plane rotation of the barium p orbital suggest a model in which charge transfer leading to Ba^+ is favored for large impact parameter collisions which achieve a Σ configuration at the crossing seam.

Orbital alignment dependence and angular distributions are reported in Chapter V for ions produced in collision of $Ba(^1P_1)$ with NO_2 and O_3. These highly exoergic

reactions yield several ionic product channels, and the energy dependence of the cross sections is used, in conjunction with the alignment dependence, to reveal a rich spectrum of reactive behavior.

Chapter VI presents work performed with Dr. Jean-Michel Mestdagh and his group at the Centre d'Etudes Nucleaire de Saclay in Paris, as part of a NATO sponsored collaboration. Doppler methods were developed to study electronically inelastic collisions of $Ba(^1P_1)$ with O_2 and N_2. The contour maps of $Ba(^3P_2)$ flux obtained from simulations of measured Doppler scans reveal dramatic contrasts in the dynamics for this collision process in O_2 and N_2.

References

1. R. E. Continetti, B. A. Balko and Y. T. Lee, J. Chem. Phys. **93**, 5419 (1990).
2. J. Z. H. Zhang and W. H. Miller, J. Chem. Phys. **91,** 1528 (1989).
3. Y. T. Lee, J. D. McDonald, P. R. LeBreton and D. R. Herschbach, Rev. Sci. Instr. **40**, 1402 (1969).
4. P. E. Siska, J. M. Parson, T. P. Schaefer and Y. T. Lee, J. Chem. Phys. **55**, 5762 (1971).
5. C. H. Becker, P. Casavecchia, P. W. Tiedemann, J. J. Valentini and Y. T. Lee, J. Chem. Phys. **73**, 2833, (1980).
6. W. B. Miller, S. A. Safron and D. R. Herschbach, Disc. Faraday Soc., **44**, 292 (1967).
7. D. R. Herschbach, Disc. Faraday Soc., **33**, 149 (1962).
8. R. E. Minturn, S. Datz and R. L. Becker, J. Chem. Phys. **44** 1149 (1966).
9. I. V. Hertel and W. Stoll, Adv. At. Mol. Phys. **13**, 113 (1978).
10. P. S. Weiss, M. H. Covinsky H. Schmidt, B. A. Balko, Y. T. Lee and J. M. Mestdagh, Z. Phys. D **10**, 227 (1988).
11. R. Duren, H. O. Hoppe, and H. Pauly, Phys. Rev. Lett. **37**, 743 (1976).
12. D. R. Herschbach, Adv. Chem. Phys., **10**, 319 (1966).
13. E. A. Gislason, in **Alkali Halide Vapors**, 189 (Academic Press, New York, 1979).
14. R. K. Janev, Adv. At. Mol. Phys. **12**, 1 (1976).

15. J. Los and A. W. Kleyn, in **Alkali Halide Vapors**, 189 (Academic Press, New York, 1979).

Chapter II: EXPERIMENTAL

A. Introduction

All of the experiments carried out at Berkeley, described in Chapters III-V, were performed in a crossed molecular beams machine which has been described in detail elsewhere.[1-4] A supersonic barium atomic beam crossed a molecular beam at 90° under single collision conditions, typically 10^{-7} Torr for the ion experiments described here (Figure 1). The $(2\ mm)^3$ interaction region of the two beams was viewed by a triply differentially pumped quadrupole mass spectrometer which could be rotated in the plane of the two beams. Chemiions formed in the interaction region of the two beams entered a set of ion optics and retarding field energy analyzer[5] mounted on the front of the rotatable detector and were then focused into the entrance of the quadrupole mass spectrometer and detected by a Daly-type scintillation ion detector. The existing electron bombardment ionizer of the detector was either grounded or biased above ground potential to act as a further focusing element. A narrow band cw laser was directed into the interaction region in the studies of electronically excited barium atom reactions. The experimental measurements were thus angular distributions of mass selected ions as a function of laboratory scattering angle, collision energy, translational energy and laser polarization.

B. Ion Detector

The interaction region and detector were modified as shown in Figure 2 for the detection of ions. The interaction region of the collision chamber was surrounded by a stainless steel electrode and detector aperture plate maintained field-free 120 V above ground. Ions produced in the reaction were allowed to scatter in the field-free region. Those which entered the aperture attached to the detector were then accelerated to ground potential at the entrance to a quadrupole mass spectrometer through focusing lenses and a retarding electrode. Typical operating potentials are indicated in Figure 3.

The retarding potential was generated by a Keithley 230 programmable voltage source interfaced to the LSI 11/83 computer through an IEEE-488 standard general purpose interface board. The scans were controlled and recorded by the computer by means of the program IONEN, a modification of Paul Weiss' program SANG.[6] IONEN allows for communication with the CAMAC modules as well as the voltage source. Scanning ranges and step sizes were entered into the computer which subsequently sent a string of instructions to the voltage source. Scans were begun and ended by the existing Timer/Gater LBL 1350 II, independently interfaced to the computer. Step triggers for the voltage source and pulses triggering a laser flag were generated by a scaler gate generator. The gate generator could be operated in a "laser mode", in which the voltage steps operated at 4 Hz, synchronous with pulses driving a stepper motor which operated a laser flag. Alternatively, a "no-laser mode" allowed

for voltage steps at 100 Hz. The scaler gate generator also controlled the scalers which accumulated the data counts originating from the detector. The detector PMT signal was sent to a discriminator thence to all four channels of a CAMAC Quad Scaler. The $Ba(^1P_1)$ fluorescence monitored in the laser experiments was sent to the first two channels of a second quad scaler unit and gated by the scaler gate generator as well. The four recorded data channels in "laser mode" were thus 1) laser on, voltage high; 2) laser on voltage low; 3) laser off, voltage high; 4) laser off voltage low. Also recorded were: 5) fluorescence, laser on; and 6) fluorescence, laser off. In "no laser mode" only the first two data channels, corresponding to voltage high and voltage low, were recorded. Often in the ion experiments we found no laser-off background, and in such cases the laser was not flagged and the scan was conducted in "no laser mode", to increase the effective scan time. The scaler gate generator is a CAMAC module triggered by the LSI 11, but no handshaking has been incorporated into its design.

Probably owing to the constraints imposed by the limited space available between the interaction region and the detector, energy-dependent focusing discussed below hampered the full use of the energy analyzer in some of these experiments. The entrance and exit lenses were adjusted to give maximum signal while minimizing the energy-dependent focusing. One useful modification for any future ion experiments would be to substitute a microchannel plate detector for the Daly detector, thereby allowing for the detection of both positive and negative ions. As we had expected, in most cases the identity of the corresponding negative ion was implied by

the detected positive ion. But sometimes it was not clear whether the positive ion was accompanied by a negative ion or a neutral and a free electron. The ability to detect mass selected negative ions would certainly eliminate any ambiguity.

For the translational energy scans, the retarding potential was applied as a 100 mV, 100 Hz square wave riding on a DC voltage, stepped up through the energy range of interest. Data corresponding to the high and low retarding voltage steps were recorded and subtracted to yield the differential energy scans. At the low energy region, signals are often the result of subtraction of two large numbers. The error bars are thus larger at the low energy regions of the spectra. Some minor energy-dependent focusing was observed when retarding potential was applied as mentioned above. At angles of intense signal, when low energy signal is very small, a small variation in transmission of high energy signal resulting from the applied retarding potential can appear as negative signal in the first few points of the scans. For the experiments reported here, this was sufficiently far from the region where the product signal appeared to cause no interference. In addition, owing to the cylindrical symmetry of the scattering process with respect to the relative velocity vector, we need not rely on product appearing at low laboratory energies to obtain a complete picture of the flux distribution.

C. Barium Source

A supersonic barium beam was formed by expanding mixtures of barium and rare gas from the 0.007" nozzle of a resistively heated one-piece molybdenum oven assembly, to be described in detail in a forthcoming publication.[7] Under typical operating conditions, the nozzle was ~1500°C, while the barium reservoir was maintained about 300°C cooler. An auxiliary radiative graphite heating element surrounding the barium reservoir allowed its temperature to be adjusted independently of the nozzle temperature. The barium beam passed through a heated molybdenum skimmer and a collimating slit, then to the collision chamber maintained at ~10^{-7} Torr.

Owing to the relatively strong ion signal in these experiments, a somewhat lower intensity barium beam was used than has been the case in studies involving neutral reaction products. Typical operating parameters were 1.7 v.a.c., 400 A on the oven body and 4.0 v.a.c., 75 A on the graphite heater. Under these conditions, a single load of barium was sufficient for more than 40 hours of operation. The seed gases used in these experiments were argon, neon, helium and a 50% helium, 50% neon mixture, and typical stagnation pressures of 250-600 Torr. This resulted in barium beam velocities ranging from 1200 m/s in argon to 3200 m/s in helium. The velocity in helium corresponds to a barium kinetic energy of >5 eV, sufficient to ionize it on impact. Neutral reaction products are also subject to impact ionization owing to the large laboratory velocities under these conditions, so care was required in interpreting ion signals when helium was used as the seed gas.

D. Molecular Beam Source

The bromine beam was produced by expanding a 3% Br_2/He mixture at a total pressure of 550 Torr through a 0.075 mm nozzle heated to 200°C. The mixture was obtained by bubbling helium from a vacuum regulator through a pyrex bubbler containing bromine which was immersed in a bath at -25 °C. The total pressure was monitored by means of a Baratron pressure gauge on the inlet line. The bromine beam passed through a skimmer and collimating slit to cross the barium beam at 90° in the main collision chamber.

The NO_2 and O_3 beams were also seeded ~10% in helium, and the same source was used as for the Br_2 beam, with the nozzle again heated to 200 °C to inhibit cluster formation. Typical stagnation pressures for these beams were 400 Torr. The NO_2 beam was produced by passing the helium carrier gas through a bubbler maintained at -50 °C. Two different methods were used to generate the ozone beam: for most experiments, the ozone was trapped on silica gel in a pyrex container at dry ice/acetone temperature (-80 °C), with care taken to exclude moisture. The trap was purged with helium to remove excess adsorbed oxygen and then warmed to about -40 °C to release ozone, with the helium seed gas passing through the trap. The O_3 concentration was monitored by means of its absorbance of 280 nm light, and the trap warmed when necessary to keep the concentration constant. This method inevitably results in residual O_2 contamination, typically about 10% of the O_3 concentration. The residual O_2 generally produced no interference in the ion experiments since the ion

channels in the O_3 reaction are so much more exoergic than for O_2. But at some collision energies and for some channels, notably BaO_2^+ which is weak in the O_3 reaction, the O_2 contamination was intolerable. For the cases in which O_2 contamination was unacceptable, the ozone was condensed and the residual oxygen pumped away. This was accomplished by opening the purged silica gel trap to a bubbler at liquid nitrogen temperature and passing helium over the trap as it was rapidly warmed to -20 °C. After the ozone was condensed, the liquid nitrogen Dewar was carefully exchanged for an isopentane slush (-160 °C, P_{O3} 10 Torr) for the experiment. The O_3 pressure was kept low at all times, particularly when substantial O_2 was present, and nothing untoward has happened using this technique.

E. Barium Optical Pumping

Electronically excited barium atoms were prepared by optical pumping at the interaction region by means of a single-frequency ring dye laser tuned to the Ba(^{1}S-^{1}P) transition at 554 nm (Figure 4), typically operating at about 250 mw. Metastable D states (1.1 and 1.4 eV above the ground state) are also populated by radiative decay from the P state, and the ^{138}Ba composition of the beam is estimated to be ~35% ground state Ba, ~35% Ba(^{1}P) and 30% Ba(^{1,3}D). For most of the ions studied, no reaction is energetically possible from the ground state. In some cases it is weakly observed but negligible compared to the excited state reaction. The D state contribution, estimated by exciting upstream of the interaction region, was found to be

negligible in the case of Ba^+ in the bromine reaction. The measured Ba^+ comes almost entirely from $Ba(^1P_1)$, as is consistent with the strong polarization effects observed in all systems studied. The D state contribution was not carefully explored for each ion, but again the strong polarization effects, and the coincidence of observed thresholds with those expected for the P state, indicate that we are justified in neglecting the D state contribution to the ion signal.

The geometry of the laser excitation scheme is illustrated in Figure 5. The laser polarization was rotated by means of a double Fresnel rhomb driven by a stepper motor. The laser beam was directed perpendicular to the plane of the beams for the in-plane polarization rotation experiments (figure 5a), or collinear with the molecular beam (figure 5b) for the out-of-plane polarization rotation experiments. In one experiment described in Chapter V, the laser beam was sent in along the 45° crossing as shown in Figure 5c, again allowing for out-of-plane polarization rotation. The fluorescence from the $Ba(^1P_1\text{-}^1S_0)$ transition was directed through a telescope onto a photomultiplier tube and recorded along with the data in all geometries.[8] The anisotropy of this fluorescence confirmed virtually complete alignment of the $Ba(^1P_1)$ state.

The relation of the prepared orbital alignment and the collision frame[9] is illustrated in Figure 5 as well. When the orbital is rotated in the collision plane (Figure 5a), the sense of rotation is clockwise when viewed from above. β is defined as the angle between the orbital alignment or laser polarization and the nominal relative velocity vector. The location of the peak of the polarization dependence for

in-plane orbital alignment is designated β'. Some authors have referred to in-plane polarization experiments as the "out-of-plane" configuration, because the laser is perpendicular to the plane, so one must be alert when reading reports of other work. In the out-of-plane alignment experiments (Figure 5b and 5c), the angle between the orbital and the relative velocity vector is not as simply defined, because the laser is never collinear with nor perpendicular to the relative velocity vector. In this case, we simply refer to the polarization angle, Θ, i.e., the angle between the E vector of the laser and a line perpendicular to the scattering plane and remain cognizant of the (significant) deviation of the in-plane configuration from parallel to the relative velocity vector. The out-of-plane polarization scans begin with the laser polarization perpendicular to the collision plane and $\Theta = 90°$ represents the alignment in which the orbital lies in the scattering plane. In one experiment with NO_2, the laser was sent in at the 45 degree crossing, shown in Figure 5c. That allowed for near preservation of perpendicular alignment (β=90 degrees) throughout the polarization scan, because in that case the relative velocity vector was ~55° from the primary beam. The peak angle of the out-of-plane polarization scans is designated Θ'.

References

1. Y. T. Lee, J. D. McDonald, P. R. LeBreton and D. R. Herschbach, Rev. Sci. Instrum. **40**, 1402 (1969).
2. P. E. Siska, J. M. Parson, T. P. Schaefer and Y. T. Lee, J. Chem. Phys. **55**, 5762 (1971).
3. M. F. Vernon, Ph.D. Thesis, University of California, Berkeley (1983).
4. C. H. Becker, P. Casavecchia, P. W. Tiedemann, J. J. Valentini and Y. T. Lee, J. Chem. Phys. **73**, 2833, (1980).
5. F. Tully, Ph.D. Thesis, University of Chicago (1973).
6. P. S. Weiss, Ph.D. Thesis, University of California, Berkeley, (1986).
7. H. F. Davis, M. H. Covinsky, A. G. Suits and Y. T. Lee, to be published.
8. P. S. Weiss, M. H. Covinsky H. Schmidt, B. A. Balko, Y. T. Lee and J. M. Mestdagh, Z. Phys. D **10**, 227 (1988).
9. E. E. B. Campbell, H. Schmidt and I. V. Hertel, Adv. Chem. Phys. **72**, 37 (1988).

Chapter II Figure Captions

Figure II-1. Schematic view of crossed beams apparatus.

Figure II-2. View of interaction region from above illustrating modifications for detection of chemiions.

Figure II-3. Interaction region ion optics and typcial operating potentials.

Figure II-4. Important states in the optical puming scheme for atomic barium.

Figure II-5. Laser-crossed molecular beams geometries for A) in-plane, B) out-of-plane, and C) 45°-out-of-plane orbital alignment rotation.

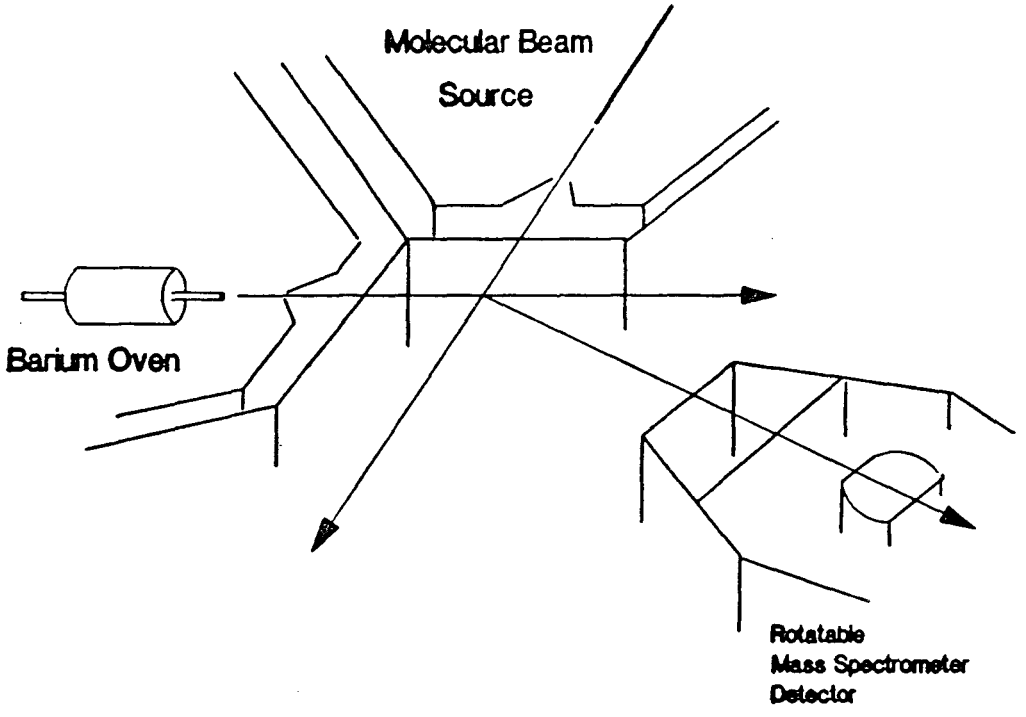
Molecular Beam
Source
Barium Oven
Rotatable
Mass Spectrometer
Detector

Figure II-1

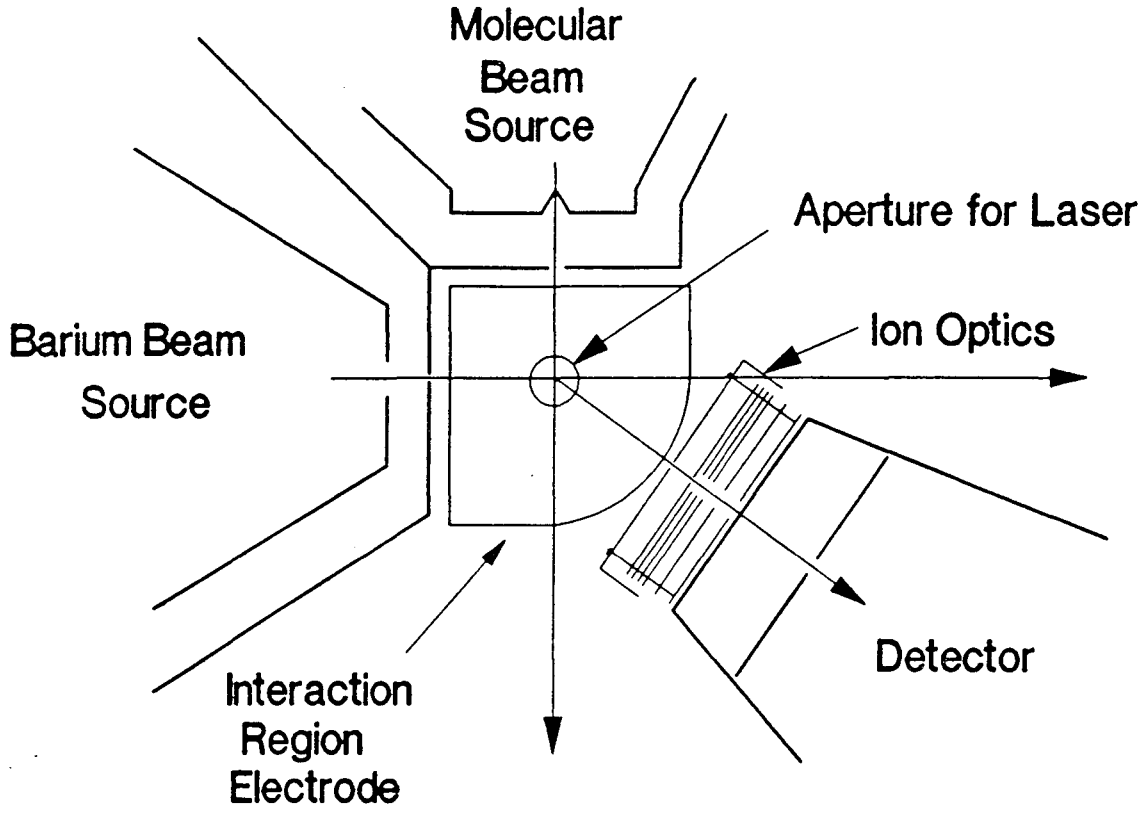
Molecular
Beam
Source
Aperture for Laser
Barium Beam
Source
Ion Optics
Detector
Interaction
Region
Electrode

Figure II-2

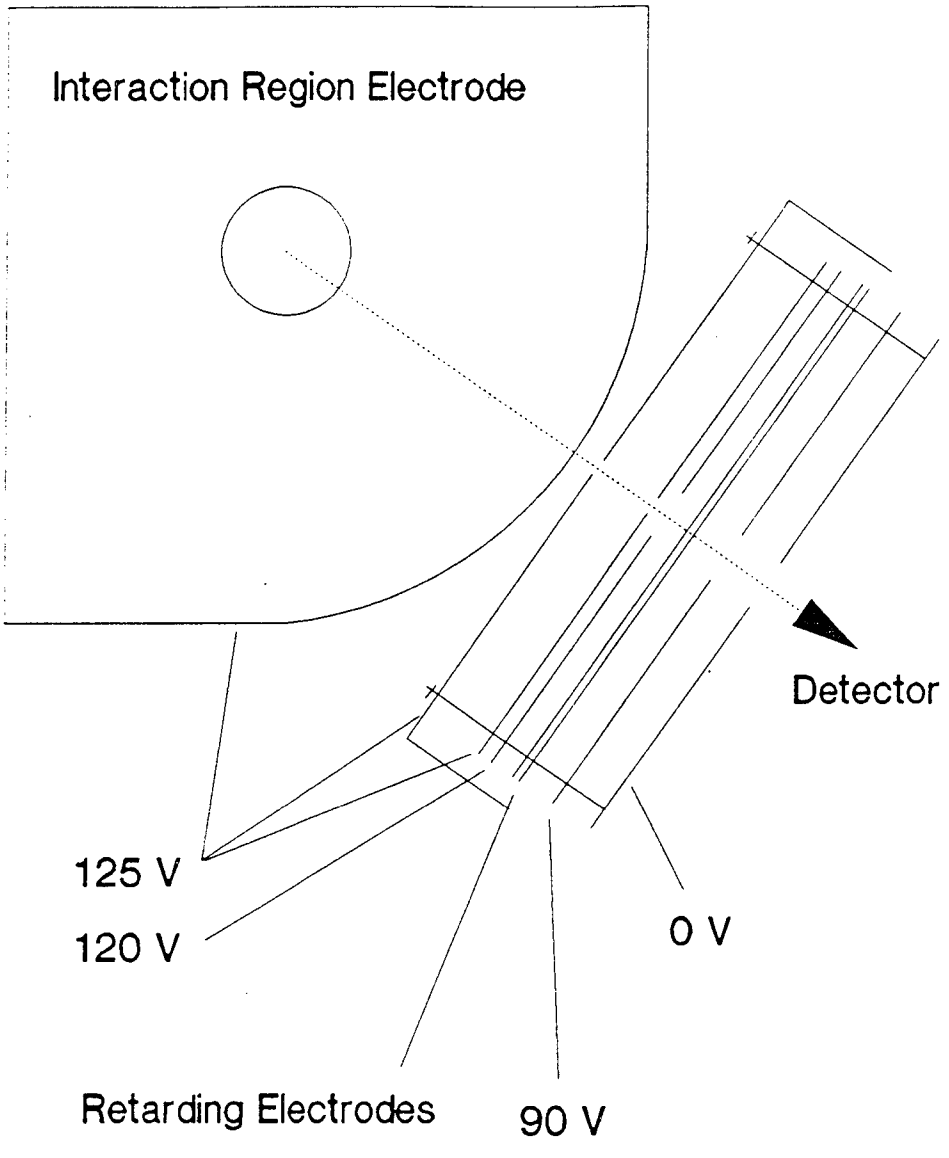
Interaction Region Electrode
Detector
125 V
120 V
0 V
Retarding Electrodes
90 V

Figure II-3

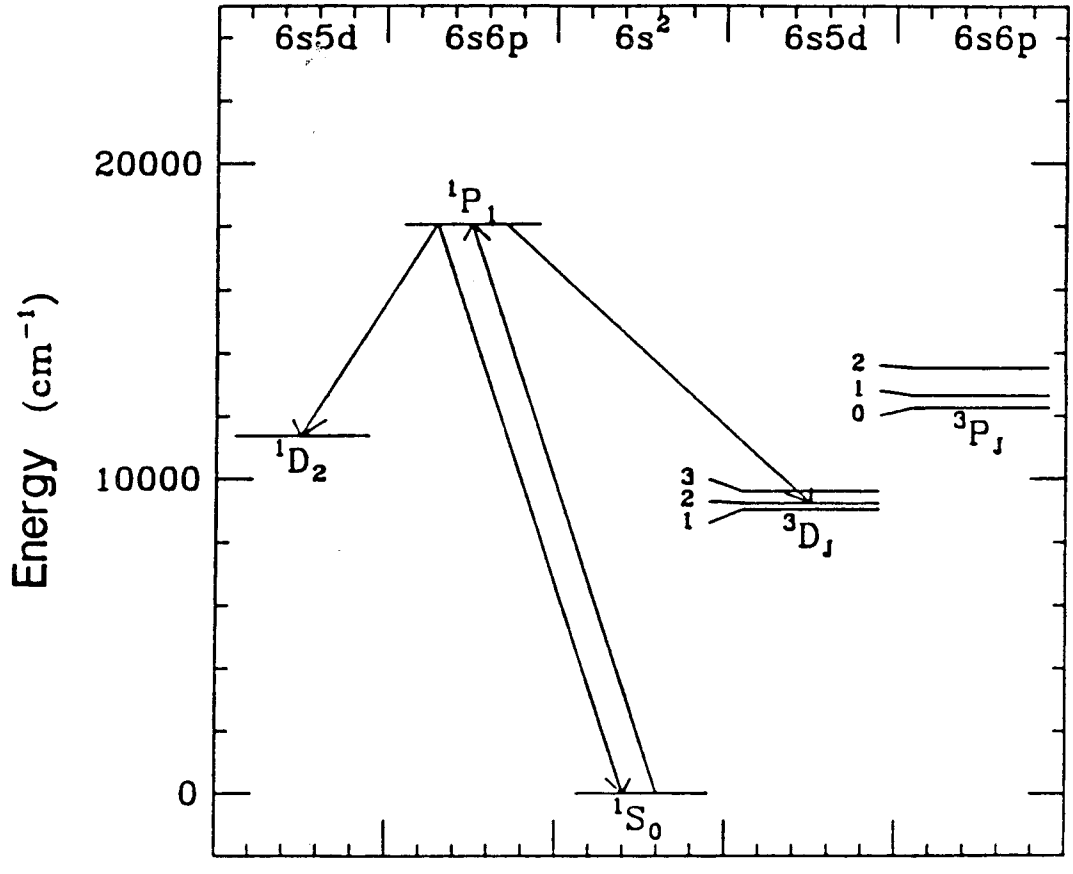
6s5d
6s6p
6s²
6s5d
6s6p
20000
10000
0
Energy (cm⁻¹)
¹P₁
¹D₂
¹S₀
³D_J
3
2
1
³P_J
2
1
0

Figure II-4

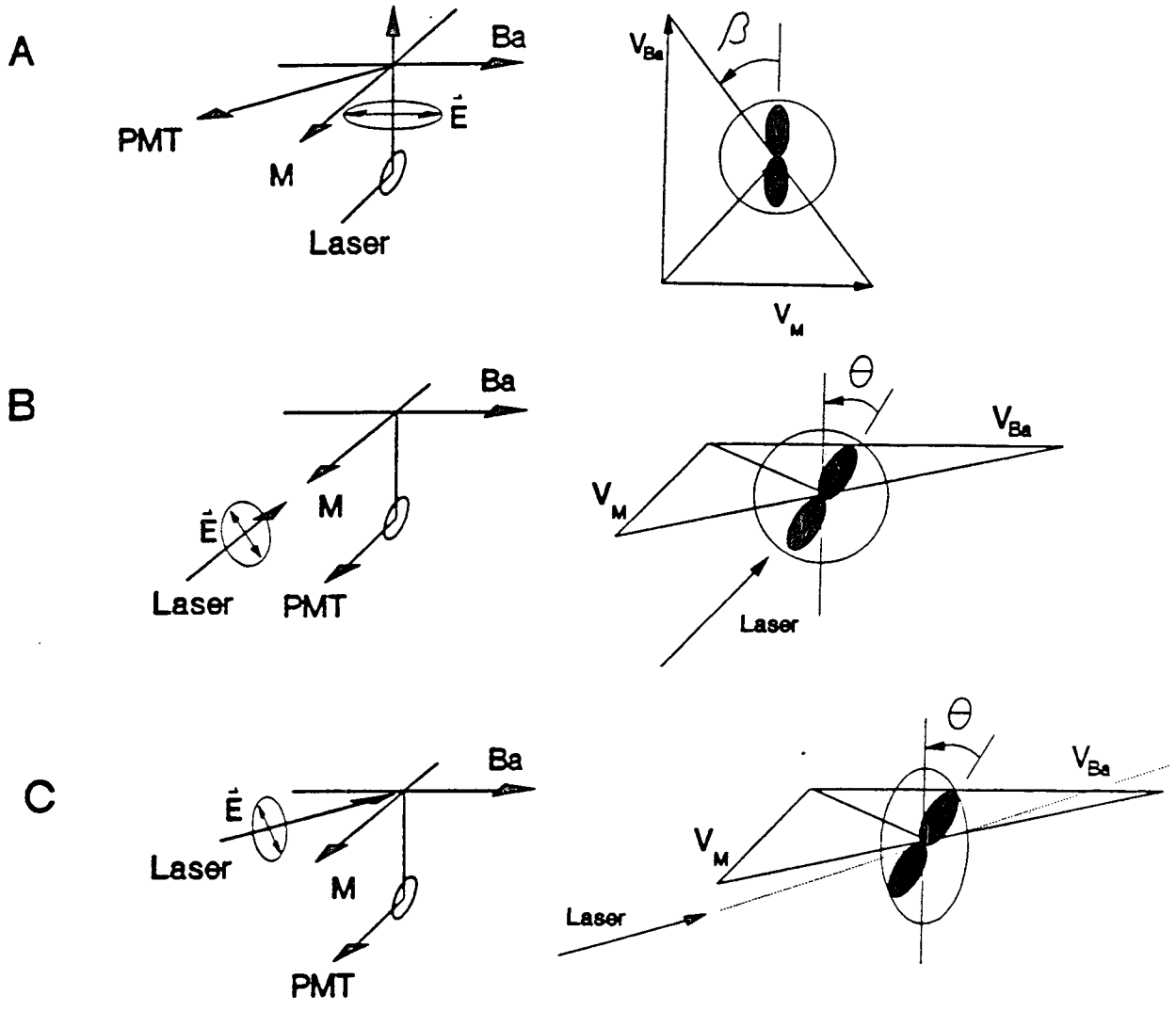
A
Ba
PMT
$\vec{E}$
M
Laser
V_{Ba}
β
V_M
B
Ba
$\vec{E}$
M
Laser
PMT
θ
V_{Ba}
V_M
Laser
C
Ba
$\vec{E}$
Laser
M
PMT
θ
V_{Ba}
V_M
Laser

Figure II-5

Chapter III: Dynamics of Ba-Br_2 Chemiionization Reactions

A. Introduction

The reaction of barium with halogen molecules represents an important prototypical case for the study of reaction dynamics in divalent systems.[1-6] Reaction may be initiated with the transfer of one electron via the celebrated "harpoon mechanism",[7-10] but there exist a range of possible product channels owing to the presence of the second valence electron on barium and a second electron-accepting halogen atom. The reaction with ground state barium is dominated by the production of the ground state, neutral radical pair BaX and X (X a halogen atom).[11,12] In addition, there also exist exoergic electronically excited neutral product channels, and a chemiion channel: BaX^+ and X^-.[13]

This chemiionization reaction corresponds to the transfer of both valence electrons from barium to the halogen molecule. The BaX^+ formation thus provides a window into the dynamics of the second electron transfer. The reaction of ground state barium with chlorine yielding $BaCl^+$ was studied under crossed beam conditions by Ross and co-workers.[14] Their results suggested either backscattering with respect to the effusive barium source, or forward-backward symmetry of the $BaCl^+$ product distribution along the relative velocity vector. They interpreted their results to indicate

the importance of a strongly coupled collision for the chemiion channel. Recently we reported clearly backscattered angular distributions of $BaCl^+$ from this reaction performed under better defined conditions,[15] confirming the importance of an intimate Ba-Cl-Cl interaction. This reaction was found to be strongly inhibited by electronic excitation of the barium, consonant with a mechanism in which the nascent BaCl formed as a result of the initial electron transfer must "pursue" the departing chlorine atom in order to reach a portion of the potential energy surface which is crossed by the doubly ionic surface correlating to $BaCl^+$ and Cl^-. Only for low impact parameter, near collinear collisions will this be possible. We here extend these studies to the measurement of translational energy and angular distributions of $BaBr^+$ product flux in an effort to achieve some quantitative understanding in the analogous Ba + Br_2 reaction. In addition, we describe a new laser dependent source of $BaBr^+$ for which no analogue appeared in the Cl_2 studies.

B. Results

The crossed beams reaction of ground state barium with Br_2 was studied at a collision energy of 1.1 eV. Translational energy scans for $BaBr^+$ products were obtained with a retarding field energy analyzer at various laboratory scattering angles. These scans are shown in Figure 1 along with fits obtained by forward convolution of assumed forms of the center of mass angular ($T(\Theta)$) and translational energy distributions ($P(E)$), assumed to be independent. The convolution includes angular

divergence of the beams and measured spreads of the beam velocities ($v/\delta v$ ~8 and 10 for barium and bromine beams, respectively).

The fits shown in Figure 1 yield the contour map of $BaBr^+$ flux shown superimposed on the nominal Newton diagram in Figure 2. Greater than 80% of the flux appears in the backward direction (forward is considered to be in the direction of the barium beam). This strongly backscattered $BaBr^+$ distribution is even more remarkable when one considers the possible smearing of the angular distribution from the range of initial recoil angles by coulomb attraction of the recoiling ion pair.

The broad translational energy distribution peaks near 0.7 eV, but >30% of the distribution results from translational energy release greater than the collision energy. The available energy is given by $E_{coll} + E_{exo} = 1.1 + 1.2 = 2.3$ eV; a substantial fraction of the products thus appear with translational energy derived from reaction exoergicity, and $BaBr^+$ is observed to the limit of the available energy.

Laboratory angular distributions for $BaBr^+$ were measured for reaction of barium with Br_2 at collision energies of 1.1 and 1.6 eV, with a single mode ring dye laser directed to the interaction region pumping the barium ($^1S_0$-$^1P_1$) transition at 553.7 nm. The laser polarization was parallel to the relative velocity vector. Figure 3 shows both laser on and laser off angular distributions, uncorrected for the fraction of the beam excited at 1.1 eV collision energy. Shown in the same figure is the laser-induced associative ionization product $BaBr_2^+$ observed under the same conditions, kinematically constrained to appear only at angles near the center of mass. The 1.1 eV collision energy result showed roughly 20-30% laser-induced inhibition of $BaBr^+$

signal, largely independent of scattering angle. This is similar to results previously obtained[15] for the chlorine reaction at 0.75 eV, and the inhibition corresponds roughly to the $Ba(^1P_1)$ population at the interaction region.

However, striking changes were observed in the distributions with the increase in collision energy to 1.6 eV, shown in figure 4. Aside from the general feature of $BaBr^+$ produced by residual ground state barium in the beam (shown as dashed line), a sharp feature appeared directly behind the center of mass. Figure 5 shows laser dependent signal for the high collision energy obtained by subtracting the contributions from the ground state Ba, and assuming the inhibition seen at the back angles corresponds to the excited state fraction of the beam. This represents the most conservative estimate of the excited state fraction. The dominant feature of course is the backscattered peak, but a substantial forward component is also apparent. The clear dip at the center of mass suggests a translational energy distribution peaking away from zero.

The associative ionization product was clearly seen at both collision energies following laser excitation, yet despite the fact that all $BaBr_2^+$ is constrained to appear clustered in the vicinity of the center of mass, the laser-dependent $BaBr^+$ at 1.6 eV was ~100 times more intense than the $BaBr_2^+$.

C. DISCUSSION

Sections through several relevant diabatic potential energy surfaces for collinear Ba-Br_2 are shown in Figure 6, estimated using a semi-empirical diatomics-in-molecules method.[18,19] We have employed the diabatic representation so that the crossing points can be more easily visualized. The Br-Br internuclear distance is fixed at 2.5 Å, somewhat larger than the equilibrium distance for the neutral molecule (2.28 Å). This represents the region of the surface likely to be important for electron transfer, owing to "prestretching" of the Br-Br bond on the adiabatic surface.[20] The Ba($^1P_1$)-Br_2 curve actually represents three curves, two of which are degenerate in the collinear configuration. Figure 6 is intended to facilitate a qualitative discussion of the dynamics of these collisions, but it should be borne in mind that the D states and the triplet surfaces have been neglected for the sake of clarity. For the ground state reaction the first crossing of the ionic and covalent potential energy surfaces (point 1 in figure 7), occurs at ~4 Å. As mentioned above, the chemiion products $BaBr^+ + Br^-$ correlate to the doubly ionic Ba^{++}-Br_2^{--} surface. The chemiion channel thus requires access to the second crossing region (2 in Figure 6). The backscattered $BaBr^+$ distribution seen in the contour map in Figure 2 reveals the nature of the stringent requirements for gaining this access: only simultaneously collinear *and* low impact parameter collisions are able to reach this second crossing point.

An understanding of the origin of these stereochemical demands requires a consideration of the competing neutral channel, the dominant channel at these collision energies.[6] In 1972 both Bernstein and coworkers[11] and Herm et al.[12] reported results for crossed beams reaction of barium with halogen molecules. The consensus for the

neutral channel was little different from that seen in the classic K + Br_2 reaction: long-range electron transfer results in a vertical transition to a repulsive region of the Br_2^- potential energy curve, resulting in rapid stretching of the $(Br\text{-}Br)^-$ bond with dissociation in the field of the positive ion. The experimental manifestation of this is forward scattered BaBr with little of the available energy appearing in translation. Beautiful studies of non-adiabatic pathways in the alkali-halogen reactions by Los and Kleyn[9,10,20] provide a deep experimental understanding of the "harpoon mechanism" outlined above. Following initial electron transfer, the rapidly changing bond distance in the vibrationally excited anion results in a corresponding change in the electron affinity, or viewed from a different perspective, the location of the crossing seam. The probability of electron transfer on exit may thus be very different from that on approach. In the case of high energy collisions of Cs-O_2, this phenomenon gave rise to oscillations in the angular distributions of Cs^+ corresponding to the vibrational period of O_2^-. The important aspect for the present discussion is that rapid stretching of the $(Br\text{-}Br)^-$ bond accompanies electron transfer. Immediately on reaching the singly ionic surface (1 in Figure 6), the reactive system rapidly escapes into the exit valley leading to neutral BaBr and Br. For collinear, low impact parameter trajectories this escape, leaving the Br atom as spectator, is simply not possible. Instead, transfer of the second electron takes place when the nascent bromine atom and the nascent BaBr are pushed together with their respective linear momentum. The result is a close collision forming a tightly packed $Ba^{2+}Br^-Br^-$ collinear intermediate. Because of the repulsion between the negatively charged bromine atoms, the backscattered $BaBr^+$

appears with a substantial fraction of the available energy released into translation. The magnitude of the chemiion cross section (0.6 $Å^2$)[13] is also consistent with the limited contribution of these sterically constrained collisions relative to the overall harpooning cross section (~50 $Å^2$).

Additional evidence for this interpretation is provided by the results for electronically excited barium. The excited state composition of the barium beam is not precisely known owing to the presence of metastable D states populated by radiative decay from the $^1P_1$. Evidence obtained by exciting upstream of the interaction region in studies with Cl_2 indicated that the D states were less effective at inhibiting the chemiion cross section than the $^1P_1$.[15] We will focus our discussion on $Ba(^1P_1)$, though these arguments are consistent with what is seen with the D states alone. For $Ba(^1P_1)$, laser excitation adds an additional 2.2 eV to the energy available to the system. Moreover, the first crossing is moved out a considerable distance: from 4 Å to 12 Å (indicated at 1* in figure 7). The implications of this in the model outlined above are apparent: the distance between the first and second crossing points has changed from ~1Å to ~9Å. Using the initial relative velocity we can estimate the time between crossings for collinear approach: about 60 femtoseconds for the ground state reaction yet 540 femtoseconds for the excited state. The vibrational period of the excited Br_2^- is ~310 femtoseconds.[10] From the excited surface, even for very nearly collinear collisions, the remaining bromine atom has ample time to escape. Moreover, even if a secondary collinear encounter between Br and highly vibrationally excited BaBr were to take place, the chances of the three atoms achieving the tightly

packed configuration corresponding to the region of the second crossing may be very limited. This probably results in redirection of flux into neutral products, yet this may represent only a minimal increase in the overall neutral cross section.

Because the associative ionization product $BaBr_2^+$ recoils from an electron, momentum conservation requires that it appear in the vicinity of the center of mass of the system. Consequently, information about its role in the dynamics of these collisions must be sought in the relative magnitude and energy and laser dependencies of the cross section, rather than in the angular or translational energy distributions. It is weakly observed from the ground state at 1.6 eV, but is greatly enhanced on laser excitation, then appearing clearly at both 1.1 and 1.6 eV. No attempt was made to discern the relative contribution of the barium P or D states to the laser enhancement of $BaBr_2^+$. The associative ionization may result from ejection of an electron at the classical turning point of the transient $Ba\text{-}Br_2$ collision if a vertical transition to a stable product ion is possible. Such a transition requires that the transient $Ba\text{-}Br_2$ complex achieve a geometry close to that of the product ion in order for the reaction to be energetically feasible. It is clear from the discussion above that the vast majority of collisions do not gain access to the deep $Br^-Ba^{++}Br^-$ well. It is not accessible in the collinear space we have considered so far. Nevertheless, there will be C_{2v} collisions and they are the most likely to achieve a geometry close to that of $BaBr_2^+$, probably after overcoming a potential energy barrier. Electron transfer at the outer crossing is not favored by A_1 and B_1 configurations in C_{2v} geometry, so a close collision from the covalent surface is quite plausible. The additional photon energy

may simply serve to bring the total energy over the ionization threshold for a greater number of collisions, allowing the system to reach the region of the potential energy surface where electron ejection may occur.

The source of the laser enhanced $BaBr^+$ observed at 1.6 eV may now be considered. The signal shown in Figure 5 displayed a sharp threshold behavior: it was not evident at all at collision energies much below 1.5 eV. As discussed above, one of the important consequences of electronic excitation of the barium atom is to move the first crossing to very large Ba-Br distance. Even for near collinear collisions the second Br atom may behave as a spectator in the initial interaction, but at this higher collision energy it may not escape prior to a second collision with the newly formed, highly vibrationally excited BaBr. If one assumes no initial transfer of momentum from the second Br atom to BaBr, one obtains the BaBr center of mass recoil velocity in the "spectator limit", and this is indicated in Figure 5. A secondary BaBr-Br collision would be characterized by this same velocity, so the circle shown in Figure 5 represents the elastic maximum for a secondary encounter in the spectator limit. All of the laser dependent $BaBr^+$ falls well within this maximum. The tendency to backscattering is a consequence of the fact that these secondary collisions can only result from near collinear trajectories. The low translational energy release may thus be understood to result naturally from conservation of linear momentum in both collisional encounters. Yet the final translational energy appears to peak sharply at approximately half of the velocity anticipated assuming the spectator limit and an elastic secondary encounter. This reveals the deviation from the limiting assumptions,

and two cases may be considered corresponding to failure of one or the other of these assumptions. If we hold the initial collision to the spectator limit, then the inelastic secondary collision must result in effective coupling of the translational energy into Ba-Br vibration, since the final recoil velocity is less than otherwise expected. This coupling is likely to occur when the BaBr-Br approach is in phase with the Ba-Br vibration. Alternatively, there may be substantial repulsion between the bromine atoms following initial electron transfer. If we assume an elastic secondary encounter, we can estimate how far from the spectator stripping limit the initial collision could be. A simple calculation assuming an elastic secondary collision suggests initial Br-Br relative velocity of 900 m/s at the point of the second collision.

This suggests a dynamic rather than energetic explanation for the sharp threshold. The features of a secondary collision are very sensitive to the initial vibrational period of the halogen molecular ion and the phase of this vibration relative to the approaching barium atom. Very different behavior would be expected for Cl_2, and indeed no analogous laser dependent signal was observed for $BaCl^+$ in previous studies at several collision energies from 0.75 to 3.0 eV.

We have not addressed the question of the final product states: both $BaBr^+ + Br^-$ and $BaBr^+ + Br + e^-$ are possible product channels, the latter approximately thermoneutral for $Ba(^1P_1) + Br_2$. The $BaBr^+$ might result from autoionization of highly vibrationally excited BaBr resulting from the second collision. Alternatively, favorable second collisions may achieve the tightly packed geometry at the region of an inner crossing to the doubly ionic $BaBr^+ + Br^-$ potential energy surface. Both product

channels appear plausible, and negative ion detection would be useful to discriminate between them.

D. CONCLUSION

The ground state, neutral products which dominate the reaction of barium with halogen molecules reveal little of the dynamical richness that is present. By studying ions produced in these reactions at modest collision energies, the dynamics in this prototypical divalent system may be drawn out. The chemiion products $BaBr^+$ and Br^- were found to result from near-zero impact parameter, collinear collisions. These severe stereochemical constraints arise out of competition with the dominant neutral channel. At 1.1 eV, the reaction was inhibited from the $Ba(^1P_1)$-Br_2 excited surface, again owing to the dynamic competition with the neutral channel. At 1.6 eV a laser dependent $BaBr^+$ signal appeared, probably also the result of collinear collisions, but derived from the neutral channel and involving a secondary encounter. A laser dependent associative ionization channel was observed at both collision energies studied, more than 100 fold weaker than the chemiion reaction. This associative ionization reaction probably results from ejection of an electron at the classical turning point of a $BaBr_2$ collision for those C_{2v} collisions which gain access to a region of the neutral potential energy surface for which the nuclear geometry resembles the product ion.

References

1. Michael Menzinger, The M + X_2 Reactions: A Case Study, in **Gas Phase Chemiluminescence and Chemi-Ionization**, A. Fontijn, ed., Elsevier Science Publishers, B.V., 1985, pp.25-66, and references therein.
2. C. D. Jonah and R. N. Zare, Chem. Phys. Lett. **9**, 65 (1971).
3. D. J. Wren and M. Menzinger, Chem. Phys. Lett. **27**, 572 (1974).
4. C. T. Rettner and R. N. Zare, J. Chem. Phys. **77**, 2416 (1982).
5. H. F. Davis, A. G. Suits, H. Hou and Y. T. Lee, Ber. Bunsenges. Phys. Chem., in press.
6. M. Menzinger, J. Phys. Chem. **94**, 1899 (1990).
7. D. R. Herschbach, Adv. Chem. Phys. **10**, 319 (1966).
8. R. Grice, Adv. Chem. Phys. **30**, 247 (1975).
9. M. M. Hubers, A. W. Kleyn and J. Los, Chem. Phys. **17**, 303 (1976).
10. J. Los and A. W. Kleyn, Ion Pair Formation, in **Alkali Halide Vapors**, P. Davidovits and D. L. McFadden, eds., Academic Press, New York, (1979) pp. 275-331.
11. J. A. Haberman, K. G. Anlauf, R. B. Bernstein and F. J. Van Itallie, Chem. Phys. Lett., **16**, 442 (1972).
12. Shen-Maw Lin, Charles A. Mims, and Ronald R. Herm, J. Chem. Phys. **58**, 327 (1973).
13. G. J. Diebold, F. Engelke, H. U. Lee, J. C. Whitehead, and R. N. Zare, Chem. Phys. **30**, 265 (1977).

14. R. H. Burton, J. H. Brophy, C. A. Mims and J. Ross, J. Chem. Phys. **73**, 1612 (1980).

15. A. G. Suits, H. Hou and Y. T. Lee, J. Phys. Chem. **94**, 5672 (1990).

16. H. F. Davis, M. H. Covinsky, A. G. Suits and Y. T. Lee, to be published.

17. Y. T. Lee, J. D. McDonald, P. R. LeBreton and D. R. Herschbach, Rev. Sci. Instrum. **40**, 1402 (1969).

18. F. O. Ellison, J. Am. Chem. Soc., **85**, 3540 (1963).

19. E. M. Garfield, E. A. Gislason and N. H. Sabelli, J. Chem. Phys. **82** 3179 (1985).

20. J. A. Aten and J. Los, Chem. Phys. **25**, 47 (1977).

Chapter III Figure Captions

Figure III-1. Translational energy scans for $BaBr^+$ from reaction of ground state Ba with Br_2 at a collision energy of 1.1 eV, shown with fits obtained by forward convolution as described in text. Laboratory scattering angles are shown, measured with respect to the Ba beam.

Figure III-2. $BaBr^+$ flux-velocity contour map obtained from the fit shown in Figure 2 for $Ba(^1S_0) + Br_2 \rightarrow BaBr^+ + Br^-$ at 1.1 eV collision energy, shown superimposed on the nominal Newton diagram.

Figure III-3. Laboratory angular distribution of $BaBr^+$ from reaction of Ba with Br_2 for ground state Ba (circles) and with a laser saturating the $Ba(^1S_0\text{-}^1P_1)$ transition at the interaction region (squares) at 1.1 eV collision energy. Also shown is the associative ionization product $BaBr_2^+$ (triangles) for the laser-on case, enhanced 25-fold.

Figure III-4. Laboratory angular distribution of $BaBr^+$ from reaction of Ba with Br_2 for ground state Ba (circles) and with a laser saturating the $Ba(^1S_0\text{-}^1P_1)$ transition at the interaction region (squares) at 1.6 eV collision energy. Dotted line shows estimated contribution of ground state reaction to the laser excited signal.

Figure III-5. Laboratory angular distribution of laser-dependent $BaBr^+$ (circles) and $BaBr_2^+$ (triangles) obtained from the data shown in Figure 4. The nominal Newton diagram is shown with the circle corresponding to the

magnitude of the BaBr recoil velocity in the spectator stripping limit. Laboratory angles 20 and 60 degrees are indicated by dotted lines. LAB and center of mass velocity vectors of BaBr in the spectator stripping limit are indicated. The associative ionization product $BaBr_2^+$ is shown enhanced 25 fold.

Figure III-6. Sections through several diabatic potential energy surfaces for collinear $Ba\text{-}Br_2$ obtained as described in text.

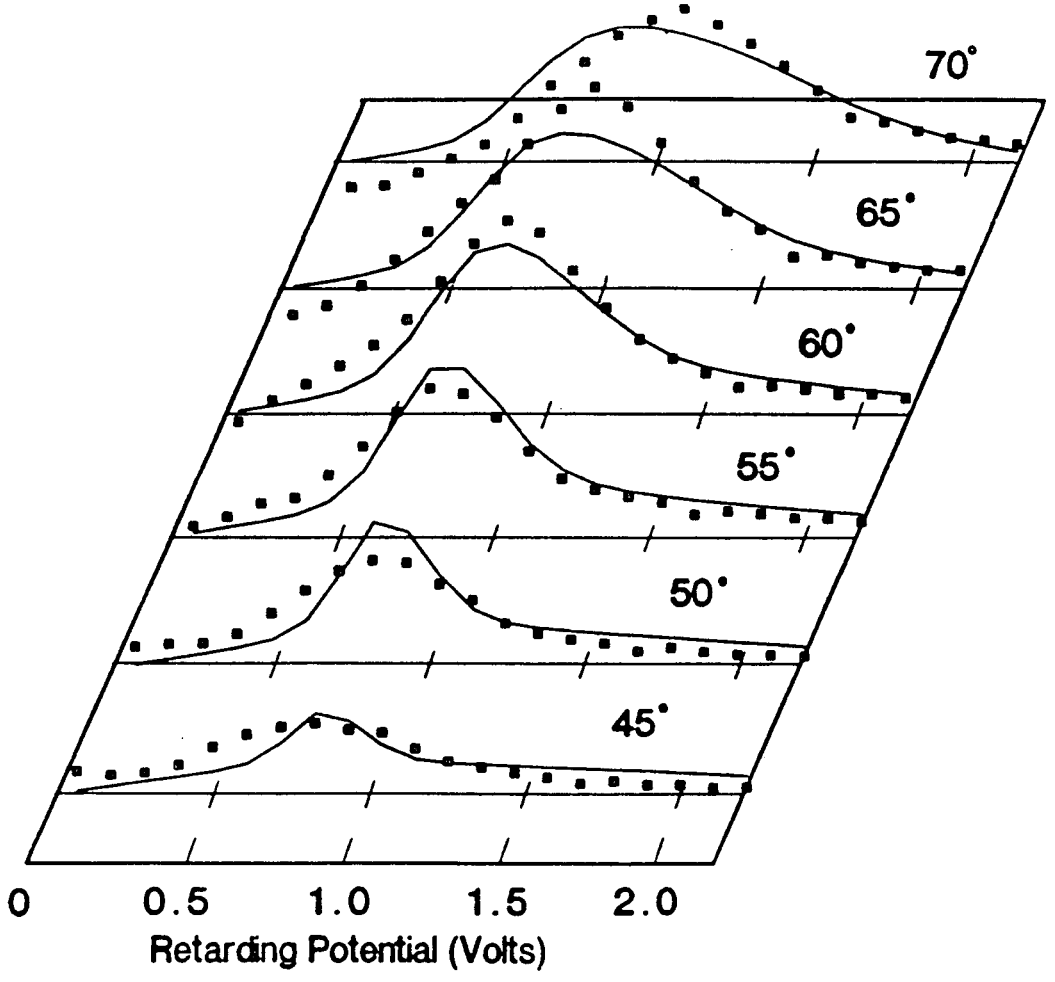

Figure III-1

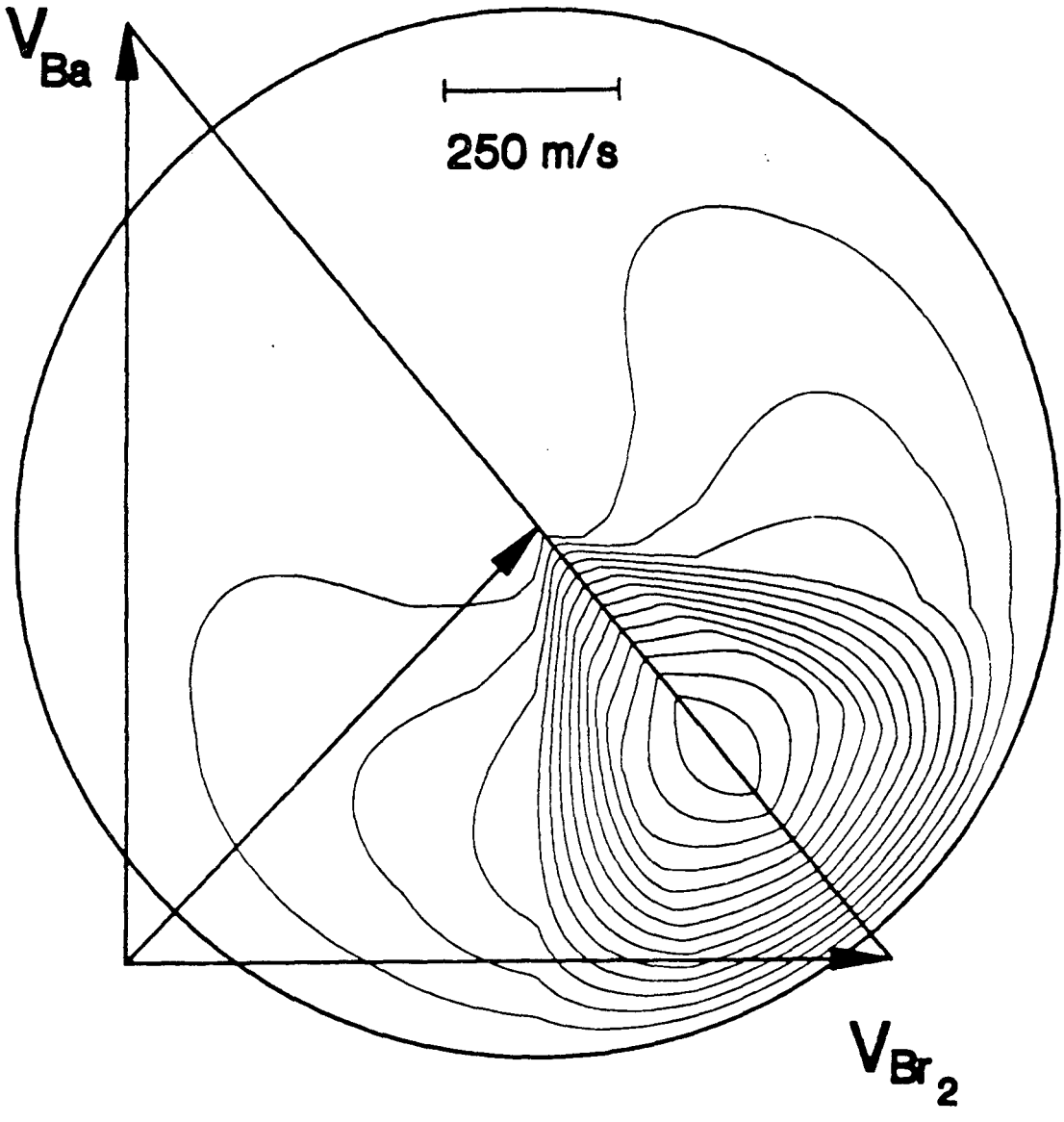

Figure III-2

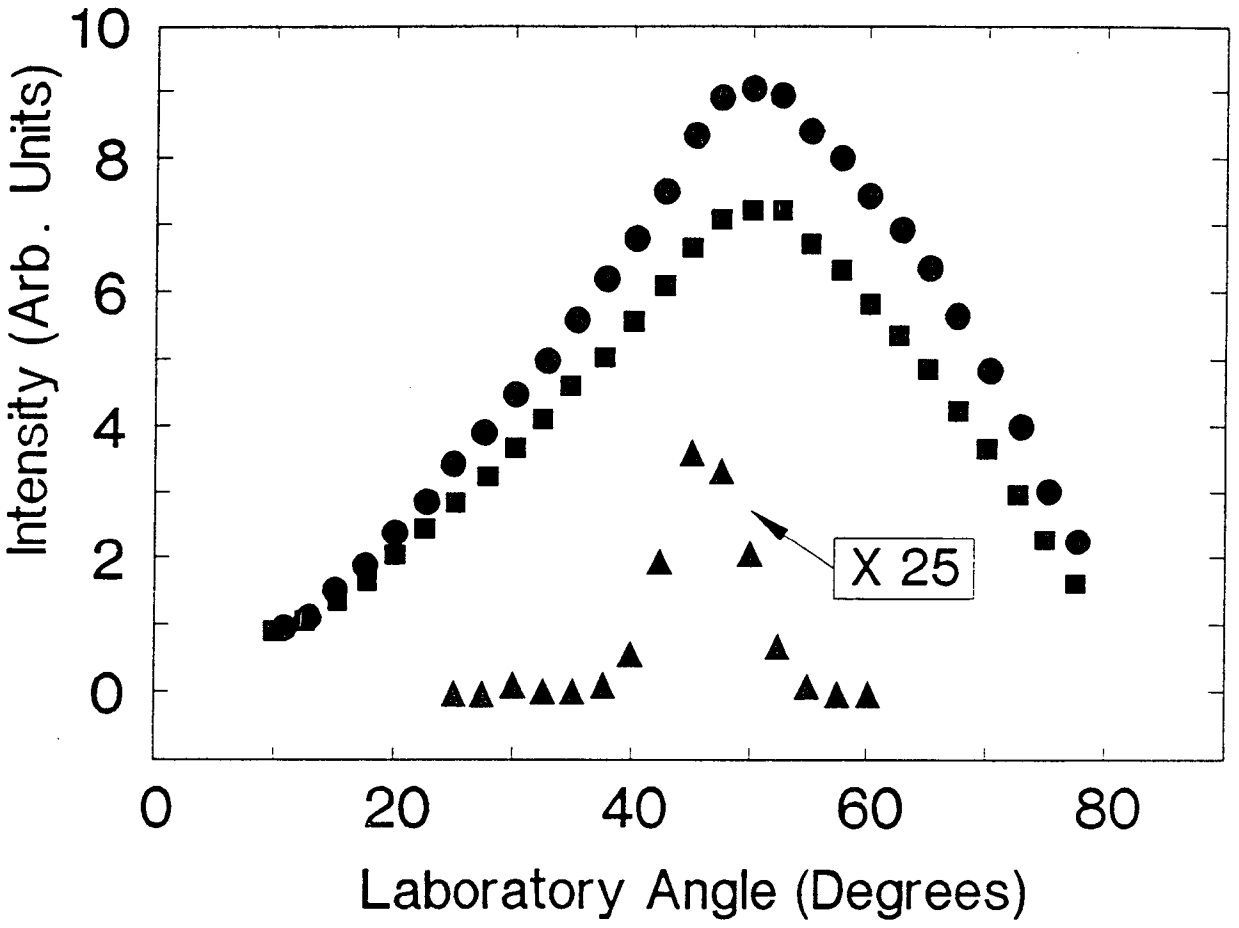
Intensity (Arb. Units)
10
8
6
4
2
0
0
20
40
60
80
Laboratory Angle (Degrees)
X 25

Figure III-3

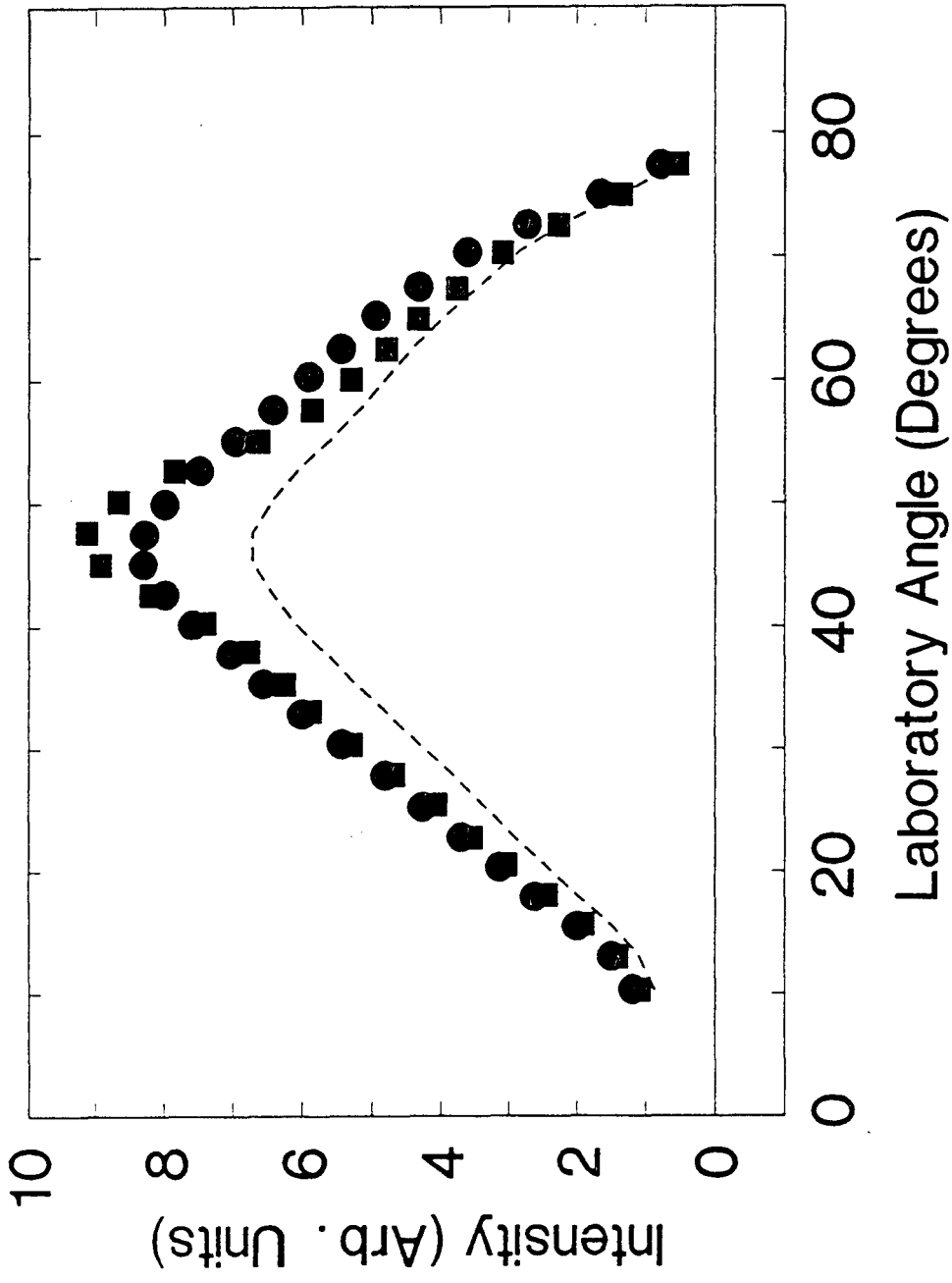
Intensity (Arb. Units)
0
2
4
6
8
10
0
20
40
60
80
Laboratory Angle (Degrees)

Figure III-4

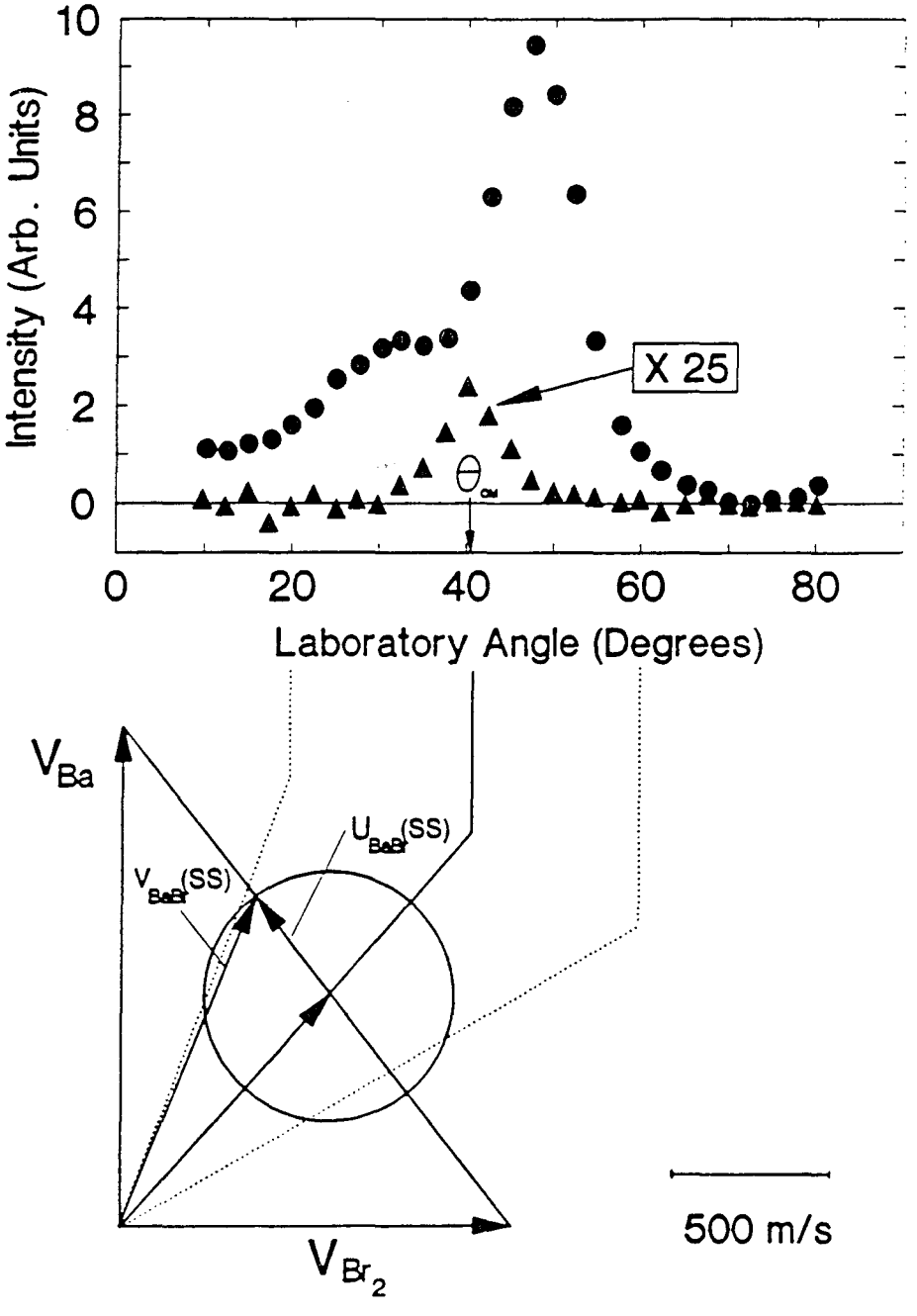
Intensity (Arb. Units)
10
8
6
4
2
0
X 25
θ_{cm}
0
20
40
60
80
Laboratory Angle (Degrees)
V_{Ba}
U_{BaBr}(SS)
V_{BaBr}(SS)
V_{Br_2}
500 m/s

Figure III-5

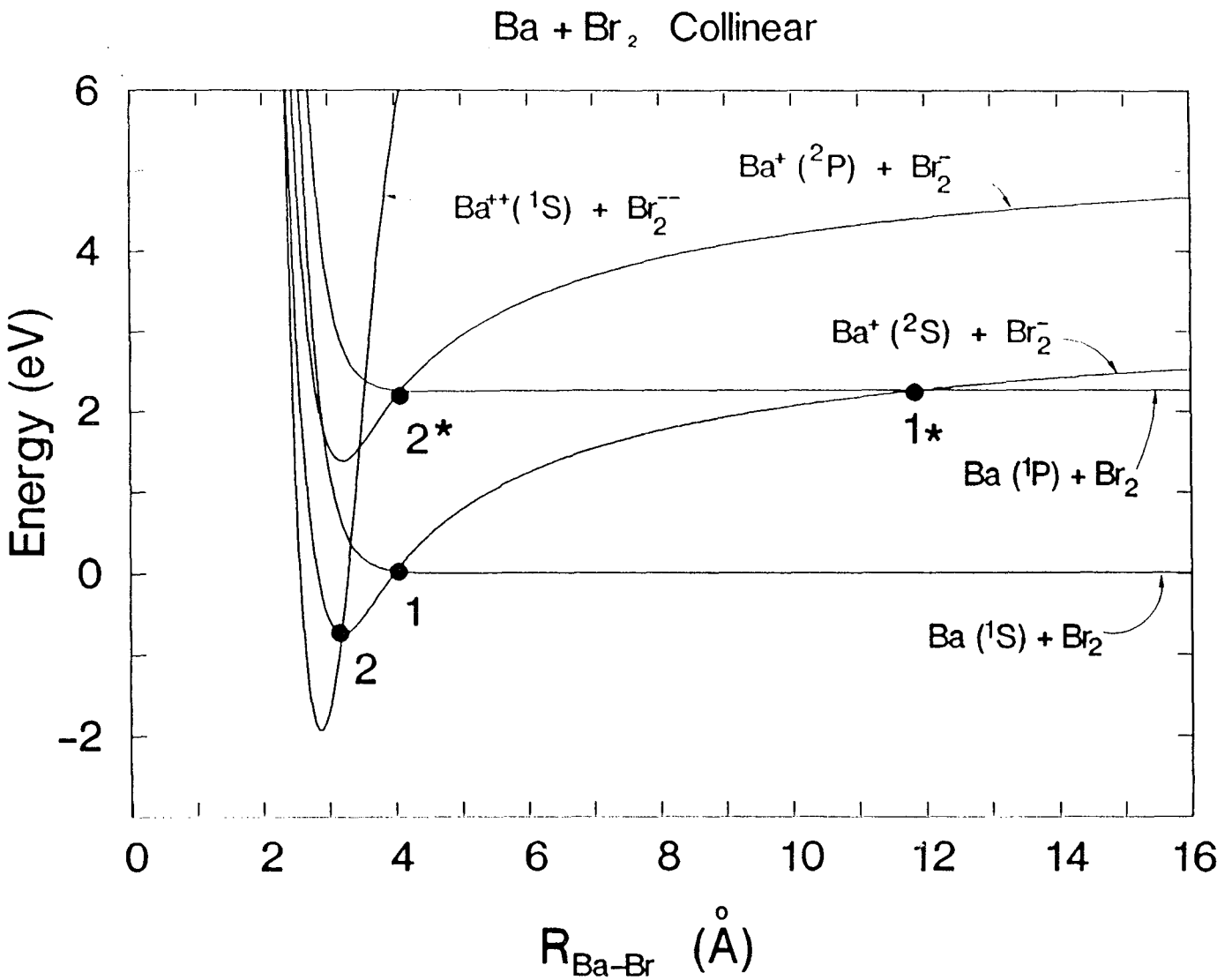
Ba + Br2 Collinear
Energy (eV)
6
4
2
0
-2
0
2
4
6
8
10
12
14
16
R Ba-Br (Å)
Ba+ (2P) + Br2-
Ba++(1S) + Br2--
Ba+ (2S) + Br2-
Ba (1P) + Br2
Ba (1S) + Br2
2*
1*
1
2

Figure III-6

Chapter IV: Reaction Geometry from Orbital Alignment Dependence of Ion Pair Production in Crossed Beams $Ba(^1P_1)$-Br_2 Reactions

A. Introduction

A simple relation exists between impact parameter and scattering angle in atom-atom scattering, so angular distributions in crossed beams experiments have been used with considerable success to study the distance dependence of interatomic forces.[1-3] Extremely accurate interatomic potentials are now routinely obtained from elastic scattering results. For inelastic atom-molecule scattering there exists no simple correspondence between scattering angle and impact parameter owing mainly to the tremendous possible variation in scattering angle with collision geometry. Yet the differential cross sections still contain a wealth of information, and crossed beams experiments have been used to explore the anisotropy of the atom-molecule interaction potential directly in the differential cross section, as in the atom-atom experiments, and indirectly through such phenomena as rotational rainbows.[4-6] Reactive scattering represents the greatest challenge to the crossed beams technique because large numbers of states, even entirely different product channels, may be accessible. These may exhibit varying partitioning of the available energy between internal modes and translation, so there may not exist strong correlations between these quantities. The

dynamics may be thus obscured by a broad and overlapping range of final state distributions. Nevertheless, scattering results often provide remarkable insight into the microscopic features of reactive collisions, particularly when translational energy distributions are also obtained, or when the reaction occurs by way of some constrained geometries[7] or shows distinctive dynamic behavior.[8] In recent years it has become possible, through use of electrostatic focusing techniques, polarized narrow band lasers and related methods, to prepare oriented or aligned atomic and molecular reagents.[10-11] The use of such prepared reagents in crossed beams experiments provides a means of extending the power of crossed beams techniques to explore the full geometry of the collisional encounter.

For barium excited to the ($^1P_1$) electronic state, thermal energy collisions with halogen molecules can yield the ion pair Ba^+ and X_2^-. The use of a linearly polarized laser to prepare the electronically excited barium atoms allows for alignment of the excited state orbital with respect to the relative velocity vector, which is itself well-defined under crossed beams conditions. Because the electronic potential energy surfaces possess different symmetries depending on initial orbital alignment, branching into non-adiabatic reaction pathways may be strongly modulated by means of laser polarization.[12,13] Furthermore, this preparation of aligned reactants breaks the cylindrical symmetry which prevails in crossed beams experiments. For scattering dominated by orbital angular momentum, Π^+ and Π^- configurations may be defined with respect to the scattering plane.[14] In effect, the detector may act as a polarizer: in

favorable cases we may distinguish products for which the initial nuclear and electronic orbital angular momentum vectors are either parallel or perpendicular. If the symmetries of the electronic wavefunctions are known for relevant states of the collision complex, the dependence of reaction cross section on initial orbital alignment may be used to infer the internuclear geometry at the critical configuration at which electron transfer occurs.

The study of collisions involving aligned orbitals has proceeded rapidly in recent years. As a result of pioneering studies by Pauly[15-17], Hertel[18-20], Leone[21-22] and others in the late 70's and early 80's, there now exist several "well-understood cases" in atom-atom scattering. In contrast alignment dependence in atom-molecule scattering, both inelastic[23,24] and reactive, has seldom been reported and is not as well understood. Earlier work in our laboratory described significant polarization effects for crossed beams reaction of Na(4D) with O_2.[25,26] Parallel alignment of the sodium d orbital with respect to the relative velocity vector led to efficient quenching via the ground state O_2^- ion. Formation of the reactive product, however, required a close collision from the covalent surface, and led to sharply backscattered NaO. In addition, the location of the peak in the polarization dependence changed with laboratory scattering angle, demonstrating the importance of a collinear nuclear geometry at the critical configuration. In 1982 Rettner and Zare reported remarkable polarization effects on product state branching and cross sections in reaction of $Ca(^1P_1)$ with HCl and Cl_2 in a beam-gas experiment.[27] In the former reaction they found

chemiluminescence from the CaCl(A $^2\Pi$) state enhanced by initial Π orbital geometry, while the CaCl(B $^2\Sigma$) state was favored by Σ geometry. They attributed the dependence of final electronic state on initial orbital alignment to a preservation of the symmetry of the initially prepared state through the reactive encounter, with reaction initiated by transfer of the calcium s rather than p electron. In the Cl_2 reaction, however, all products were found to be favored by the Π configuration. This was ascribed to an alignment dependence of the probability for transfer of the p electron at the outer crossing of the potential energy surfaces, with reaction favored by broadside approach. These arguments have some bearing on the work presented here, and will be considered in detail in the ensuing discussion.

We previously reported strong orbital alignment dependence for Ba^+ produced from crossed beams reaction of $Ba(^1P_1)$ with Cl_2 at a collision energy of 3 eV.[28] This alignment dependence was only observed at back angles with respect to the barium beam, although unfavorable kinematics precluded viewing angles significantly forward of the center of mass. The analogous reaction with Br_2 was expected to show many of the same features as the Cl_2 reaction, while the kinematics are considerably more favorable. The alignment dependence for Ba^+ produced from reaction of $Ba(^1P_1)$ with Br_2 was found to be strongly dependent on laboratory scattering angle, and different dependence was observed for in-plane and out-of-plane rotation of the orbital. All observations can be reconciled by a mechanism in which large impact parameter

collisions dominate in long-range electron-transfer of those collisions which achieve a Σ configuration (in the molecular reference frame) at the crossing seam.

B. Results

The charge transfer reaction of $Ba(^1P_1)$ with Br_2 at 1.6 eV collision energy was studied as a function of orbital alignment and laboratory scattering angle for both in-plane and out-of-plane rotation of the barium p orbital. Beta, the angle between the relative velocity vector and the laser polarization, is taken to be in the positive direction for clockwise rotation of the orbital viewed from above. For out-of-plane rotation the positive sense of polarization rotation is taken to be clockwise when viewing into the bromine beam.

1. In-Plane Polarization Rotation

Figure 1 shows laboratory angular distributions of Ba^+ taken with parallel (β=0°) perpendicular (β=90°) and $\beta = \pm 45°$ alignment for in-plane rotation of the orbital. All polarizations showed forward or forward-sideways scattered angular distributions. Little change was seen between the perpendicular and parallel polarizations for the most forward laboratory angles, but the location of the peak shifted back substantially for the perpendicular result and showed a much larger

contribution from angles behind the center of mass. Both $\beta = \pm 45°$ alignment scans were intermediate between the parallel and perpendicular, with neither showing as large a contribution at back angles. The $\beta = +45°$ angular distribution showed greater wide angle scattering than the $\beta = -45°$. The narrow angular distributions indicate that considerable energy remains in Br_2^- vibration.

Figure 2 shows a series of polarization scans of Ba^+ taken at a range of laboratory scattering angles for in-plane rotation of the p orbital. These were obtained by monitoring the Ba^+ flux at a given laboratory angle as a function of laser polarization. All scans are fit by the expression[19]

$$I(\beta) = \frac{(I_{max}+I_{min})}{2} + \frac{(I_{max}-I_{min})}{2}\cos 2(\beta-\beta').$$

The values of $(I_{max}-I_{min})/I_{min}$ and β' obtained from the fits are shown in Table 1. The alignment dependence is quite strong, reaching 1.2 at back angles, but varies significantly with angle and no clear trend appears. The location of the peak (β') changes monotonically with scattering angle, almost through a full 180°, but the change at the back angles is much slower than at the forward angles.

The polarization scans of Figure 2 were scaled using the measured angular distributions to yield the alignment-angular distributions shown in Figure 3. Each grid

point thus corresponds to a measured data point. The maximum flux occurred for β=90°, perpendicular alignment of the p orbital with respect to the relative velocity vector, while the minimum appeared for parallel polarization.

2. Out-of-Plane Polarization Rotation

Figure 4 shows Ba^+ flux as a function of scattering angle and alignment angle for out-of-plane rotation of the p orbital. The in-plane polarization (θ=90°) corresponds to β = 35° because the laser is directed parallel to the bromine beam, 55° from the relative velocity vector. The out-of-plane polarization (θ=0°) corresponds to β = 90°. The widest laboratory angle accessible in this experimental geometry was 35°; beyond this the laser was obstructed by the detector. The out-of-plane polarization rotation results summarized in Figure 4 show the domination of in-plane alignment, independent of laboratory angle. In addition, Figure 4b suggests a correlation between laboratory scattering angle and the magnitude of the alignment effect. The ratio $(I_{max}-I_{min})/I_{min}$ ranged from a minimum of 1 at 35°, to a maximum of 4 at 10°.

C. DISCUSSION

Reaction of ground state barium with Br_2 at thermal energies is dominated by the production of the neutral radical pair BaBr and Br[29] via the celebrated "harpoon mechanism". Reaction is initiated with electron transfer from the metal atom to the halogen molecule at a distance at which the Coulomb interaction of the nascent ion pair compensates for the energy deficit of the electron transfer. Vertical electron attachment to Br_2 results in rapid stretching of the $(Br\text{-}Br)^-$ bond with subsequent dissociation in the field of the positive ion. Little momentum is transferred to the "spectator" bromine atom and forward scattered, vibrationally excited BaBr results.[30] Analogy with the extensively studied $K\text{-}Br_2$ system suggests that the neutral reaction dominates up to collision energies in the range 2-5 eV. At higher collision energies, formation of the ion pair M^+ and Br_2^- dominates and the cross section for neutral reaction products becomes negligible.[31]

Studies of ion pair formation in 5-1000 eV alkali metal-halogen molecule collisions have provided remarkable insight into the dynamics of these non-adiabatic processes. A generalized Landau-Zener treatment[32-37] gives the probability for remaining on a given adiabatic potential surface after passage through the crossing region:

$$p = 1-e^{-\delta}$$

where

$$\delta = \frac{2\pi H_{12}^2 R_c^2}{v}\left(1-\frac{b^2}{R_c^2}\right)^{-\frac{1}{2}}$$

in which v is the initial relative velocity, b the impact parameter and R_c the internuclear distance at the crossing point. For an atom-molecule collision, the coupling matrix element H_{12} may have a strong dependence on the angle ϕ between the molecular axis and the radius vector, largely as a consequence of the symmetries of the diabatic surfaces.[38]

Olson et al., have compiled a large number of measured and calculated coupling matrix elements for atom-atom systems to obtain a semi-empirical expression relating coupling matrix element to crossing distance:[39]

$$H_{12}^{*} = R_x^{*}\exp(-0.86R_x^{*})$$

in atomic units, where

$$H_{12}^{*} = \frac{H_{12}}{\sqrt{I_1 I_2}}$$

and

$$R_c^{*} = (\sqrt{I_1}+\sqrt{I_2})R_c$$

are the reduced coupling matrix element and reduced crossing distance, respectively, and I_1 and I_2 are the initial and final ionization potentials of the transferred electron. This expression yields values within a factor of three for >80% of the compiled data, over a range of 10 orders of magnitude of the reduced coupling matrix element. The semi-empirical coupling elements may be used with the Landau-Zener result above to examine the dependence of electron transfer probability on crossing distance and collision parameters. At low to moderate collision energies, exclusively adiabatic behavior is predicted for crossing distances below about 7 Å, with a very rapid transition to non-adiabatic behavior with increasing crossing distance. This is illustrated in Figure 6 for conditions relevant to the Ba-Br_2 system. The dependence of adiabatic transition probability on crossing distance is shown for reactions of $Ba(^1P_1)$, using an ionization potential of 3 eV, a relative velocity of 2000 m/s and impact parameter b = 0 and 10 Å, while the electron affinity is allowed to vary.

Although the slopes are somewhat different, the general features of these curves are the same: the adiabatic transition probability falls rapidly in the region from 10 Å to 15 Å.

This exponential dependence of the coupling on the crossing distance yields the "bond-stretching" phenomenon which is perhaps the central feature of the dynamics of ion pair formation in alkali metal-halogen molecule collisions.[40] Following electron transfer on approach, the consequent stretching of the $(X\text{-}X)^-$ bond results in a substantial increase in the X_2 electron affinity, with a corresponding increase in the crossing distance and decrease in the coupling matrix element. As the molecular ion vibrates, the electron affinity varies considerably. The probability for electron transfer on exit may thus undergo oscillations, and in general will be very different from that on approach. Alternatively, nonadiabatic behavior on approach will lead to another opportunity for ion pair formation, in electron transfer on exit (the "covalent" trajectories). Because electron transfer on approach (the "ionic" trajectories) results in greater opportunity for the ion pair to experience the strong Coulomb attraction, the ionic trajectories in general will be deflected to larger scattering angles than the covalent trajectories.

The foregoing discussion derives largely from studies of ion pair formation in relatively high energy (5-1000 eV) collisions of ground state alkali atoms with halogen molecules. The nonadiabatic behavior in that case is largely a consequence of the high velocity through the crossing region. Nonadiabatic transitions are observed even

though the crossing distances may be relatively small. The use of electronically excited atoms also promotes nonadiabatic behavior, but through effects on the coupling matrix elements directly since different potential energy surfaces are involved. Excitation of Ba to the (^{1}P) state results in a lowering of its ionization potential from 5.2 to 3.0 eV. This moves the first crossing for the Ba-Br_2 system from ~4 Å to ~12 Å. As noted above, this is the region at which the coupling matrix element, hence the adiabatic transition probability, is dropping rapidly as a function of crossing distance. Another important effect of laser excitation on the coupling matrix element results from the change in the symmetries of the diabatic surfaces. The Ba(^{1}P)-Br_2 system actually represents three distinct potential energy surfaces, and their intersection with the $Ba^+(^2S)$-Br_2^- surface is schematically illustrated for $C_{\infty v}$ and C_{2v} geometries in Figure 7. This outer crossing represents a conical intersection[41] of the potential surfaces, and the coupling matrix elements are expected to show a ϕ dependence[42] given by:

$$(H_{12}(\phi))^2 = (H_{12}^o)^2 \sin^2(\phi) \quad \textit{for } p_x$$

$$(H_{12}(\phi))^2 = (H_{12}^o)^2\cos^2(\phi) \quad \textit{for } p_z$$

$$(H_{12}(\phi))^2 = 0 \qquad \textit{for } p_y.$$

The coupling matrix element, hence the probability of electron transfer, will thus be sensitive to alignment of the barium p orbital.

The Σ orbital alignment in $C_{\infty v}$ results in an avoided intersection at this outer crossing. In C_{2v} geometry this orbital alignment corresponds to A_1 symmetry, for which there is no interaction with the B_1 symmetry σ^* orbital of Br_2. The two favorable configurations for electron transfer are Σ in $C_{\infty v}$ and B_1 in C_{2v}. One may thus use the orbital alignment dependence of the cross sections for different reaction channels to make inferences about the important nuclear geometries, and this is the basis of the argument presented by Rettner and Zare for their $Ca(^1P_1) + Cl_2$ alignment dependence.[27] But to make sense of alignment effects, the relation between the asymptotically prepared orbital alignment and the geometry of the collision complex must be divined. For head-on collisions there is no ambiguity, but for finite impact parameter collisions an initially prepared Σ state may evolve into either a Σ or Π state of the collision complex, depending on the magnitude of the splitting between the Σ and Π potential energy curves: that is, depending on whether Ω is a good quantum number for the system. This is the orbital locking phenomenon, the importance of

which is now universally recognized.[43-44] In atom-atom scattering there exists both experimental and theoretical evidence for a "locking radius" at which point the body-fixed reference frame becomes the important one.[45,46] An analogous phenomenon is anticipated in atom-molecule collisions, although greatly complicated by the additional nuclear degrees of freedom and the anisotropy of the potential. Rettner and Zare argued that the alignment dependence observed for all products studied in the $Ca(^1P_1)$-Cl_2 reaction indicated the importance of electron transfer at the outer crossing region, and this is entirely consistent with our observations in the present study. In addition, they inferred from the fact that all channels were favored by Π alignment that broadside collisions were dominant and orbital following was perhaps important. Simons, in a 1987 review[47], hinted that the $Ca(^1P_1)$-Cl_2 results might alternatively be understood to result from large impact parameter collisions which are outside the locking radius for the system. Our results are clearly in accord with Simons' remark, and they suggest the model illustrated in Figure 8. Three conclusions serve to rationalize all the experimental findings: 1) The crossing point is beyond the locking radius for the system; 2) The charge transfer process is dominated by large impact parameter collisions, for which asymptotic Π alignment corresponds to Σ alignment in the body fixed frame at the crossing point; and 3) The internuclear geometry is collinear at the critical configuration.

We first consider alignment dependence of charge transfer in $Ba(^1P_1)$-Br_2 collisions for in-plane rotation of the p orbital. If one assumes initial and final nuclear

orbital angular momentum vectors to be parallel, a reasonable approximation here, then both configurations favoring electron transfer, Σ in $C_{\infty v}$ and Π in C_{2v}, require the impact parameter to lie in the scattering plane. All Ba^+ will be scattered in the scattering plane (the plane of the detector) regardless of alignment angle. This is also consistent with the results for the $Ca(^1P_1)$-Cl_2 discussed above, in which there was no scattering plane to break the cylindrical symmetry of the experiment. Several aspects of the data indicate that large impact parameter collisions dominate the production of the charge transfer process. All Ba^+ is forward or forward-sideways scattered, as expected for large impact parameter collisions. The different angular distributions for $\beta = \pm 45°$, shown in Figure 1, can be readily understood as a consequence of a negative correlation between impact parameter and scattering angle. Most importantly, the different nature of the alignment dependence for in-plane and out-of-plane polarization scans strongly suggests the dominance of large impact parameter collisions.

The out-of-plane results shown in Figures 4 and 5 enable us to determine the relative importance of C_{2v} and $C_{\infty v}$ geometries. The alignment dependence is always favored for collisions in which the orbital lies in the scattering plane. If C_{2v} geometries were dominant, then one would expect little alignment dependence for out-of-plane rotation. There is as likely to be a suitably oriented Br_2 molecule whether or not the p orbital is in the scattering plane. If collinear geometry were dominant, however, dramatic alignment effects might be anticipated. Although perpendicular

orbital alignment is most favorable for electron transfer, for out-of-plane orbital alignment this would occur only for impact parameters lying in a plane perpendicular to the scattering plane: most products would thus scatter out of the plane containing the detector. Figures 3 and 4 thus strongly suggest that large impact parameter collisions which achieve a collinear nuclear configuration and Σ orbital alignment at the crossing point dominate this process.

These conclusions find further support in the angular distributions of figure 1. The increased flux seen for perpendicular over parallel polarization appears to be less forward scattered. This is consistent with preliminary translational energy scans which suggest that perpendicular alignment leads to an increase in the sideways scattered product. These distributions may be understood with recourse to figure 6. The perpendicular alignment favors electron transfer for the large impact parameter collisions. These will not necessarily lead to forward scattering, however. The long-range coulomb interaction may still produce significant deflection even in these collisions. As mentioned above, the most forward scattered flux will be that which originates from covalent trajectories: those for which electron transfer occurs on exit rather than on approach.[40] Parallel alignment favors lower impact parameter collisions. In this case, electron transfer on approach results in a strong interaction which probably favors neutral products or the chemiion channel.[28] The charge transfer channel may only be possible for low impact parameter collisions via the covalent trajectories. Parallel alignment thus produces the most forward scattered flux. The β

$= \pm 45°$ results further indicate that for these still relatively large impact parameter collisions ($b = 10/\sqrt{2} = 7.1$ Å), electron transfer occurs on approach rather than on exit. For $\beta = +45°$, the tendency to wide angle scattering reveals that this orbital alignment favors positive center of mass scattering angles. The more forward laboratory angular distribution for $\beta = -45°$ indicates that this results in scattering into negative center of mass angles, as illustrated schematically in Figure 9.

Orbital locking is expected when Ω-splitting of the potentials is large relative to the angular velocity of the collision. This Ω-splitting may be expressed as a precession frequency of the electronic orbital angular momentum vector about the internuclear axis[48]:

$$\omega_{prec}(R) = \Delta V(R)/\hbar \ .$$

The condition for orbital locking then becomes:

$$\omega_{prec}(R) >> \dot{\phi}(R) \ ,$$

where $\dot{\phi}(R)$ is the angular velocity of the collision. A "locking radius", R_L, may be defined at some internuclear distance smaller than which this condition is considered to hold. Manders et al., in semi-classical trajectory studies of alignment effects in Ne**-Ar collisions, have found the condition

$$\omega_{prec}(R_L) = 4\dot{\phi}(R_L)$$

provides a reasonable definition for this locking radius.[49] Applying these considerations we can estimate the magnitude of Ω-splitting necessary to induce orbital locking in the $Ba(^1P_1)$-Br_2 system. For an impact parameter of $R_c/\sqrt{2} = 7$Å, the

splitting between the potentials would have to exceed 4 meV at 10Å in order for orbital locking to be possible there. Splitting of this magnitude seems unlikely at such long range. Although the discussion is strictly appropriate only for atom-atom collisions, it is useful to provide a sense for the magnitude of the forces involved, and is unlikely to be seriously in error at the large Ba-Br_2 distances considered.

From the foregoing discussion we might not anticipate orbital locking to be important for this system. Indeed, although they do not preclude the possibility of orbital locking, the experimental results argue the importance of the space fixed reference frame throughout the collision. The observed Π alignment dependence implies that for these dominant geometries, the laboratory-prepared orbital alignment is precisely that which is relevant in the collision. If this were not the case, we would anticipate a dominant orbital alignment somewhat shifted from perpendicular, which could evolve to the favorable geometry through rotation of the molecule fixed frame as the internuclear distance changed from R_L to R_C.

The narrow angular distributions in Figure 2 are consistent with the limited energy available to translation following electron attachment to Br_2. The inner circle represents the maximum Ba^+ velocity based on the vertical electron affinity of Br_2: ion pair production via vertical electron attachment is 1.4 eV endoergic. Most of the distribution falls within this limiting circle. This Ba^+ production following vertical electron attachment requires effective coupling of the initial translational energy into the reaction coordinate. Yet for the dominant large impact parameter collisions the

radial velocity (the reaction coordinate) may be very small at the moment of electron transfer. Moreover, similar results were obtained at 1 eV collision energy, yet this is below the endoergicity of the process for a simple vertical electron transfer. Several alternatives may be considered to account for this apparent discrepancy. Ion pair production is consistently observed in alkali-halogen molecule collisions below thresholds based on the vertical electron affinities: in fact thresholds for ion pair production yield good values for the adiabatic electron affinities of halogen molecules.[50] This results from "prestretching" of the halogen bond in the presence of the alkali atom, and it has been shown to be important even up to collision energies of 120 eV.[40,51] Yet prestretching may be less important at the large distances considered here. Alternatively, although the vertical electron affinity of Br_2 is given as 1.6 eV, owing to the steepness of the Br_2^- potential in this region the Franck-Condon envelope is >0.8 eV wide, so a broad range of Br_2^- vibrational states may be reached. Furthermore, the low vibrational frequency of Br_2 (325 cm^{-1}) implies a substantial vibrationally excited population. Under the conditions of our experiment and assuming no vibrational relaxation in the supersonic expansion, >20% of the Br_2 is in v=1. For Br_2 (v=1), vertical electron transfer may reach deep into the Br_2^- well, resulting in the release of considerably more energy to the reaction coordinate. All of the foregoing considerations are probably relevant and classical trajectory calculations would be useful to address these questions.

It is interesting to note that in the $Ca(^1P)$-Cl_2 system studied by Rettner and Zare, and the Na(4D)-O_2 and $Ba(^1P)$-Br_2 studies from our laboratory, the conditions were such that adiabatic transition probability, as given by the Landau-Zener treatment discussed above, was significantly different from both one and zero. That is, the experiments were performed in the region in which the coupling varies rapidly as a function of crossing distance (and in which its dependence on orbital alignment may have some measurable effect). Furthermore, in all these examples of strong alignment effects for reactive scattering, it is in non-adiabatic channels that these alignment effects are observed. In these channels the dominant adiabatic flux contributes no background. This suggests a general prescription for those seeking to exploit orbital alignment effects in the study of reactive scattering: 1) choose systems in which the adiabatic transition probability is changing rapidly as a function of crossing distance, and 2) study the non-adiabatic channels in these systems.

D. CONCLUSION

A strong dependence of the charge transfer cross section on orbital alignment was used to explore the stereochemical requirements of the initial electron transfer in $Ba(^1P_1)$-Br_2 collisions. The orbital alignment dependence observed for Ba^+ production is striking in several respects. The magnitude of the effect, reaching $(I_{max}-I_{min})/I_{min} = 4$, is unprecedented in studies of atom-molecule scattering, particularly for reactive

processes. In addition, the continuous change of the location of the polarization peak with scattering angle suggests important changes of impact parameter or nuclear geometry with alignment angle. Finally, there is an apparent contradiction between the in-plane result, which shows a maximum for perpendicular orbital alignment, and the out-of-plane result, which shows a minimum for perpendicular orbital alignment. These differences in the alignment dependence for in-plane and out-of-plane rotation of the barium p orbital indicate that the reaction is dominated by large impact parameter collisions for which the perpendicular orbital alignment corresponds to a Σ state in the molecular reference frame at the critical configuration.

References

1. J. M. Parson, T. P. Schaefer, F. P. Tully, P. E. Siska, Y. C. Wong and Y. T. Lee, J. Chem. Phys. **53**, 2123 (1970).
2. P. E. Siska, J. M. Parson, T. P. Schaefer, F. P. Tully, Y. C. Wong and Y. T. Lee, Phys. Rev. Lett., **25**, 271 (1970).
3. H. Pauly and J. P. Toennies, Adv. At. Mol. Phys. **1**, 195 (1965).
4. F. P. Tully and Y. T. Lee, J. Chem. Phys. **57**, 866 (1972).
5. R. Schinke and J. Bowman, in **Molecular Collisions Dynamics**, (Springer-Verlag, Berlin, 1983).
6. P. L. Jones, U. Hefter, A. Mattheus, J. Witt, K. Bergmann, W. Muller,W. Meyer and R. Schinke, Phys. Rev. L ett. **46**, 915 (1981).
7. D. R. Herschbach, Disc. Faraday Soc., **33**, 149 (1962).
8. W. B. Miller, S. A. Safron and D. R. Herschbach, Disc. Faraday Soc., **44**, 292 (1967).
9. R. E. Minturn, S. Datz and R. L. Becker, J. Chem. Phys. **44** 1149 (1966).
10. I. V. Hertel and W. Stoll, Adv. At. Mol. Phys. **13**, 113 (1978).
11. D. H. Parker, H. Jalink, and S. Stolte, J. Phys. Chem. **91**, 5427 (1987).
12. I. V. Hertel, Adv. Chem. Phys. **45**, 341 (1981).
13. E. E. Nikitin, J. Chem. Phys. **43**, 744 (1965).

14. E. E. B. Campbell, H. Schmidt and I. V. Hertel, Adv. Chem. Phys. **72**, 37 (1988).

15. R. Duren, H. O. Hoppe, and H. Pauly, Phys. Rev. Lett. **37**, 743 (1976).

16. L. Huwel, J. Maier, R. K. B. Helbing and H. Pauly, Chem. Phys. Lett. **74**, 459 (1980).

17. L. Huwel, J. Maier and H. Pauly, J. Chem. Phys. **76**, 4961 (1982).

18. A. Fischer and I. V. Hertel, Z. Phys. A **304**, 103 (1982).

19. W. Reiland, G. Jameison, U. Tittes and I. V. Hertel, Z. Phys. A **307**, 51 (1982).

20. A. Bahring, I. V. Hertel and H. Schmidt, Z. Phys. A **320**, 141 (1985).

21. M. O. Hale, I. V. Hertel and S. R. Leone, Phys. Rev. Lett. **53**, 2296 (1984).

22. W. Bussert, D. Neuschafer and S. R. Leone, J. Chem. Phys. **87**, 3833 (1987).

23. W. Bussert and S. R. Leone, Chem. Phys. Lett. **138**, 269 (1987)

24. W. Bussert and S. R. Leone, Chem. Phys. Lett. **138**, 276 (1987).

25. P. S. Weiss, M. H. Covinsky H. Schmidt, B. A. Balko, Y. T. Lee and J. M. Mestdagh, Z. Phys. D **10**, 227 (1988).

26. H. Schmidt, P. S. Weiss, J. M. Mestdagh, M. H. Covinsky and Y. T. Lee, Chem. Phys. Lett. **118**, 539 (1985).

27. C. Rettner and R. N. Zare, J. Chem. Phys. **77**, 2416 (1982).

28. A. G. Suits, H. Hou and Y. T. Lee, J. Phys. Chem. **94**, 5672 (1990).

29. J. A. Haberman, K. G. Anlauf, R. B. Bernstein and F. J. Van Itallie, Chem. Phys. Lett., **16**, 442 (1972).

30. Shen-Maw Lin, Charles A. Mims, and Ronald R. Herm, J. Chem. Phys. **58**, 327 (1973).

31. C. W. A. Evers, Chem. Phys. **30**, 27 (1978).

32. L. D. Landau, J. Phys. (USSR) **2**, 46 (1932).

33. C. Zener, Proc. Roy. Soc. (London) **A137**, 696 (1932).

34. E. E. Nikitin, Opt. Spectrosc. **11**, 246 (1961).

35. R. K. Janev, Adv. At. Mol. Phys. **12**, 1 (1976).

36. Y. N. Demkov, Sov. Phys. JETP **18**, 138 (1964).

37. D. Rapp and W. E. Francis, J. Chem. Phys. **37**, 2631 (1962).

38. E. A. Gislason and J. G. Sachs, J. Chem. Phys. **62**, 2678 (975).

39. R. E. Olson, F. T. Smith and E. Bauer, Appl. Optics, **10**, 1848 (1971).

40. J. Los and A. W. Kleyn, in **Alkali Halide Vapors**, 189 (Academic Press, New York, 1979) and references.

41. G. Herzberg, **Electronic Spectra of Polyatomic Molecules** (Van Nostrand, Princeton NJ 1967).

42. E. E. Nikitin, Chem. Phys. Lett. **1**, 266 (1967).

43. G. C. Schatz, L. J. Kovalenko and S. R. Leone, J. Chem. Phys. **91**, 6961, (1989).

44. B. Pouilly and M. H. Alexander, Chem. Phys. **145**, 191 (1990).

45. L. J. Kovalenko, S. R. Leone and J. B. Delos, J. Chem. Phys. **91**, 6948 (1989).

46. J. P. J Driessen, Ph.D. Thesis, Eindhoven University (1989).

47. J. P. Simons, J. Phys. Chem. **91**, 5378 (1987).

49. J. P. J. Driessen, F. J. M. v. d. Weijer, M. J. Zonneveld, L. M. T. Somers, M. F. M. Janssens, H. C. W. Beijerinck and B. J. Verhaar, Phys. Rev. Lett., **62**, 2369 (1989).

50. M. P. I. Manders, W. B. M. van Hoek, E. J. D. Vredenbregt, G. J. Sandker, H. C. W. Beijerinck and B. J. Verhaar, Phys. Rev. A **39**, 4467 (1989).

50. A. P. M. Baede, D. J. Auerbach and J. Los, Physica **64**, 134 (1973).

51. J. A. Aten and J. Los, Chem. Phys. **25**, 47 (1977).

Table 1: Ba^+ In-Plane Alignment Dependence

Lab Angle	$(I_{max}-I_{min})/I_{min}$	β'
10.0°	.89	35°
12.5°	.91	23°
15.0°	.71	16°
17.5°	.41	1°
20.0°	.27	159°
22.5°	.27	137°
25.0°	.35	120°
27.5°	.46	111°
30.0°	.52	105°
32.5°	.68	100°
35.0°	.85	93°
37.5°	.95	89°
40.0°	1.06	85°
42.5°	1.23	82°
45.0°	1.25	77°
47.5°	.19	72°
50.0°	.94	66°
52.5°	.70	59°
55.0°	.53	56°
57.5°	.50	52°
60.0°	.44	57°

Table 1: Ba^+ alignment dependence for in-plane orbital rotation. Values of $(I_{max}-I_{min})/I_{min}$ and β' were obtained from the fits shown in Figure 2.

Chapter IV Figure Captions

Figure IV-1. Laboratory angular distributions of Ba^+ from the reaction $Ba(^1P_1)$ + Br_2 -> Ba^+ + Br_2^- at 1.6 eV collision energy shown with the nominal Newton diagram. The orbital alignment was $\beta = 90°$(circles), 0°(diamonds), -45°(squares) or +45°(triangles). The solid and dashed circles represent maximum Ba^+ recoil velocity based on adiabatic and vertical Br_2 electron affinities, respectively.

Figure IV-2. Experimental polarization dependences of Ba^+ at a collision energy of 1.6 eV for in-plane rotation of the barium p orbital at the indicated laboratory angles. Beta is the angle of the polarization with respect to the relative velocity vector. Also shown is a typical example of the $Ba(^1P_1)$ fluorescence intensity, which was monitored simultaneously for all scans.

Figure IV-3. The data of Figure 2 scaled by the angular distributions of Figure 1 to yield a polarization-laboratory angular distribution.

Figure IV-4. Experimental polarization-laboratory angular distribution of Ba^+ at a collision energy of 1.6 eV for out-of-plane rotation of the barium p

orbital. The polarization angle is taken to be zero when the laser polarization is perpendicular to the scattering plane.

Figure IV-5. The data of Figure 5 scaled so that the polarization maxima at each laboratory angle are equal.

Figure IV-6. Adiabatic transition probability calculated as described for $Ba(^1P_1)$ collisions at a relative velocity of 2000 m/s and impact parameter b = 0 Å (solid line) or b = 10 Å (dotted line).

Figure IV-7. Schematic illustration of possible reaction geometries.

Figure IV-8. Model illustrating important orbital alignment at the outer crossing for the $Ba(^1P_1)$-Br_2 charge transfer reaction.

Figure IV-9. Qualitative illustration of different laboratory scattering angles for $\beta = \pm 45°$ orbital alignment.

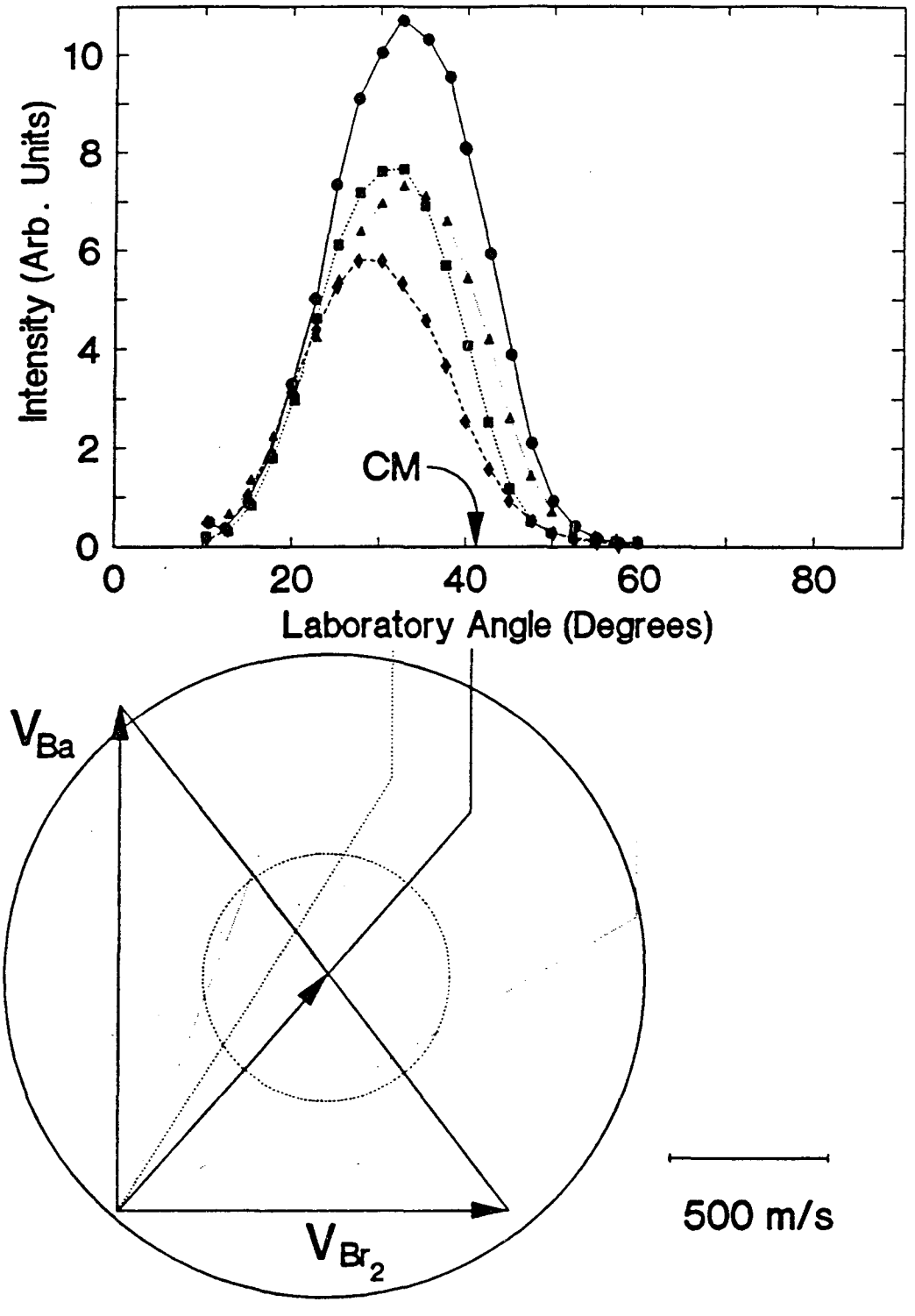
Intensity (Arb. Units)
10
8
6
4
2
0
0
20
40
60
80
CM
Laboratory Angle (Degrees)
V_{Ba}
V_{Br_2}
500 m/s

Figure IV-1

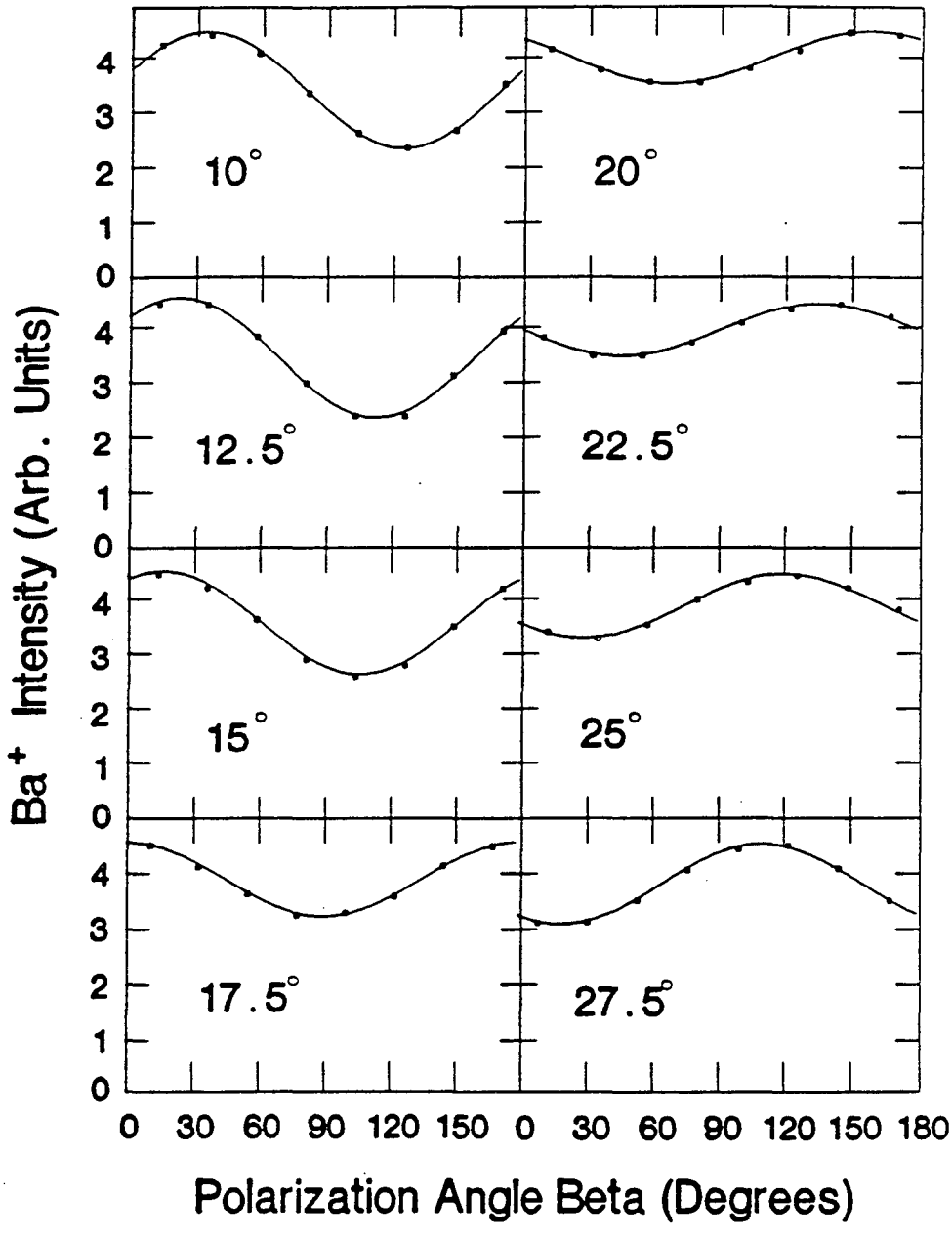
10°
20°
12.5°
22.5°
15°
25°
17.5°
27.5°
Ba+ Intensity (Arb. Units)
0 30 60 90 120 150 0 30 60 90 120 150 180
Polarization Angle Beta (Degrees)

Figure IV-2a

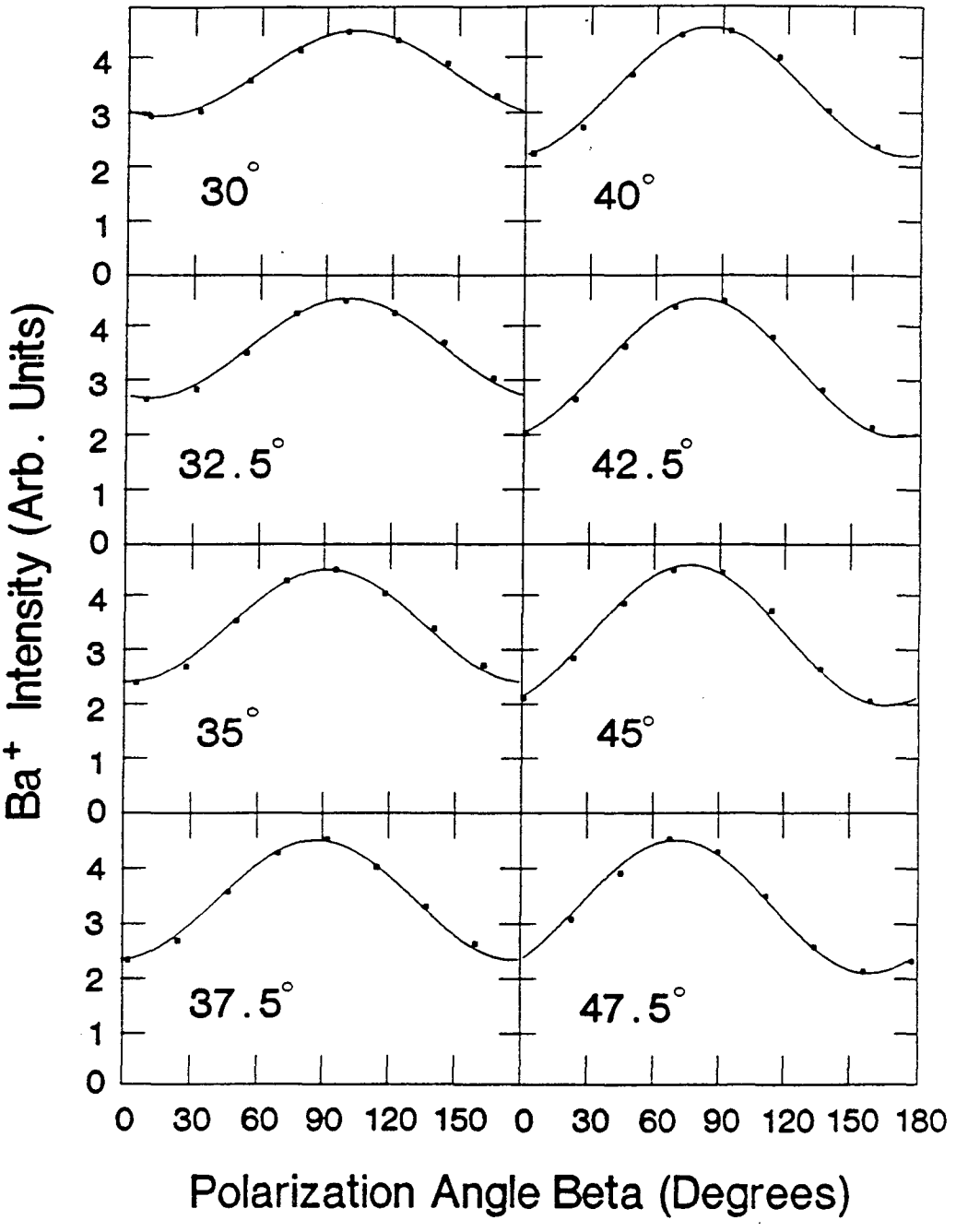
Ba+ Intensity (Arb. Units)
30°
40°
32.5°
42.5°
35°
45°
37.5°
47.5°
0 30 60 90 120 150 0 30 60 90 120 150 180
Polarization Angle Beta (Degrees)

Figure IV-2b

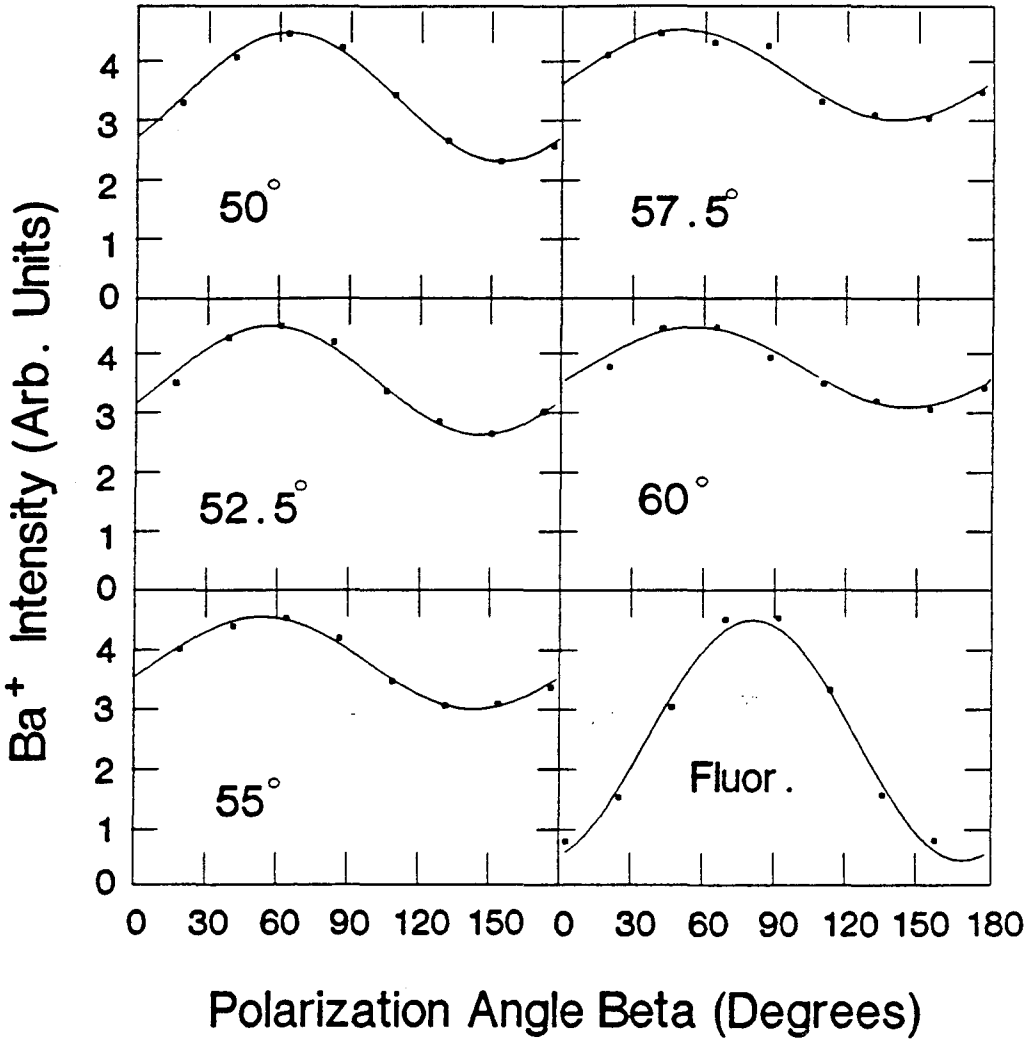
Ba+ Intensity (Arb. Units)
50°
57.5°
52.5°
60°
55°
Fluor.
0 30 60 90 120 150 0 30 60 90 120 150 180
Polarization Angle Beta (Degrees)

Figure IV-2c

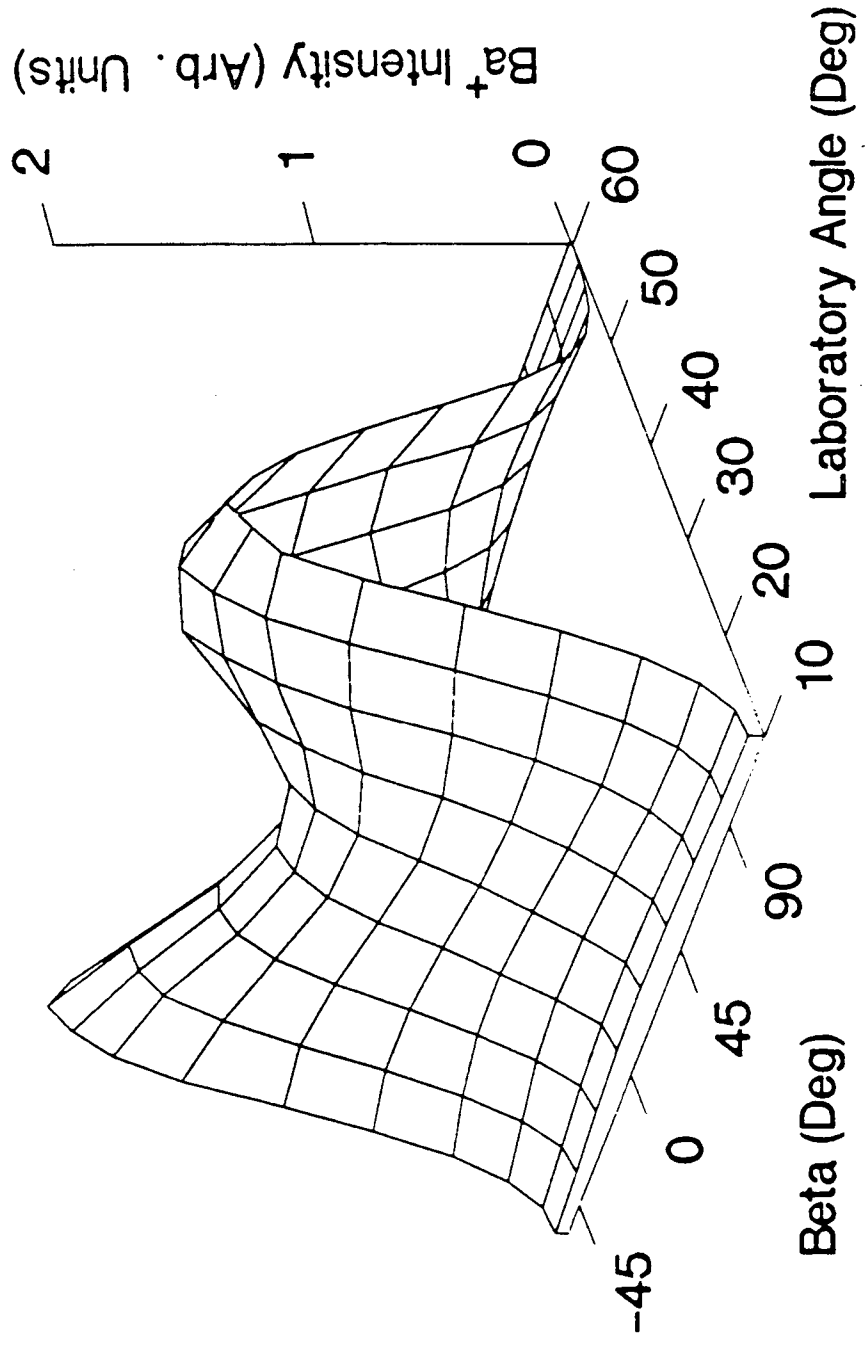
Ba+ Intensity (Arb. Units)
2
1
0
60
50
40
30
20
10
Laboratory Angle (Deg)
90
45
0
-45
Beta (Deg)

Figure IV-3

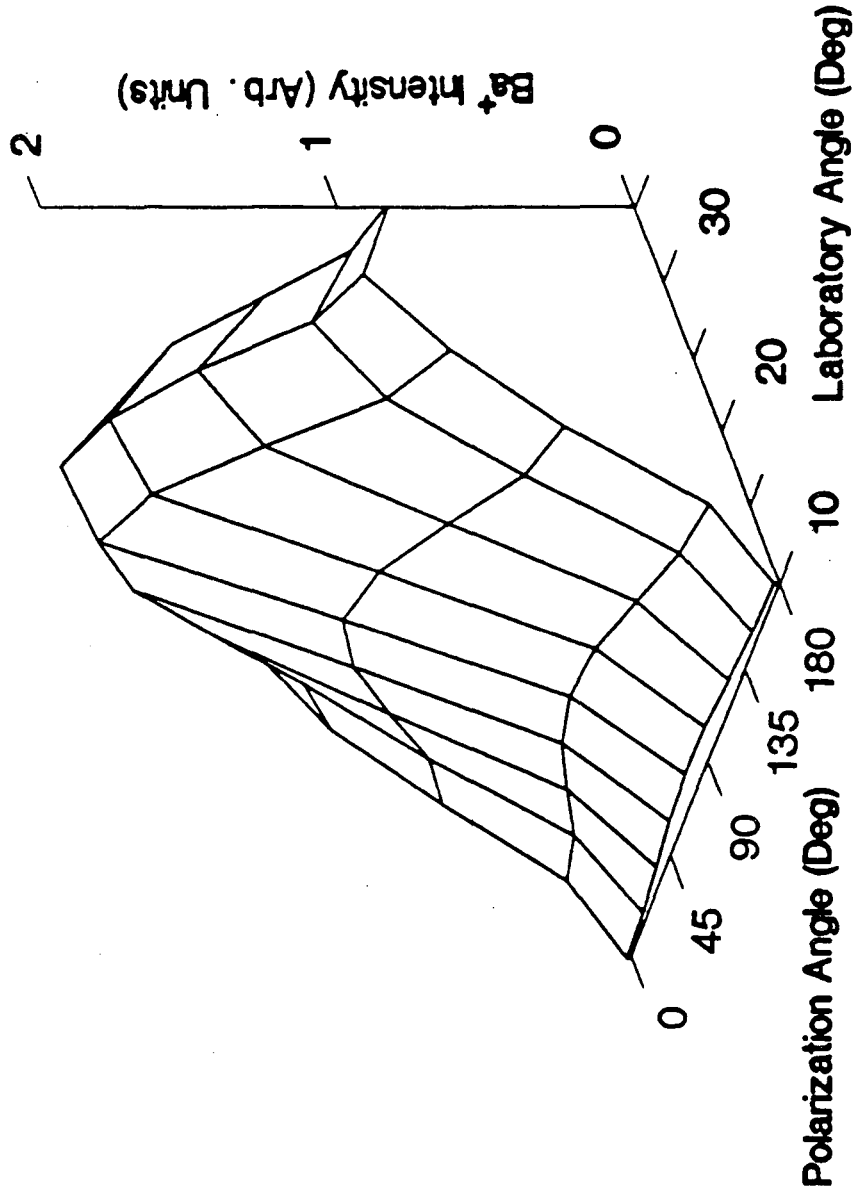
Ba+ Intensity (Arb. Units)
2
1
0
Laboratory Angle (Deg)
30
20
10
Polarization Angle (Deg)
0
45
90
135
180

Figure IV-4

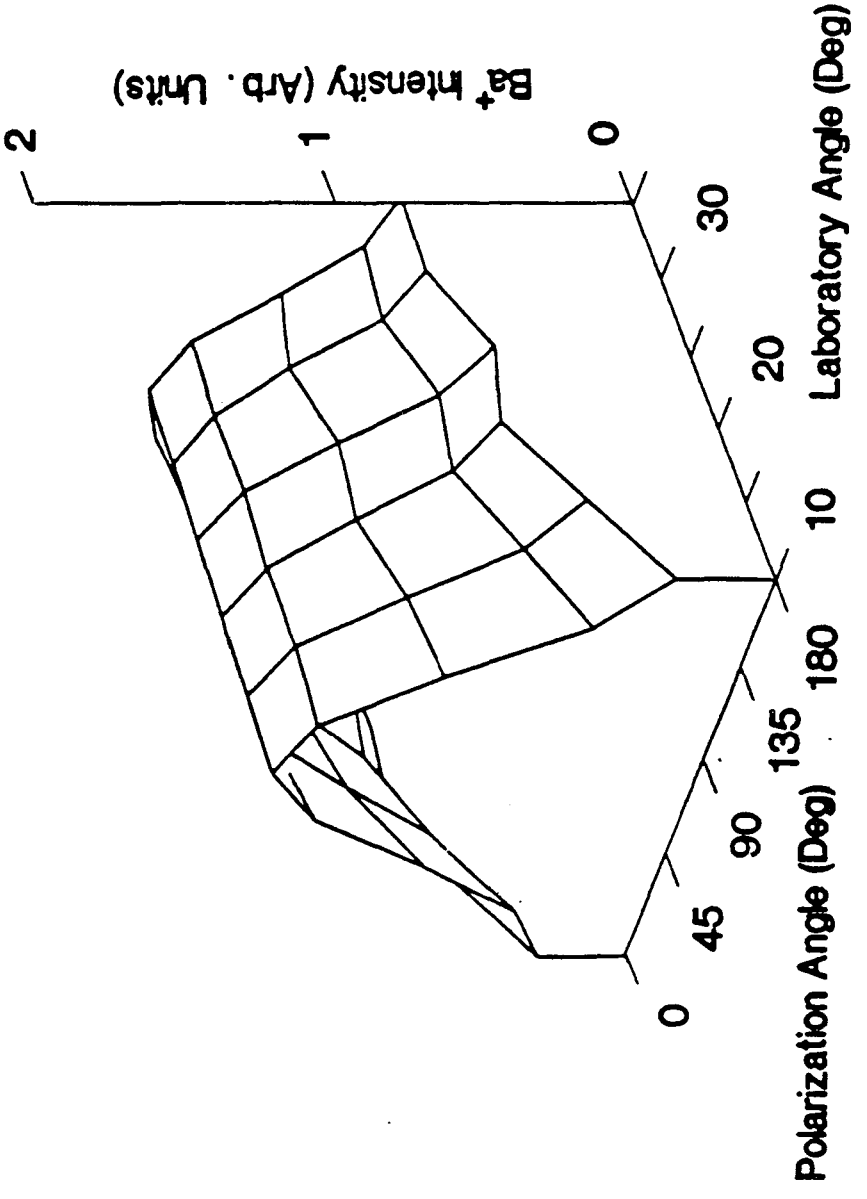
Ba+ Intensity (Arb. Units)
2
1
0
Laboratory Angle (Deg)
30
20
10
Polarization Angle (Deg)
0
45
90
135
180

Figure IV-5

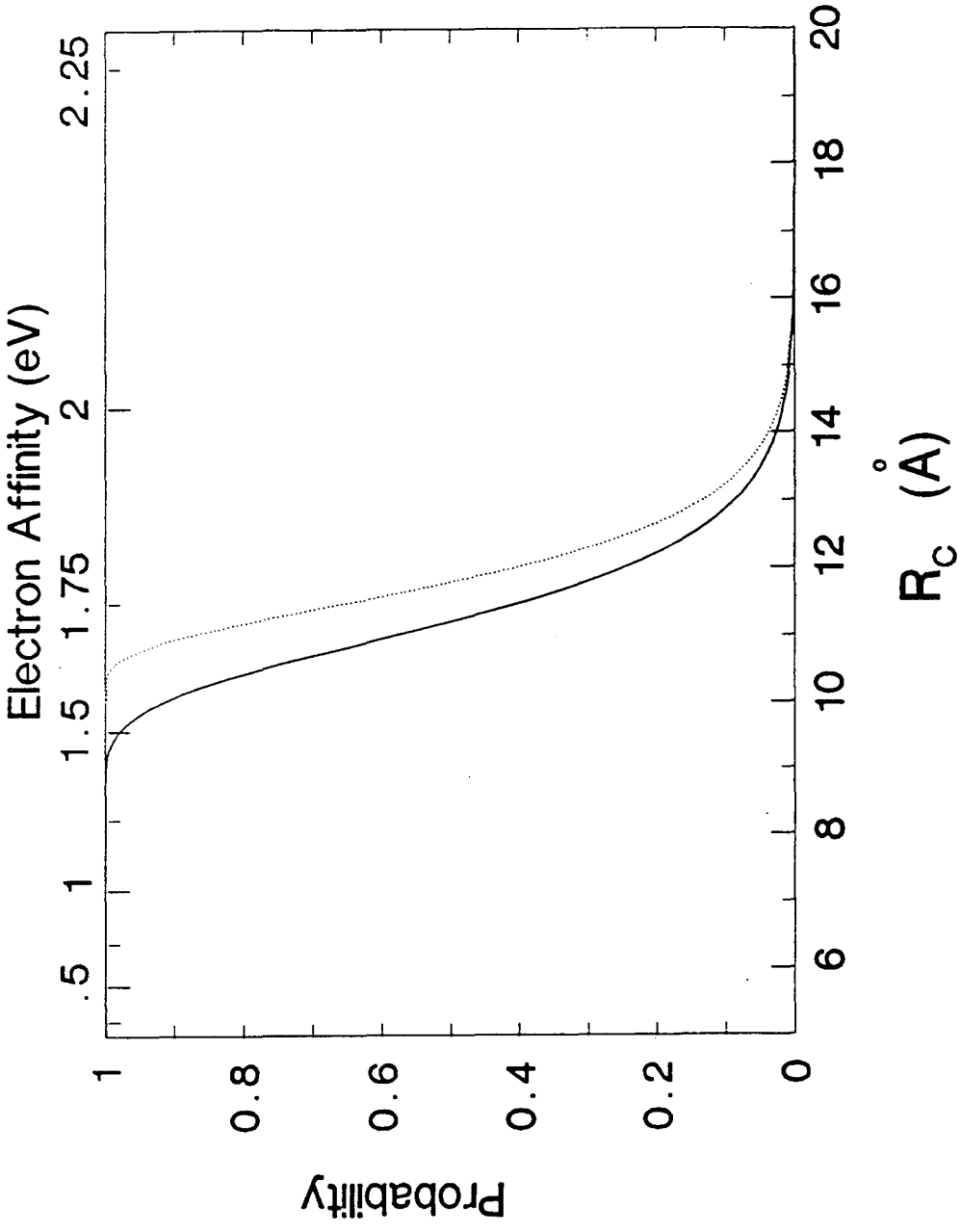
Electron Affinity (eV)
.5
1
1.5
1.75
2
2.25
Probability
1
0.8
0.6
0.4
0.2
0
6
8
10
12
14
16
18
20
R_C (Å)

Figure IV-6

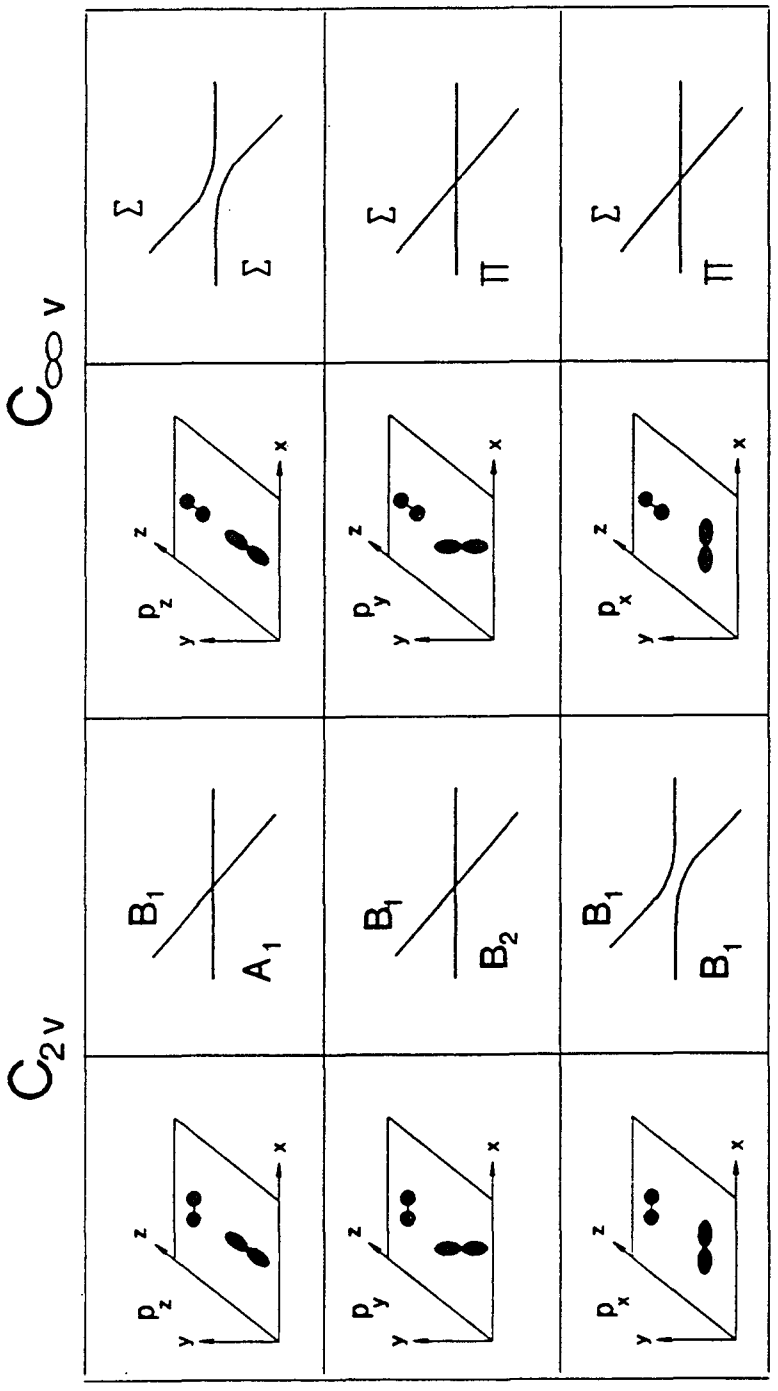

Figure IV-7

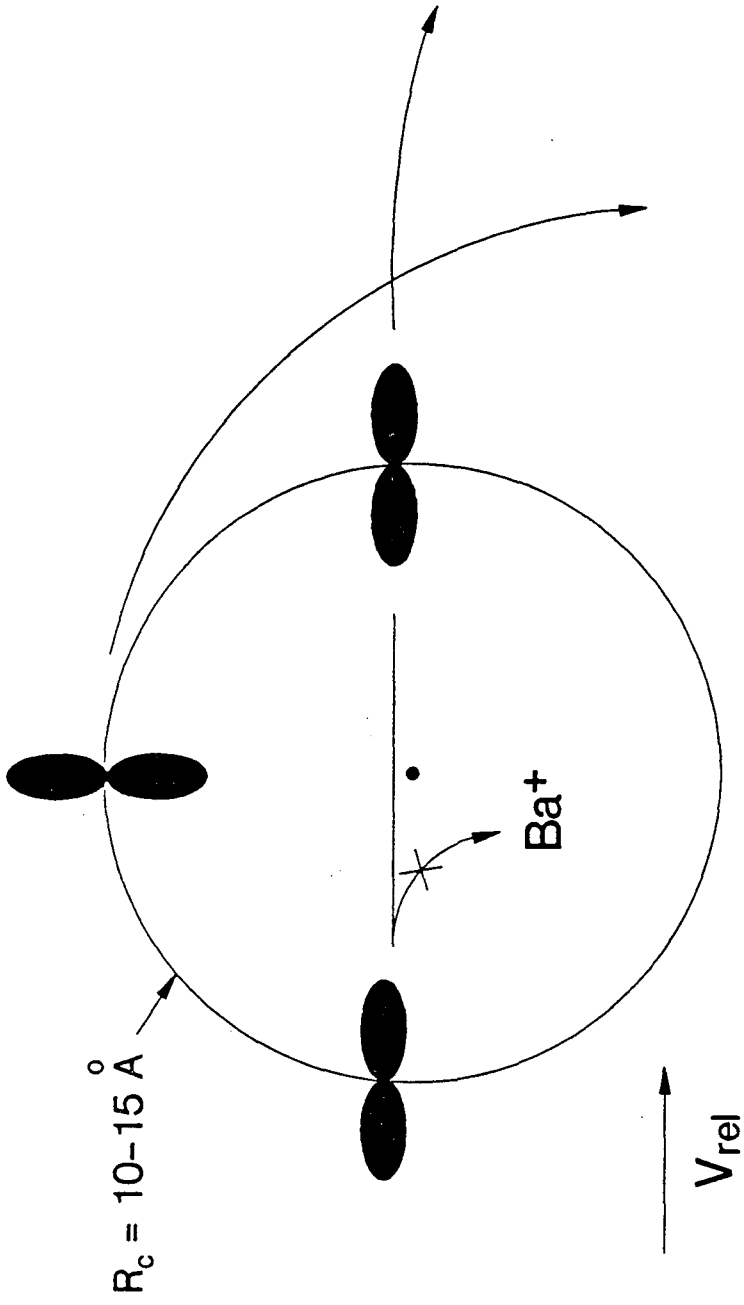

Figure IV-8

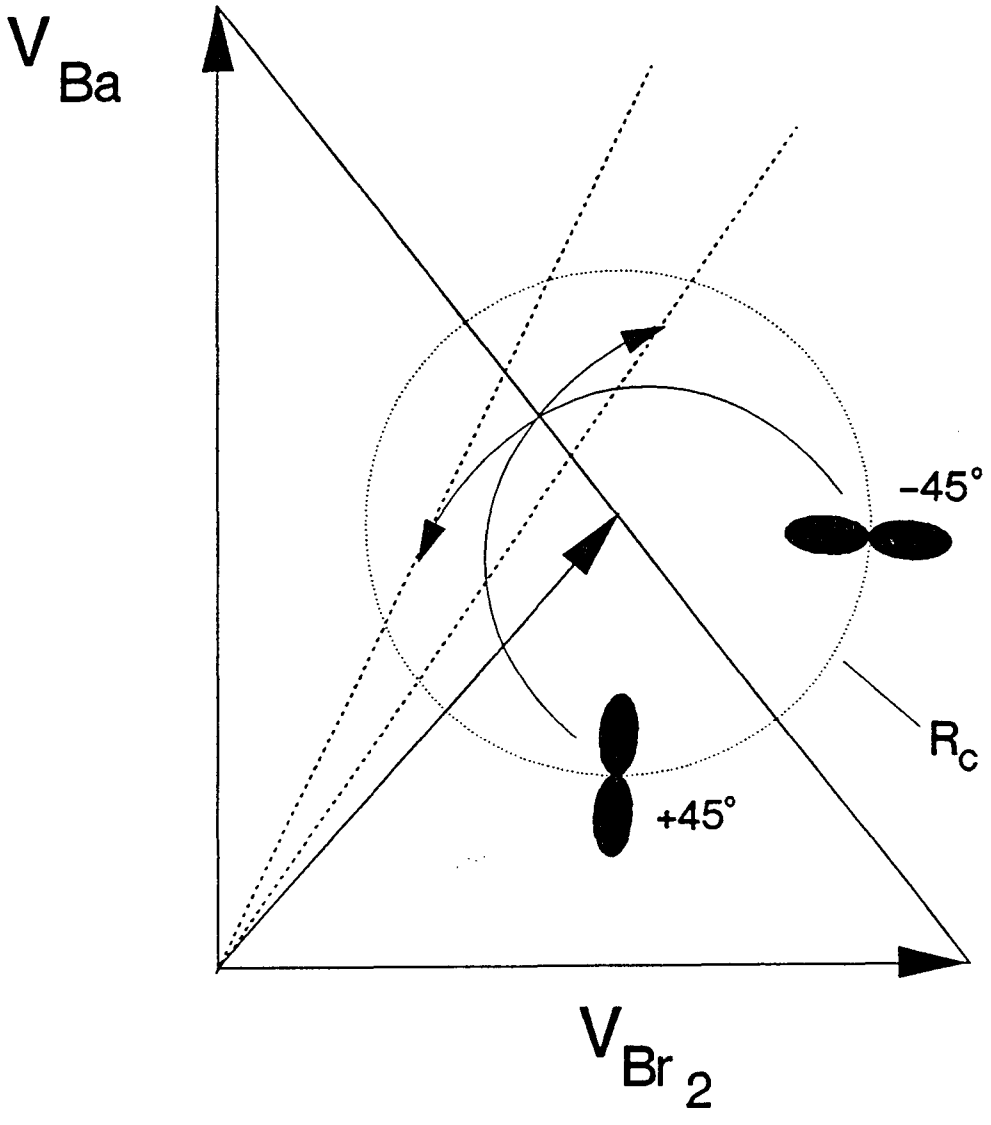

Figure IV-9

Chapter V: Reaction Dynamics from Orbital Alignment Dependence and Angular Distributions of Ions Produced in Collision of $Ba(^1P_1)$ with NO_2 and O_3.

A. Introduction

The reactions of ground state barium with ozone and NO_2 are tremendously exothermic process yielding both ground state and electronically excited products.[1-3] Owing to the high yield of chemiluminescent BaO^*, the reactions were extensively studied in the early 70s as possible media for a visible-wavelength laser.[4-7] Although the predominance of ground state products eventually dissolved the dreams of a barium chemical laser, these reactions have proved to be a fruitful source of insight into the reaction dynamics of divalent systems.

Studies of the neutral products from reaction of $Ba(^1S_0)$ with ozone and NO_2 in our laboratory have shown that, despite the large exoergicity (> 4 eV), the ground

state reaction involves a long-lived (several rotational periods) collision complex. A direct reaction, probably responsible for the electronically excited states of BaO, is also observed.[8] In addition, from the ozone reaction we reported the first gas phase observation of BaO_2, which appeared to result exclusively from long-lived $Ba\text{-}O_3$ complexes. The maximum BaO_2 translational energy release yielded a lower bound of 120 kcal/mole for the $Ba\text{-}O_2$ bond energy, implying very large reaction exoergicities (-4.42 eV) for this channel as well.[9] The existence of a long-lived complex despite the presence of these exoergic product channels implies a substantial barrier to its decay. This is also suggested by the translational energy distributions which are observed to peak away from zero. At higher translational energy the novel product BaNO was observed from the NO_2 reaction, though its forward-sideways scattered angular distribution indicated a direct reaction in that case. In general, these reactions are initiated by long-range electron transfer yielding the singly ionic complexes $Ba^+\text{-}O_3^-$ or $Ba^+\text{-}NO_2^-$. However, both ground state BaO and BaO_2 are thought to be well represented as doubly ionic species[25]. The production of ground state products from the initially formed complex requires substantial electronic rearrangement. The long lived complexes thus probably result from a barrier to the transfer of the second electron. The structure of these complexes and the dynamics of their decay remain interesting unanswered questions.

Excitation to the $Ba(^1P_1)$ electronic state adds an additional 2.1 eV to the system. As discussed in Chapters III and IV, this results in the occurrence of the first

intersection of the ionic and covalent potential energy surfaces at very long range. The vertical electron affinity of O_3 is 2.1 eV[10], implying an outer crossing distance of 14.8 Å. The inner crossing, corresponding to the transfer of the barium s electron, occurs at just 4.0 Å. At the outer crossing, the coupling between the diabatic surfaces is considerably weakened[11-14] so that nonadiabatic transitions become increasingly important, just as has been discussed in Chapter III for Br_2. In Chapter III the dependence of chemiionization cross sections and angular distributions on alignment of the barium p orbital was used to explore the full geometry of reaction in the case of Br_2. For ozone, the additional energy and increased complexity of the system allow for a range of ionic product channels, and these provide a valuable opportunity for the study of reaction dynamics involving many electronic potential energy surfaces and possible product channels. Furthermore, the energy dependence of the relative cross sections may be used in conjunction with the alignment dependences and angular distributions of the various chemiion channels to provide a complete picture of the underlying dynamics, despite the inherent complexity of the system. Some of the results will provide insight into the direct components of the neutral reaction channels as well.

Values for several thermodynamic quantities result directly or indirectly from these studies. For example, appearance thresholds may be used in conjunction with known bond energies to obtain lower limits for ionization potentials. In addition to reaction with ozone, the associative ionization reaction with O_2 was studied to obtain a

threshold for BaO_2^+ formation. This value is of some importance in considering the fate of Ba^+ in the atmosphere,[15] as well as having direct bearing on the thermodynamics of the ozone reaction.

The chemiion channels in reaction of $Ba(^1P_1)$ with O_3 and NO_2 show many remarkable similarities; in fact the results are almost identical except where the different thermodynamics dictate obvious differences. As a result, we have chosen to focus our study on O_3, where the extra exoergicity affords stronger ion signal. We will present some results for NO_2, however, to document the parallel behavior and to facilitate a discussion of this somewhat surprising result.

B. Results

Positive ions resulting from reaction of $Ba(^1S_0)$ and $Ba(^1P_1)$ with ozone were studied as a function of scattering angle, orbital alignment and collision energy. At a nominal collision energy of 1.1 eV, only BaO_2^+ and BaO_3^+ were observed from the ground state reaction, and both were very weak. However, from the excited state reaction at this collision energy all barium containing positive ions were observed: Ba^+, BaO^+, BaO_2^+, and BaO_3^+. Laboratory angular distributions were measured for all of these products of the excited state reaction. In addition, for Ba^+ and BaO^+, dependence of the cross sections on alignment on the barium p orbital was measured

at several laboratory angles. The signal intensity for BaO_2^+ and BaO_3^+ was too low to provide useful alignment dependences.

1. Thresholds for BaO_2^+ and BaO_3^+ formation

A threshold for the appearance of BaO_2^+ was obtained in studies of the ground state associative ionization reaction of barium with molecular oxygen. No BaO_2^+ was observed at a nominal collision energy of 0.9 eV. At 1.5 eV, the reaction was observed, very weakly, at the center of mass angle. This threshold is substantially higher than the only previously reported value,[16] 0.2 eV, and possible sources of the discrepancy will be considered in the discussion.

The threshold for associative ionization of ground state Ba with O_3 could be fixed at a collision energy of 1.2 ± 0.1 eV because the BaO_3^+ signal appeared as the O_3 concentration of the O_3/He beam was lowered, i.e., as the O_3 beam velocity was increased slightly. This implies that the collision energy was very near threshold.

2. Orbital Alignment Dependence and Angular Distributions at 1.1 eV

a. Ba^+

The Newton diagram for collision of Ba with O_3 at 1.2 eV collision energy is shown in Figure 1. The analogous Newton diagram for NO_2, not shown, is almost identical. Angular distributions of Ba^+ from reaction of $Ba(^1P_1) + O_3$ are shown in Figure 2. The two scans represent alignment of the p orbital in the collision plane and either along or perpendicular to the relative velocity vector. These angular distributions are quite reminiscent of the those obtained for Ba^+ from reaction with Br_2 presented in Chapter IV. Both distributions in Figure 2 are largely forward of the center of mass, and the result for perpendicular alignment is substantially higher in intensity. In addition, the perpendicular distribution shows a larger contribution from angles behind the center of mass.

The dependence of scattered Ba^+ signal on alignment of the Ba p orbital is shown for in-plane rotation of the laser polarization in Figure 3 for reaction with O_3. These polarization scans are shown along with the fluorescence intensity which was recorded simultaneously. Both are fit by the expression:[17]

$$I(\beta) = \frac{(I_{max} + I_{min})}{2} + \frac{(I_{max} - I_{min})}{2} \cos 2(\beta - \beta').$$

This yields values for $(I_{max}-I_{min})/I_{min}$ and β', which are presented in Table 1 for the data of Figure 3. A definite trend is evident in β', which ranges from 47° at the rearmost angles to ~110° for the most forward scattered Ba^+. The ratio $(I_{max}-I_{min})/I_{min}$ shows a trend as well, reaching a value of 2.2 at the back angles and dropping to .14 at 7.5°. In-plane alignment dependence for Ba^+ from reaction with NO_2 is shown at laboratory angles of 15° and 20°, along with the corresponding O_3 results, in Figure 4. Although the polarization effect appears weaker in the NO_2 case, the experiments were performed under somewhat different conditions so that it would be difficult to draw conclusions from the relative magnitude of the effect. But the location of the alignment peak, β', is nearly identical for the two molecules at both angles.

Results for out-of-plane rotation of the barium p orbital are shown in Figure 5 for O_3. These represent a striking contrast to the out-of-plane results for Ba^+ from reaction with Br_2. Figure 5 reveals substantial variation of the peak orbital alignment angle with laboratory scattering angle, while the Br_2 result showed a strong preference for in-plane alignment of the p orbital independent of scattering angle. Table 2 lists the magnitude of the polarization effect, $(I_{max}-I_{min})/I_{min}$, and the location of the polarization peak (Θ') for the out-of-plane results of Figure 5. Shown in Figure 6 are

several out-of-plane alignment scans of Ba^+ from reaction with NO_2 in which the laser was directed 45° from the barium beam, only ~10° from the relative velocity vector. These all thus represent collisions in which the orbital is nearly perpendicular to the relative velocity vector, but the alignment with respect to the scattering plane is varied. The forward angles favor ~30° inclination of the orbital out of the scattering plane, in the direction of the detector. The back angles favor a ~45° tilt out of the scattering plane, in the opposite direction. Analogous measurements were not made in the case of O_3.

b. BaO^+

The angular distribution of BaO^+ from the reaction of $Ba(^1P_1)$ with O_3 is shown in Figure 7 for in-plane ($\beta = 35°$) and out-of-plane alignment of the p orbital. These distributions show several important differences from the Ba^+ result. The out-of-plane orbital alignment dominates at most angles, quite the reverse of what is observed for Ba^+. In addition, although the BaO^+ is seen to peak somewhat forward of the center of mass angle, nearly 50% of the distribution results from angles behind the center of mass.

Figure 8 shows the orbital alignment dependence recorded for BaO^+ for out-of-plane rotation of the p orbital at laboratory angles 10 and 15 degrees. The BaO^+ appears somewhat favored by out-of-plane alignment of the orbital, with little

difference on going from 10° to 15°. β for the analogous Ba^+ result shifted ~90° between these two angles. The angular distributions of Figure 7 further suggest little change for other scattering angles.

c. BaO_2^+,BaO_3^+

The laboratory angular distribution of BaO_3^+ from reaction of $Ba(^1P_1)$ with O_3 is presented in Figure 9. Because the associative ionization product BaO_3^+ is recoiling from an electron, with less than $1/10^5$ its mass, conservation of momentum requires that it appear in the vicinity of the center of mass angle.

Because associative ionization reaction with O_2 contamination of the O_3 beam was found to yield an unacceptable background BaO_2^+ signal, the BaO_2^+ channel was studied using purified O_3 as described in Chapter II. These conditions resulted in a slightly higher collision energy (1.23 vs. 1.1 eV) and a shift in the location of the center of mass from ~15° to ~17°. The BaO_2^+ appears slightly forward scattered, with none of the tail which was associated with the BaO^+ distribution.

3. Energy dependence of the relative cross sections.

Angular distributions were obtained for Ba^+, BaO^+, BaO_2^+ and BaO_3^+ products at 4 collision energies: 0.7, 0.9, 1.2 and 1.9 eV. The angular distributions were

integrated and scaled by the relative barium beam flux (obtained from the fluorescence intensity and beam velocities) to explore the energy dependence of the relative cross sections. These angular distributions were all performed using purified liquid ozone, so that O_2 contamination was minimal. No attempt was made to obtain center of mass distributions, so the integrated intensities are uncorrected for the LAB→CM transformation Jacobian. In cases in which a portion of the forward distribution was too close to the barium beam to be measured, its contribution was estimated and included. This results in relative cross sections accurate to within perhaps a factor of three between ions and significantly better for the energy dependence of a given ion. Figure 11 shows the trends which emerge from these measurements. In Figure 11a, the integrated intensities are all plotted on the same scale so that their relative magnitudes may be gauged. In Figure 11b, the same data is rescaled as indicated so that the nature of the energy dependence of the weaker channels may be discerned.

The most striking feature of Figure 11 is the obvious parallel between the behavior of Ba^+ and BaO_2^+, despite the fact that the cross sections differ by nearly two orders of magnitude. The strong increase with collision energy suggests nonadiabatic behavior. In fact the result for Ba^+ is not unexpected considering the results for ion pair formation in alkali metal-halogen molecule collisions discussed in Chapter III.[30] But the similarities indicate that Ba^+ and BaO_2^+ are indeed very closely related channels.

The BaO^+ results, however, clearly imply a different origin. The energy dependence suggests a barrier with little change in cross section at energies beyond the threshold region. This is similar to the behavior seen for BaO_3^+, but for the latter, the barrier probably represents simply the endoergicity of the associative ionization process.

C. Discussion

1. Thresholds for BaO_2^+ and BaO_3^+ formation

The thermodynamic quantities obtained above are presented in Figure 12, along with established values for a variety of the reactions considered. The previously reported value[16] of 0.2 eV for the threshold for BaO_2^+ formation in Ba-O_2 collisions was obtained in an experiment in which a sputtered Ba beam, containing kinetic energies in the range from thermal to >100 eV, was crossed by a supersonic O_2 beam. The threshold was obtained from the maximum scattering angle observed, which was assumed to correspond to the center of mass angle of the slowest reacting Ba atoms. The O_2 beam velocity was not measured, and its angular and velocity spreads were neglected in obtaining the threshold. Unfortunately, owing to the strategy of obtaining the barium beam velocity from the center of mass angle, an error in the O_2 beam velocity would result in an relative error of magnitude (O_2 velocity error)^2 in the value

of the threshold. Although a number of the assumptions employed are somewhat crude, it is nevertheless difficult to explain the large difference between the previously reported 0.2 eV and our 1.3 eV thresholds. The question of O_2 dimers was not discussed in the previous work, and perhaps this is the source of the discrepancy. The O_2 velocity given (740 m/s) implies a room temperature nozzle, which would certainly result in the formation of dimers. If dimers were responsible for the maximum scattering angle (taken to be 8°) this would imply a threshold for $Ba + (O_2)_2 \rightarrow BaO_2^+ + O_2^-$ or $BaO_2^+ + O_2 + e^-$ of 1.48 eV, more in line with our result. Further support for the higher value comes when considering the implications for the ionization potential of BaO_2. We previously obtained a value of 5.2 ± 0.5 eV for $D_o(Ba\text{-}O_2)$.[27] Assuming that the thresholds derive from the fastest components of our beams, a 10% spread in beam velocity suggests an appearance energy for $Ba + O_2 \rightarrow BaO_2^+ + e^-$:

$$1.0 < E_{th} < 1.7 \text{ eV} .$$

When combined with the value for the bond energy given above, this implies

$$6.2 \pm 0.5 \text{ eV} < \text{I.P. } BaO_2 < 6.9 \pm 0.5 \text{ eV} .$$

The corresponding value given the previously reported BaO_2^+ threshold is only 5.4 eV, only slightly higher than the ionization potential of atomic barium. The ionization potential of BaO has been fixed in several experiments at 6.9 ± 0.2 eV. It seems reasonable, particularly given the strong BaO_2 bond, that the ionization potentials of the two species, BaO and BaO_2, should be comparable. Owing to the weakness of the BaO_2^+ signal observed from ground state reaction with O_2 even at 1.5 eV collision

energy, we suggest that the actual threshold is nearer the higher energy, and recommend a value of 6.7 ± 0.5 eV for the ionization potential of BaO_2.

The threshold obtained for BaO_3^+ from ground state Ba reaction with O_3 may be used to estimate the Ba-O_3 binding energy. BaO_3 has not been directly observed in the gas phase before, but the existence of long-lived complexes in Ba-O_3 reactions implies a substantial bond energy. If Ba-O_3 is assumed to be a single electron ionic bond, then the ionization potential of BaO_3 should, like BaBr, be somewhat lower than that of atomic barium (5.1 eV); for BaBr the value is 4.8 eV. This yields a value for the bond energy of Ba-O_3:

$$D_o(Ba\text{-}O_3) = IP_{BaO3} - E_{thr}$$

$$= 4.8 \pm 0.2 - 1.2 \pm 0.1 \quad = 3.6 \pm 0.3 \text{ eV}$$

$$= 82 \pm 7 \text{ kcal/mole.}$$

This provides the estimated location of the neutral BaO_3 shown in Figure 12.

2. Ba^+

The angular distributions and in-plane orbital alignment dependence for Ba^+ shown in Figures 2 and 3 reproduce the qualitative features of the Br_2 results quite well, so we will draw heavily on the discussion of Chapter IV. In the bromine reaction two configurations were thought to be favorable for electron transfer owing to a conical intersection[18] of the potential energy surfaces: for broadside collisions (C_{2v}),

charge transfer is favored by perpendicular alignment in the body-fixed frame while for collinear collisions ($C_{\infty v}$), parallel alignment favors electron transfer. A strong dependence of electron transfer probability on orbital alignment and internuclear geometry thus results. The tendency to forward scattering exhibited by the parallel orbital alignment was ascribed to the importance of the covalent trajectories, those for which the ion pair is produced in electron transfer transition on exit, in ion production from low impact parameter collisions. Small impact parameter collisions were thought to favor the neutral channel or the chemiion channel yielding $BaBr^+$ and Br^-. The tendency to sideways- or less forward-scattered distributions for perpendicular orbital alignment indicated the overall importance of large impact parameter collisions. This is a consequence of the greater statistical weight associated with such collisions as well as the increased likelihood for electron transfer resulting from the prolonged excursion through the crossing region for these trajectories. The results for out-of-plane polarization rotation were interpreted assuming that initial and final orbital angular momenta were roughly equal. The fact that Ba^+ was favored by alignment of the orbital in the scattering plane independent of scattering angle strongly suggested that large impact parameter collisions were dominant. Collisions in which the orbital was aligned perpendicular to the plane resulted in scattering out of the plane of the detector. Even though those collisions favored ion production, the resulting ions were not detected. The evidence thus indicated that the initially prepared Π orbital alignment (the p orbital perpendicular to the relative velocity vector) corresponded to a Σ

configuration (in the molecular frame) at the crossing seam, and the reaction was dominated by large impact parameter collisions.

For $Ba(^1P_1)$ collision with O_3 and NO_2 the problem is vastly more complex, yet similarities between the in-plane alignment results for all three systems indicate that the solution may be simpler than the problem. Analogy with the bromine result suggests that here, too, Ba^+ production is favored from large impact parameter collisions in which the orbital is directed in toward the molecule at the crossing point. Considering C_{2v} geometry, in the case of NO_2 electron transfer from the barium atom fills the $6A_1$ orbital, resulting in a Ba^+-NO_2^- complex of overall A_1 symmetry. For ozone, this orbital is already filled, so the first electron must enter the $2B_1$ orbital. In both O_3 and NO_2 there exist excited states of the anion, but these are considerably higher in energy hence are unlikely to be important here. Nevertheless at first it might seem puzzling that, although the symmetries of the relevant orbitals are entirely different, O_3 and NO_2 show apparently identical behavior. But in fact the overall symmetry of the problem has been greatly reduced. Genuine C_{2v} collisions are exceedingly rare and of negligible importance for this atom-triatom system. The similarities between O_3 and NO_2 indicate that the dominant geometries favoring electron transfer do not even achieve C_s configuration, otherwise some distinction between them would be expected to appear. It seems reasonable to suggest that the reason for the importance of the Σ orbital alignment (in the body-fixed frame) is that

the electron density is closer to the molecule and effective interaction can occur for a wide range of internuclear geometries.

The notable distinction between results for Br_2 and the triatomics appears in the out-of-plane alignment effects. As mentioned above, for bromine the Ba^+ intensity peaked with the orbital in the plane regardless of scattering angle. This actually supports the assumption that initial and final nuclear orbital angular momentum vectors are parallel, otherwise some variation with laboratory angle or some deviation from in-plane peaking would be anticipated. The out-of-plane results for O_3 and NO_2 indicate that this assumption is no longer valid. The reduced symmetry of the collision and the likelihood of rotational excitation resulting from exit channel interaction between the nascent ions both argue for some difference between **L** and **L'**. Furthermore, the lowered symmetry may imply greater sensitivity of the electron transfer to the precise alignment of the orbital; indeed the magnitude of the alignment effect bears witness to this. The out-of-plane alignment results, even for the data of Figure 6, are not strictly perpendicular (nor parallel) to the relative velocity vector. Unfortunately this inhibits any attempt at a direct quantitative interpretation of these results.

Both the in-plane and out-of-plane alignment dependences for Ba^+ in the O_3 reaction show a rather sudden change in the location of the peak of the polarization dependence, and it occurs in the vicinity of the center of mass. This suggests that the regions where the covalent trajectories dominate, in the forward scattered flux, may be

fairly well isolated from the dominant large impact parameter collisions whose scattering shows a strong Coulombic deflection. This is just what is seen in the alkali metal-halogen collisions at high energies.

3. BaO_2^+

Ozone exhibits two resonances in dissociative electron attachment: at zero energy there is a resonance producing O^- and O_2, and at 0.4 eV another resonance yielding O_2^- and O.[19] The zero energy resonance implies that the electron affinity exceeds the O^--O_2 binding energy, and a number of measurements bear this out.[10,20,21] The adiabatic electron affinity of O_3 is well established at 2.1 eV, while several measurements have placed the O^--O_2 bond energy at 1.8 eV. The higher threshold for the appearance of O_2^- is a consequence of the lower electron affinity of O_2 (0.43 eV) versus O (1.45 eV). The existence of the zero energy resonance indicates that electron transfer is likely to produce highly excited O_3^-. Electron transfer from a barium atom to ozone will not result in this 2.1 eV being available for dissociation of the ozonide ion since, in effect, it has been harnessed to ionize the barium atom in the first place. Nevertheless, the O_3^- will be formed in a repulsive region of the potential energy surface, and dissociation in the field of the barium ion will be quite facile. The resulting fragments may subsequently interact with the departing Ba^+. For low impact parameter collisions, this will generally result in the formation of neutral products BaO

and O_2, since the ion pairs will exhibit a strong attraction for each other. For certain favorable collision geometries and large impact parameter collisions, however, the departing Ba^+ may encounter the neutral O_2 fragment from the dissociating O_3^-. Our value for the BaO_2^+ appearance threshold implies a substantial 90 kcal/mol Ba^+-O_2 bond energy, and the R^{-4} ion-induced dipole potential allows for fairly long range Ba^+-O_2 interaction. This picture is suggested by the strong parallels which appear in the Ba^+ and BaO_2^+ channels. Although the BaO_2^+ shows some tendency to forward scattering reminiscent of the Ba^+, the remarkably similar energy dependences shown by these two channels provides the most convincing evidence. The relative weakness of the BaO_2^+ signal, lower in intensity than Ba^+ by a factor of 100, is not surprising given the expected rarity of effective secondary encounters. Secondary interaction between Ba^+ and O^- is much more likely owing to the Coulomb attraction between them, but the result of this will be a contribution to the neutral BaO signal which would be very difficult to detect against the large BaO background from the ground state reaction. The BaO_2^+ thus can be thought of as deriving directly from the dominant Ba^+ channel through those relatively rare collisions in which the departing Ba^+ encounters an O_2 fragment from the dissociating O_3^-. In fact, this BaO_2^+ represents additional evidence for the importance of large impact parameter collisions in the Ba^+ channel, its parent. For low impact parameter collisions, the neutral products would certainly dominate and no BaO_2^+ would be expected.

4. BaO^+

The results for BaO^+ from reaction of $Ba(^1P_1)$ with O_3 are unlike the other ion channels in every respect. The out-of-plane orbital rotation scans of Figure 8 favored perpendicular alignment apparently independent of scattering angle. Furthermore, this was the only ion channel in these studies to feature a significant backscattered contribution in its laboratory angular distribution. Finally, the energy dependence showed a threshold at about 0.9 eV, and little change in cross section was observed at energies above this. Both the angular distributions and the insensitivity of the out-of-plane alignment results to scattering angle suggest a larger role for low impact parameter collisions in this case. However, the nature of the alignment dependence indicates that the BaO^+ results preferentially from collisions which avoid electron transfer at the outer crossing. We have argued that in general low impact parameter collisions will favor the formation of neutrals, owing to the opportunity for strong interaction between nascent ions and the fact that the neutral channels are far more exoergic. These considerations hint that the BaO^+ may in fact derive from the neutral BaO channel. This suggests the following model for the formation of BaO^+ in $Ba(^1P_1)$-O_3 collisions: for those collisions which avoid electron transfer at the outer crossing, electron transfer at the second crossing results in the formation of electronically excited BaO^* and O_2.[9] A substantial fraction of the BaO may be formed with sufficient internal energy to undergo vibrational autoionization yielding BaO^+ +

e^-. Results for neutral BaO from the ground state reaction showed translational energy distributions peaking at only ~0.5 eV despite 6 eV available energy. Although much of this is probably tied up in electronic and rotational energy of the products, the BaO is likely to be highly vibrationally excited as well. Although low impact parameter collisions may be more important for BaO^+ formation, probably a consequence of the increased probability for nonadiabaticity at the outer crossing, the angular distributions nevertheless indicate substantial forward scattering as well. Large impact parameter collisions may result in neutrals from a stripping mechanism[9] yielding highly vibrationally excited BaO, so these may also be important in BaO^+ formation.

D. Conclusions

Angular distributions, energy dependence of the relative cross sections and orbital alignment effects have been used to explore the reaction dynamics for chemiion channels in collisions of electronically excited barium with O_3 and NO_2. The general features for the Ba^+ from collision with both triatomics resembles that from the $Ba(^1P_1)$-Br_2 reaction presented in Chapter III: the product is generally forward or forward-sideways scattered, with the latter favored by the dominant perpendicular alignment of the p orbital with respect to the relative velocity vector. However, the out-of-plane alignment results show a strong dependence on scattering angle, quite unlike the results for the Br_2 reaction. This is probably a consequence of the reduced

symmetry of the collision for the triatomics and the inequality of initial and final nuclear orbital angular momentum. The parallels between the results for Ba^+ from O_3 and NO_2 suggest that the symmetry of the available orbital in the isolated molecule is not important in determining the probability for electron transfer at the outer crossing of the potential energy surfaces. Rather electron transfer appears simply to be favored for large impact parameter collisions in which the orbital is directed toward the molecule.

The BaO_2^+ from the O_3 reaction exhibits angular distributions and energy dependences which are quite reminiscent of the Ba^+ albeit two orders of magnitude lower in intensity. This, in conjunction with the threshold for BaO_2^+ formation, indicate that it derives from the Ba^+ channel as a consequence of those collisions in which the departing Ba^+ encounters a dissociating O_2 fragment.

Important differences in the dynamics for the BaO^+ channel are suggested in the angular distributions, which show a substantial backscattered component, as well as the alignment effects and energy dependence. These are used to suggest that the BaO^+ probably derives from neutral BaO^* which is sufficiently internally excited to undergo vibrational autoionization.

The profound sensitivity of these nonadiabatic channels to the factors governing electron transfer probability at intersections of the electronic potential energy surfaces allow for detailed insight into the underlying reaction dynamics. Thus, despite the complexity of the atom-triatom collision and the tremendous energies

available in these reactions, the use of orbital alignment dependences in combination with the traditional crossed beam measurements of angular distributions and energy dependences, allows the complete picture of the reaction to emerge.

References

1. C. H. Ottinger and R. N. Zare, Chem. Phys. Lett. **5**, 243 (1970).
2. C. D. Jonah, R. N. Zare and C. Ottinger, J. Chem. Phys. **56**, 263 (1972).
3. A. Schultz and R. N. Zare J. Chem. Phys. **60**, 5120 (1974).
4. J. I. Steinfeld, ed., **Electronic Transition Lasers**, (MIT Press, Cambridge, Massachusetts, 1975).
5. C. R. Dickson, S. M. George and R. N. Zare, J. Chem. Phys. **67**, 1024 (1977).
6. J. J. Reuther and H. B. Palmer, J. Chem. Phys. **76**, 83 (1982).
7. Y. C. Hsu and J. G. Pruett, J. Chem. Phys. **76** 5849 (1981).
8. H. F. Davis, A. G. Suits and Y. T. Lee, Ber. Bunsenges. Phys. Chem. **94**, 1193 (1990).
9. H. F. Davis, A. G. Suits and Y. T. Lee, manuscript in preparation.
10. S. E. Novick, Paul C. Engelkin, P. L. Jones, J. H. Futrell and W. C. Lineberger, J. Chem. Phys. **70**, 2652 (1979).
11. R. K. Janev, Adv. At. Mol. Phys. **12**, 1 (1976).
12. E. A. Gislason and J. G. Sachs, J. Chem. Phys. **62**, 2678 (1975).
13. R. E. Olson, F. T. Smith and E. Bauer, Appl. Optics, **10**, 1848 (1971).
14. J. Los and A. W. Kleyn, in **Alkali Halide Vapors**, 189 (Academic Press, New York, 1979) and references.

15. E. Murad, J. Chem. Phys. **77**, 2057 (1982).

16. R. B. Cohen, C. E. Young and S. Wexler, Chem. Phys. Lett. **19**, 99 (1973).

17. W. Reiland, G. Jameison, U. Tittes and I. V. Hertel, Z. Phys. A **307**, 51 (1982).

18. G. Herzberg, **Electronic Spectra of Polyatomic Molecules** (Van Nostrand, Princeton NJ 1967).

19. R. K. Curran, J. Chem. Phys. **35**, 1849 (1961).

20. J. F. Hiller and M. L. Vestal, J. Chem. Phys. **74**, 6096 (1981).

21. C. Lifshitz, R. L. C. Wu, T. O. Tiernan and D. T. Terwilliger, J. Chem. Phys. **68**, 247 (1978).

Table 1: Ba^+ In-Plane Alignment Dependence

Lab Angle	$(I_{max}-I_{min})/I_{min}$	β'
10.0°	.14	108°
12.5°	.79	106°
15.0°	.71	97°
17.5°	2.4	64°
20.0°	2.0	60°
22.5°	2.2	53°
25.0°	.6	47°

Table 1: In-plane alignment dependence for Ba^+ from collision of $Ba(^1P_1)$ with O_3 at 1.1 eV. Values for $(I_{max}-I_{min})/I_{min}$ and β' were obtained from the fits shown in Figure 3.

Table 2: Ba^+ Out-of-Plane Alignment Dependence

Lab Angle	$(I_{max}-I_{min})/I_{min}$	Θ'
7.5°	1.0	81°
10.0°	.40	81°
12.5°	.16	66°
15.0°	.33	148°
17.5°	.29	138°
20.0°	1.6	105°
22.5°	1.6	104°
25.0°	.84	100°

Table 2: Out-of-plane alignment dependence for Ba^+ from collision of $Ba(^1P_1)$ with O_3 at 1.1 eV. Values for $(I_{max}-I_{min})/I_{min}$ and Θ' were obtained from the fits shown in Figure 5.

Chapter V Figure Captions

Figure V-1. Newton diagram for collision of Ba with O_3 at 1.1 eV.

Figure V-2. Laboratory angular distributions of Ba^+ from $Ba(^1P_1)$-O_3 collision at 1.1 eV for perpendicular (diamonds) and parallel (squares) alignment of the p orbital with respect to the relative velocity vector. Lines are drawn to guide the eye.

Figure V-3. Orbital alignment dependence of Ba^+ from $Ba(^1P_1)$-O_3 reaction for in-plane alignment of the p orbital. Laboratory angles are indicated. Also shown is a representative record of the $Ba(^1P_1)$ fluorescence monitored simultaneously.

Figure V-4. Orbital alignment dependence of Ba^+ from $Ba(^1P_1)$ reaction with O_3 (A and B) and NO_2 (C and D) at the indicated laboratory angles for in-plane polarization rotation.

Figure V-5. Orbital alignment dependence of Ba^+ from $Ba(^1P_1)$-O_3 reaction for out-of-plane alignment of the p orbital. Laboratory angles are indicated.

Figure V-6. Orbital alignment dependence of Ba^+ from $Ba(^1P_1)$-NO_2 reaction for out-of-plane alignment of the p orbital, with the laser directed along the 45° crossing of the barium beam. Laboratory angles are indicated.

Figure V-7. BaO^+ laboratory angular distributions for in-plane ($\beta = 35°$) and perpendicular out-of-plane alignment of the p orbital from reaction with O_3 at 1.1 eV.

Figure V-8. Orbital alignment dependence of BaO^+ from $Ba(^1P_1)$-O_3 reaction for out-of-plane alignment of the p orbital. Laboratory angles are indicated.

Figure V-9. Laboratory angular distribution of BaO_3^+ from reaction of $Ba(^1P_1)$ with O_3 at 1.1 eV.

Figure V-10. Laboratory angular distribution of BaO_2^+ from reaction of $Ba(^1P_1)$ with O_3 at 1.2 eV.

Figure V-11. A) Energy dependence of integrated angular distributions for Ba^+ (asterisks), BaO^+ (circles), BaO_2^+ (squares) and BaO_3^+ (triangles). B) The same data as A rescaled: Ba^+(/100) (asterisks), BaO^+(/50) (circles), BaO_2^+(X5) (squares) and BaO_3^+ (X5) (triangles). Lines are drawn to guide the eye.

Figure V-12. Relative energies for electronic ground states of ion and neutral channels for Ba-O_3 reaction. Dotted lines indicate available energy for $Ba(^1P_1)$-O_3 at the 4 collision energies studied.

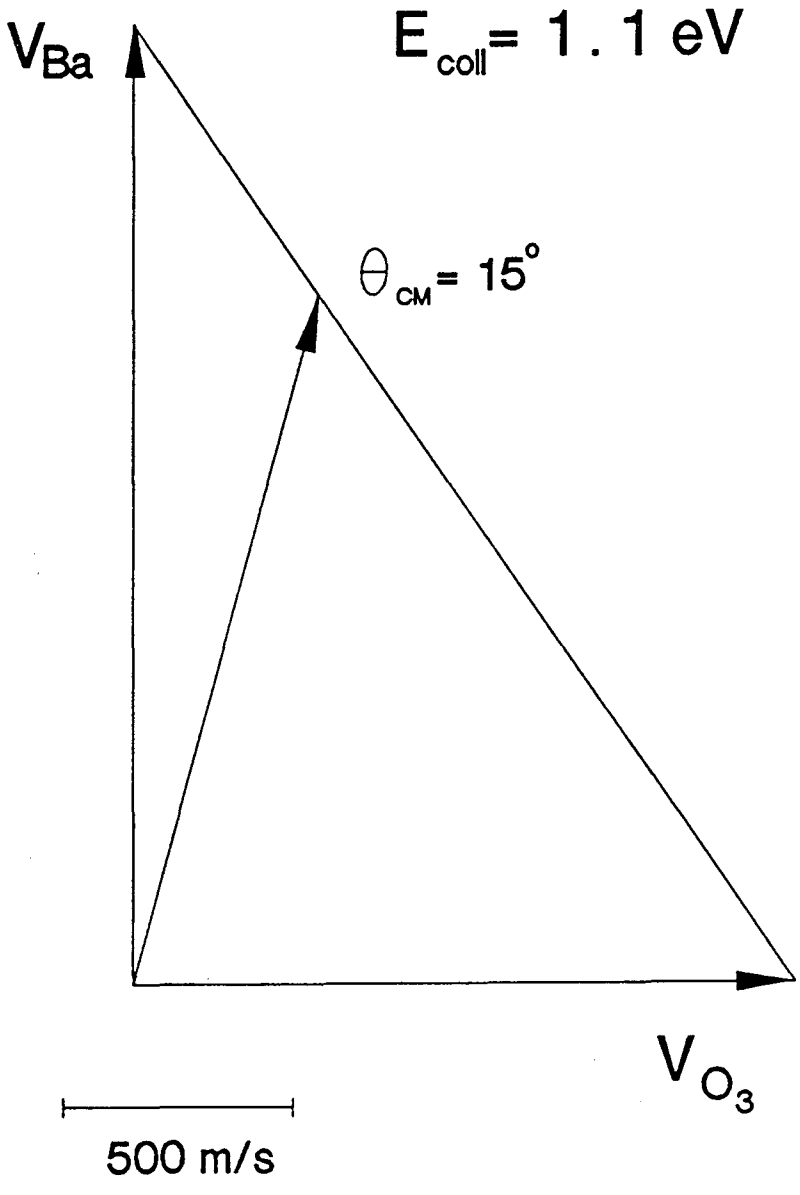

Figure V-1

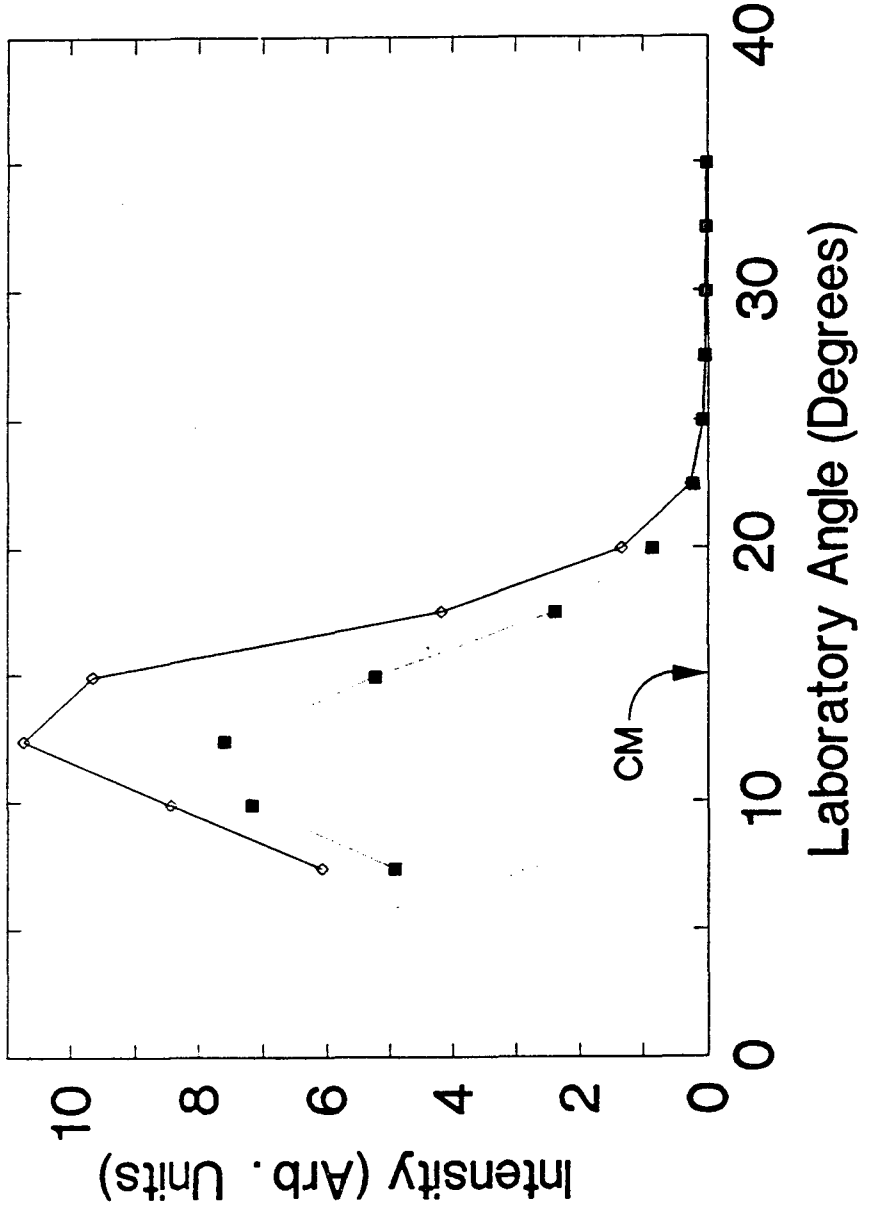
Intensity (Arb. Units)
0
2
4
6
8
10
0
10
20
30
40
Laboratory Angle (Degrees)
CM

Figure V-2

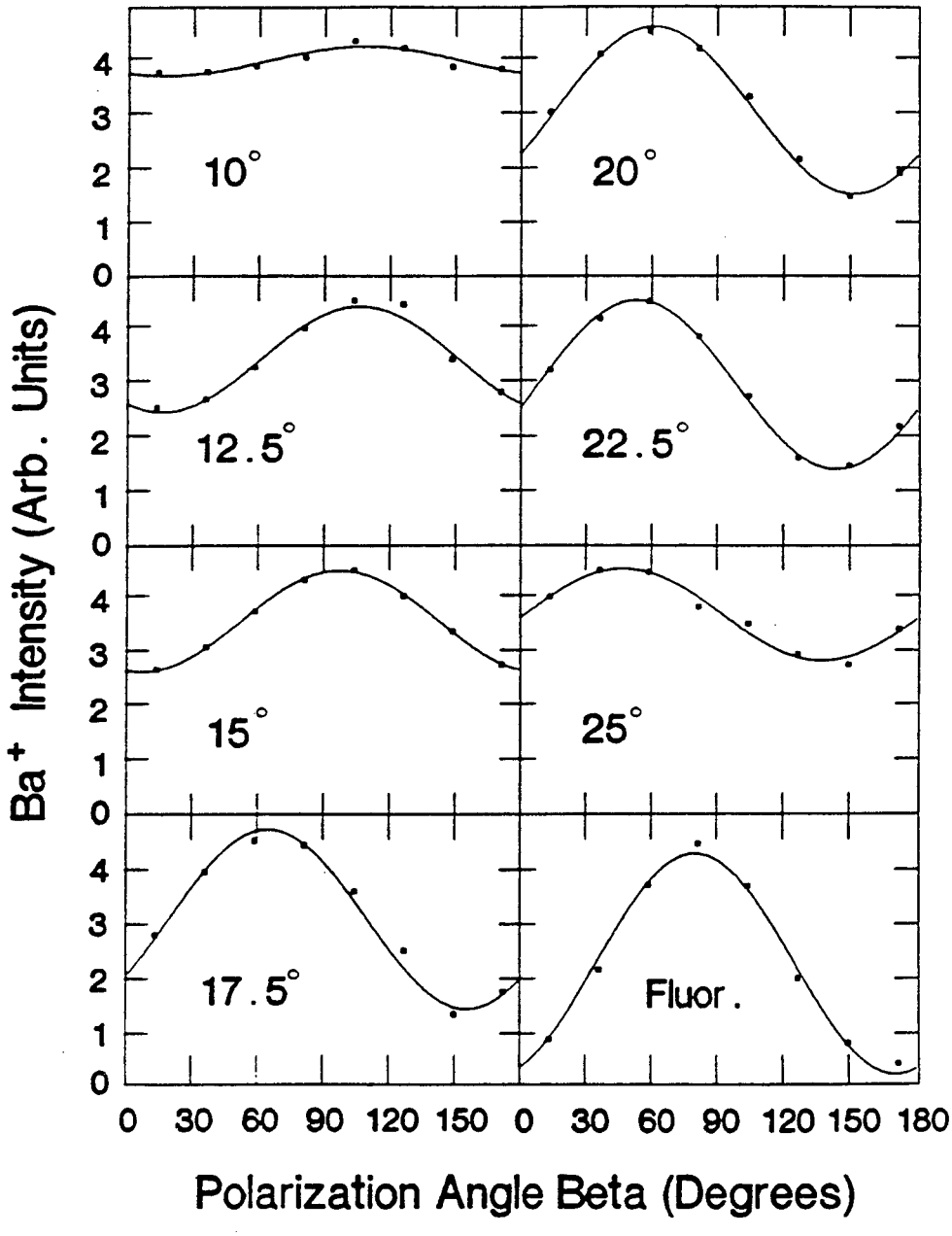
10°
20°
12.5°
22.5°
15°
25°
17.5°
Fluor.
Ba+ Intensity (Arb. Units)
0 30 60 90 120 150 0 30 60 90 120 150 180
Polarization Angle Beta (Degrees)

Figure V-3

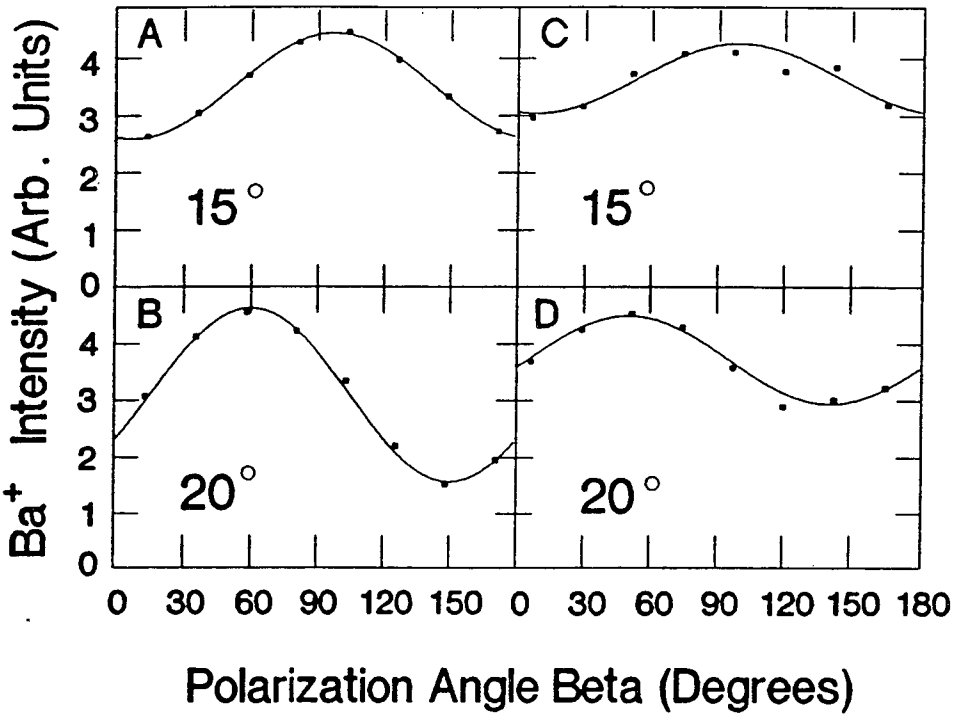
A
C
B
D
15°
15°
20°
20°
Ba+ Intensity (Arb. Units)
0 1 2 3 4
0 30 60 90 120 150 0 30 60 90 120 150 180
Polarization Angle Beta (Degrees)

Figure V-4

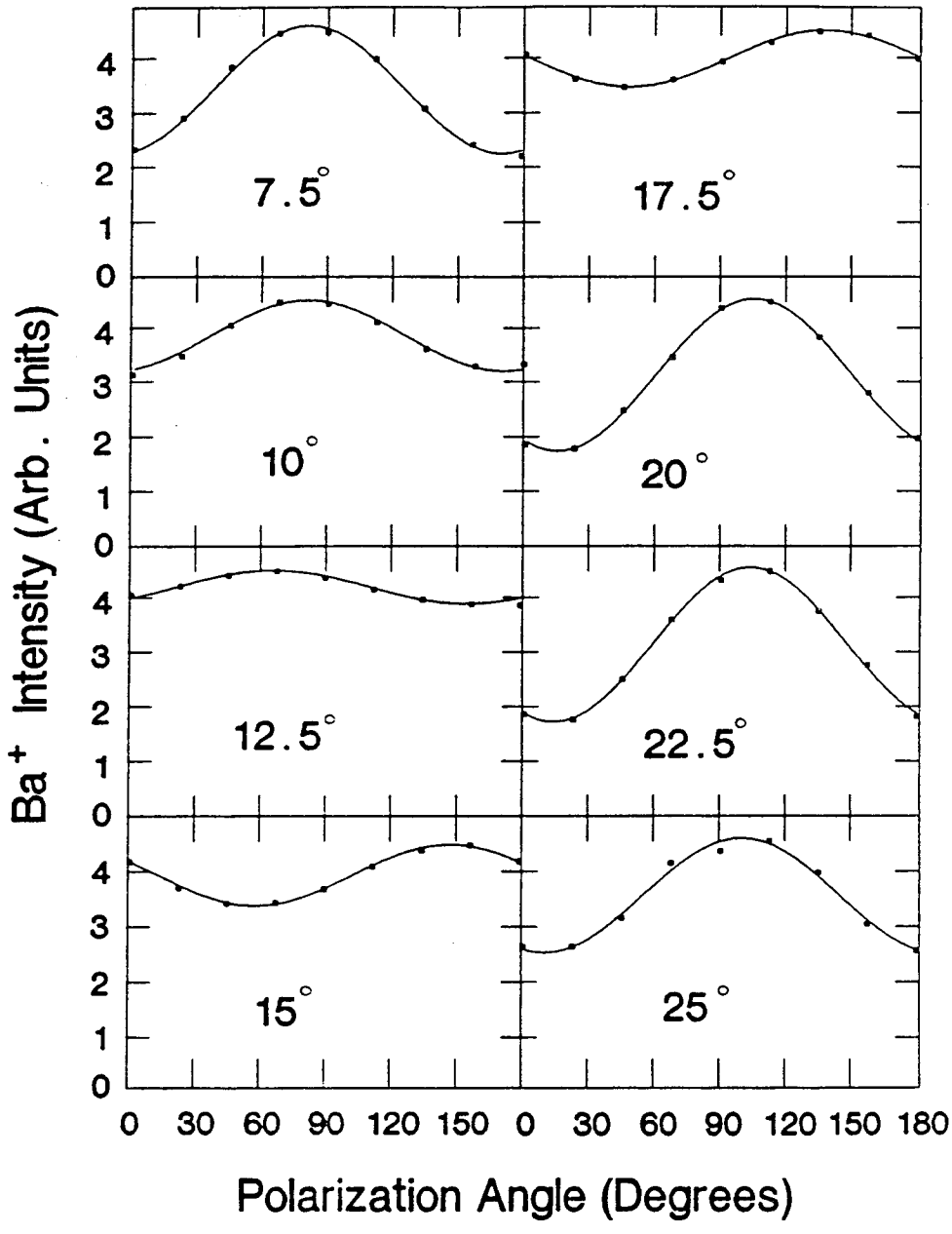
7.5°
17.5°
10°
20°
12.5°
22.5°
15°
25°
Ba+ Intensity (Arb. Units)
0 30 60 90 120 150 0 30 60 90 120 150 180
Polarization Angle (Degrees)

Figure V-5

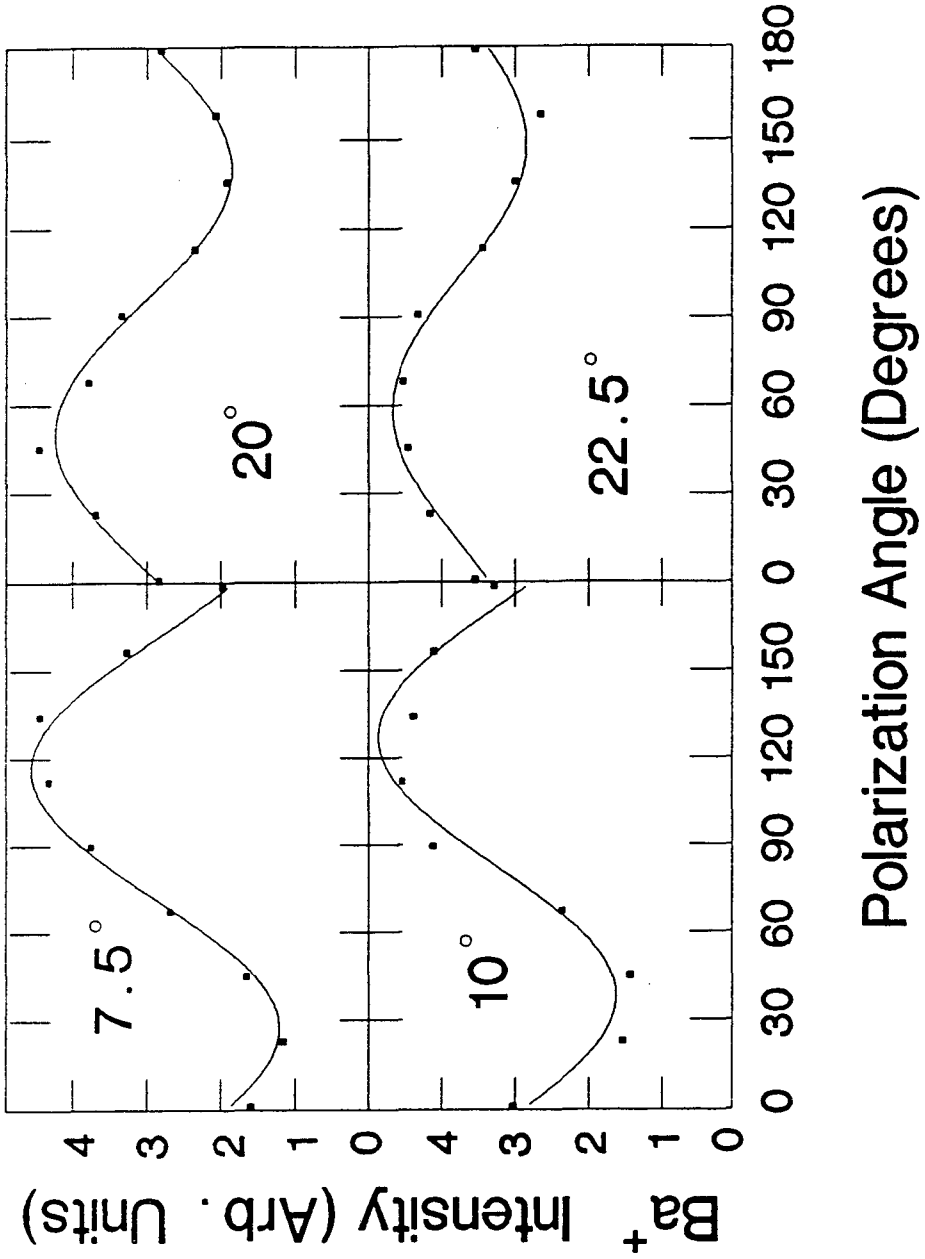
Ba+ Intensity (Arb. Units)
Polarization Angle (Degrees)
7.5°
10°
20°
22.5°
0
1
2
3
4
0 30 60 90 120 150 0 30 60 90 120 150 180

Figure V-6

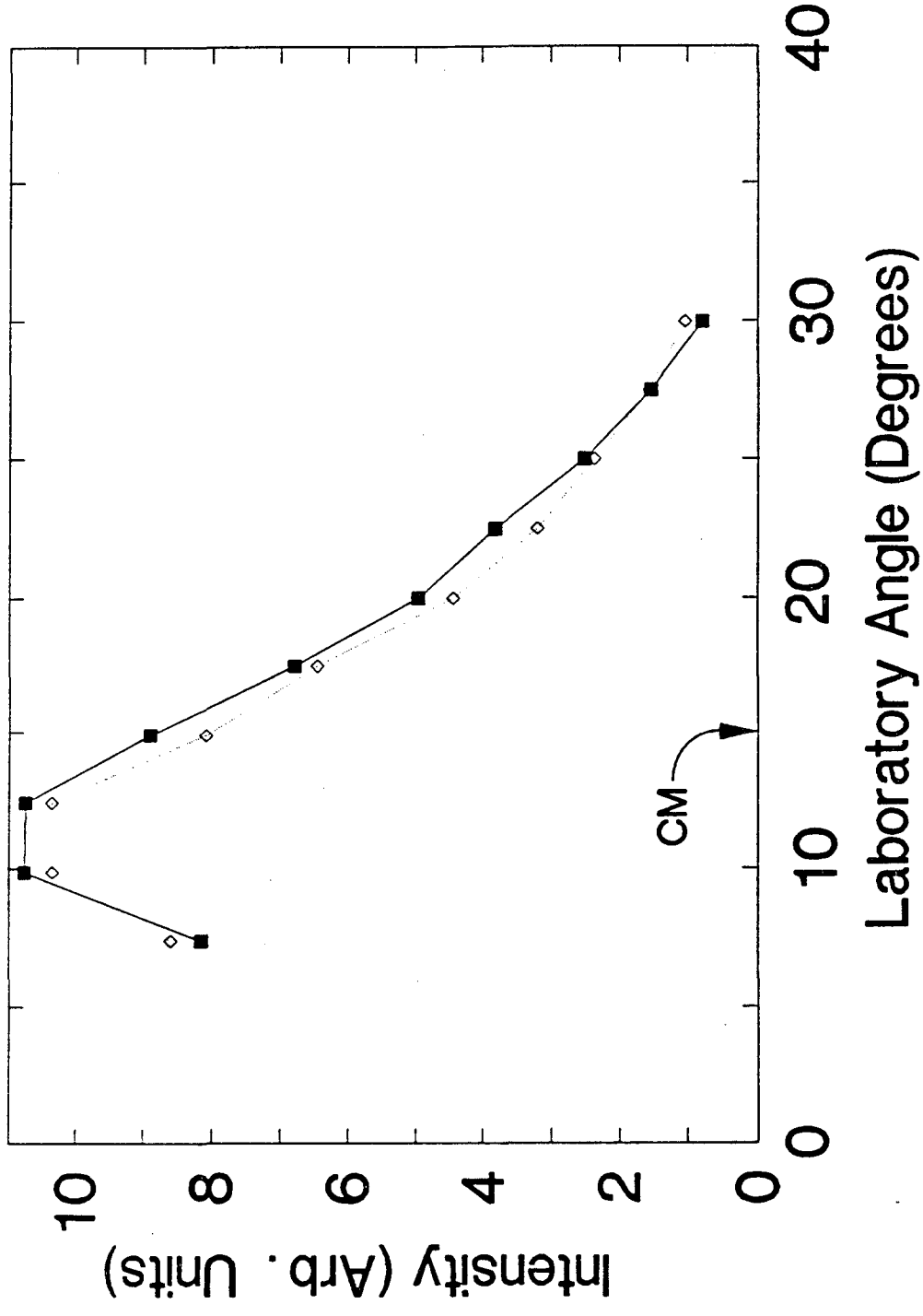
Intensity (Arb. Units)
0
2
4
6
8
10
Laboratory Angle (Degrees)
0
10
20
30
40
CM

Figure V-7

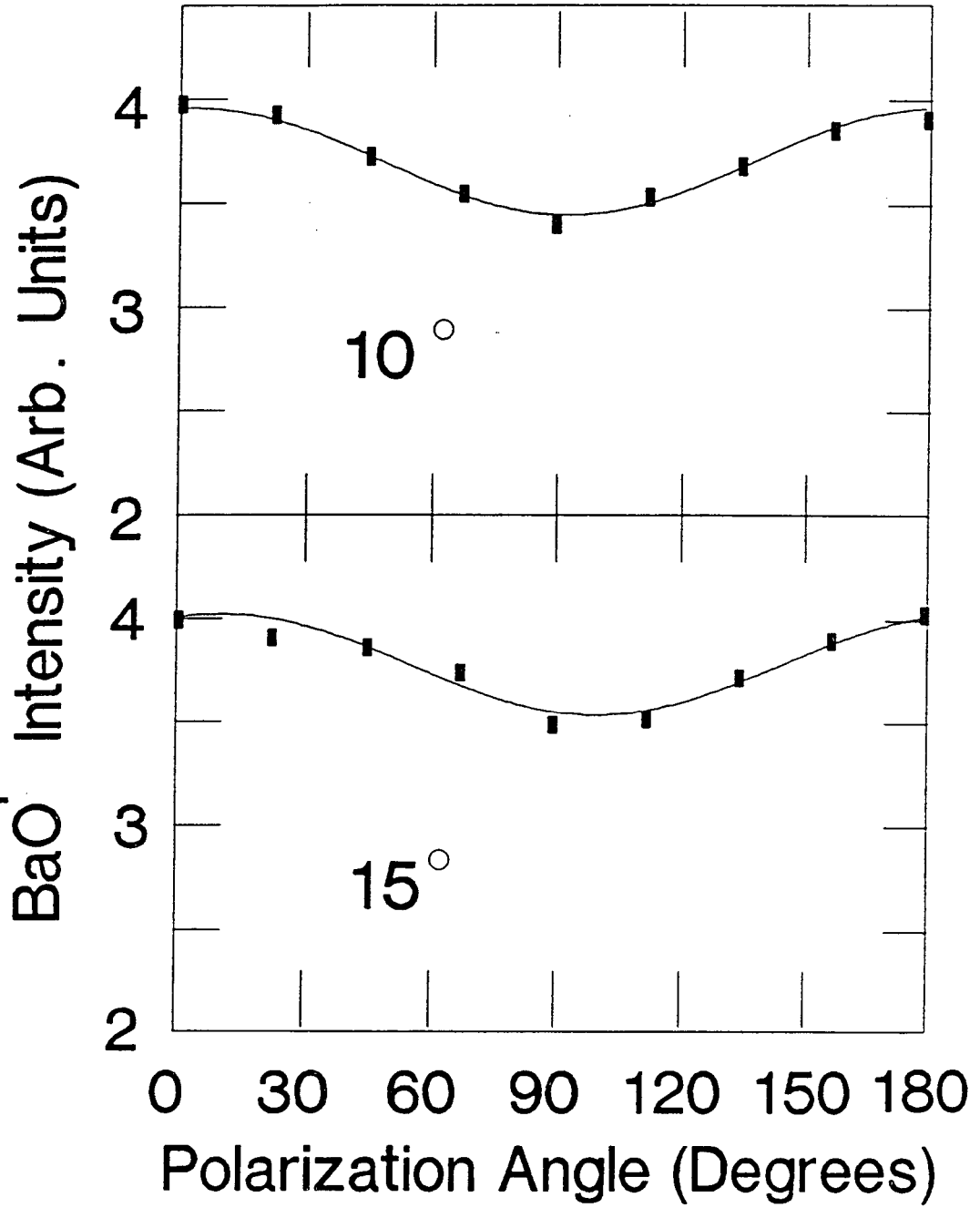
BaO+ Intensity (Arb. Units)
4
3
2
10°
4
3
2
15°
0 30 60 90 120 150 180
Polarization Angle (Degrees)

Figure V-8

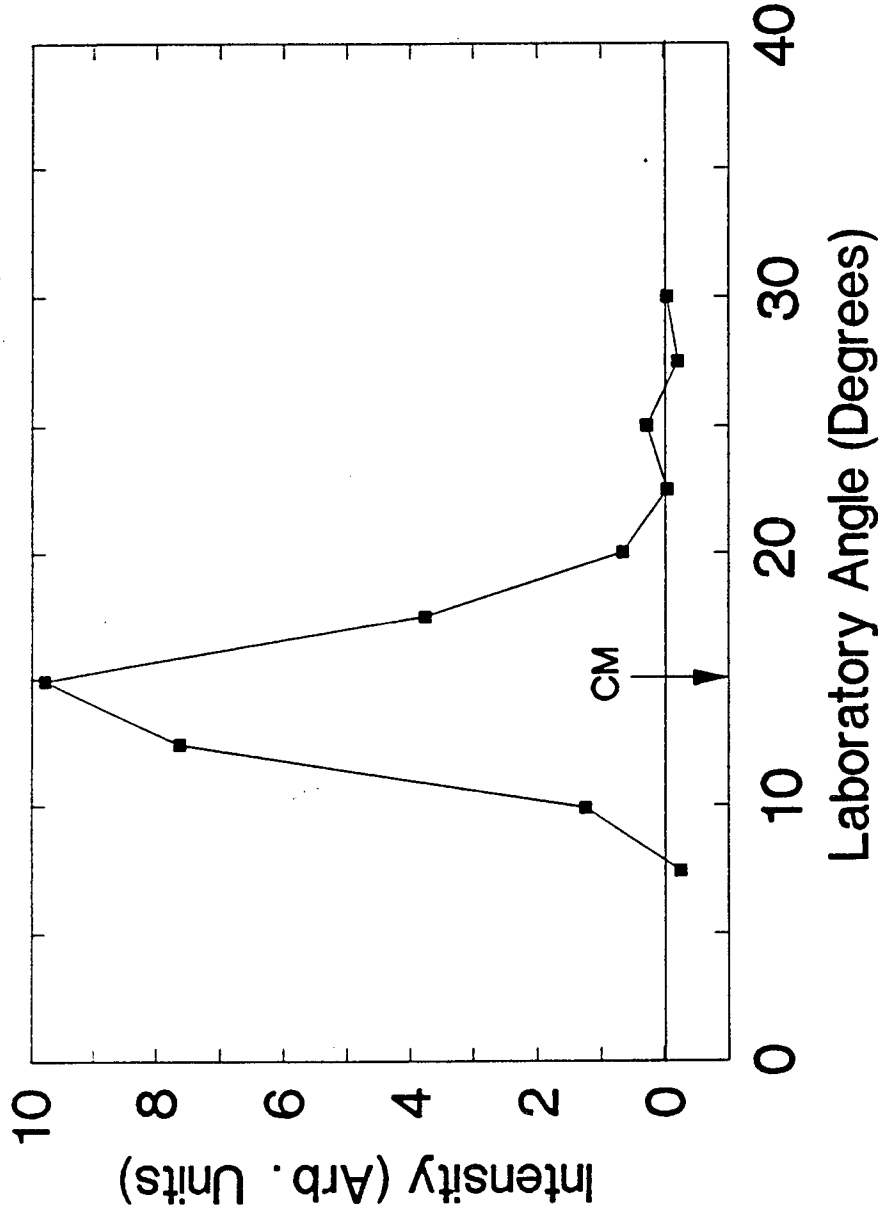
Intensity (Arb. Units)
0
2
4
6
8
10
CM
0
10
20
30
40
Laboratory Angle (Degrees)

Figure V-9

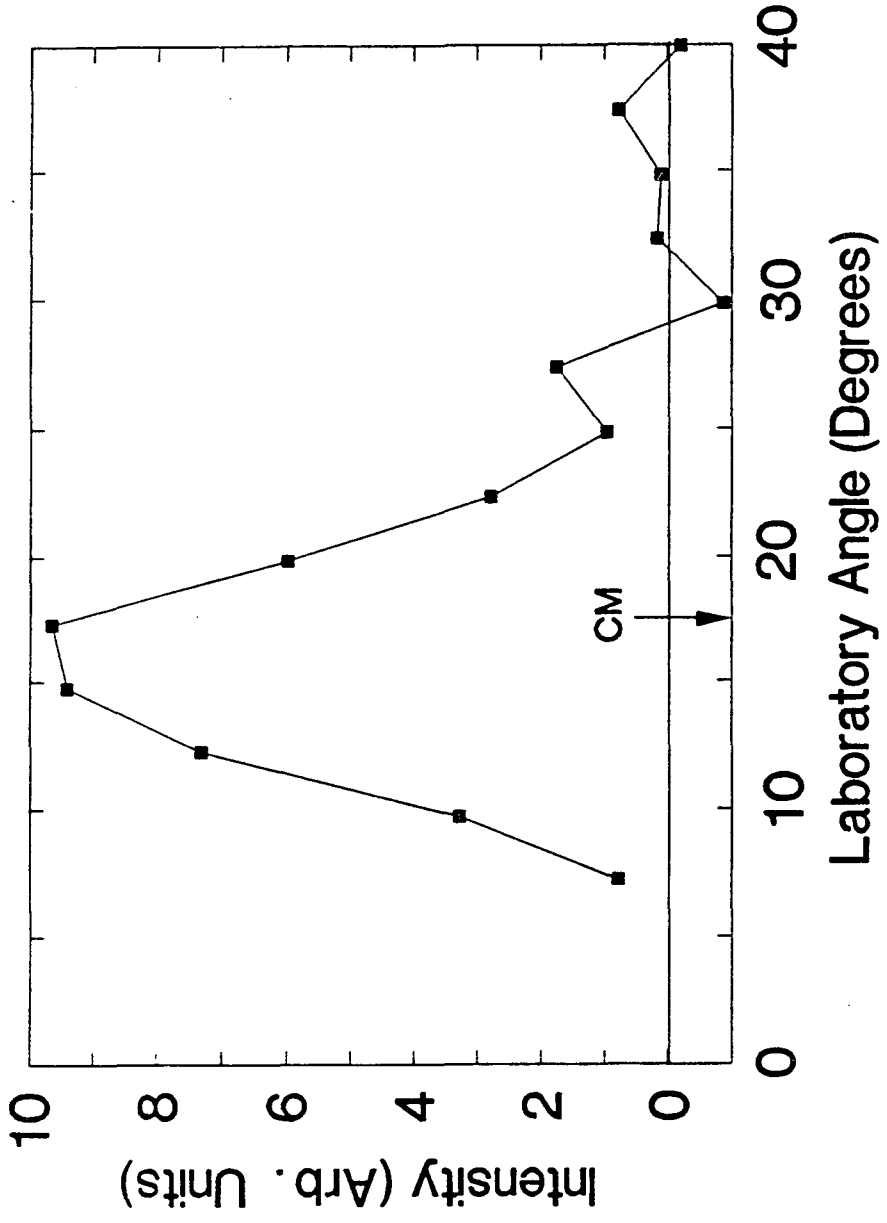
Intensity (Arb. Units)
0
2
4
6
8
10
CM
0
10
20
30
40
Laboratory Angle (Degrees)

Figure V-10

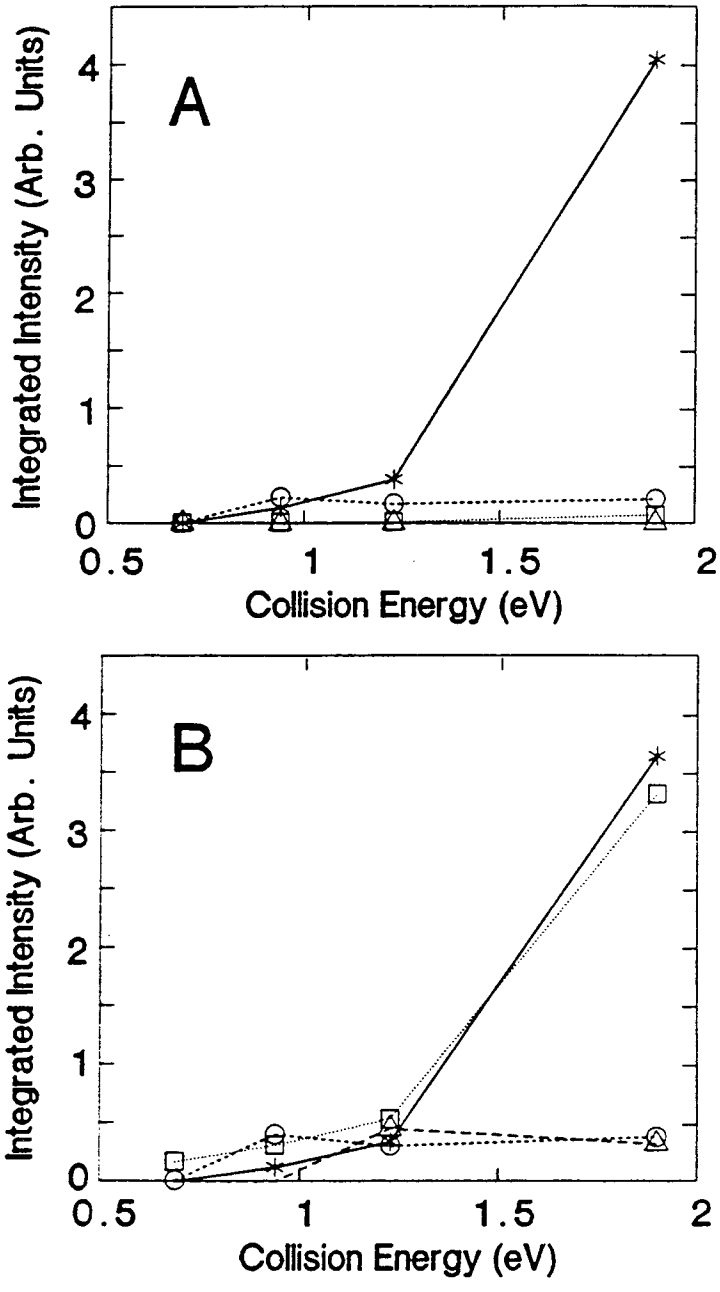
A
Integrated Intensity (Arb. Units)
0
1
2
3
4
0.5
1
1.5
2
Collision Energy (eV)
B
Integrated Intensity (Arb. Units)
0
1
2
3
4
0.5
1
1.5
2
Collision Energy (eV)

Figure V-11

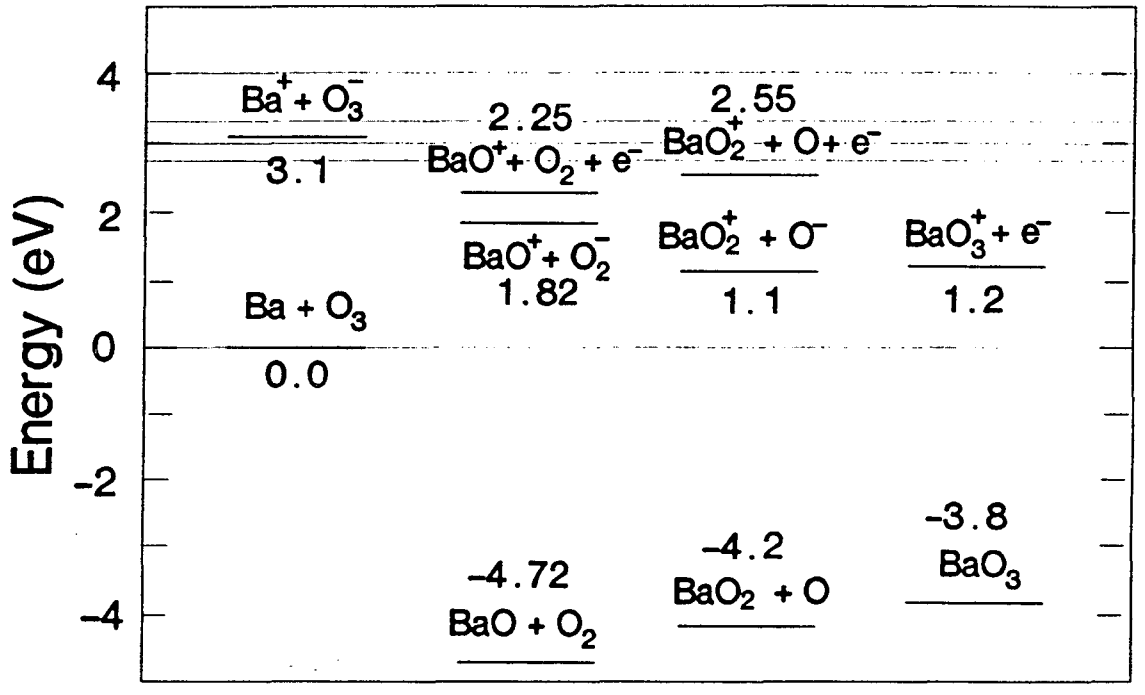
Energy (eV)
4
2
0
-2
-4
Ba+ + O3-
3.1
Ba + O3
0.0
2.25
BaO+ + O2 + e-
BaO+ + O2-
1.82
-4.72
BaO + O2
2.55
BaO2+ + O + e-
BaO2+ + O-
1.1
-4.2
BaO2 + O
BaO3+ + e-
1.2
-3.8
BaO3

Figure V-12

Chapter VI: The Dynamics of Electronically Inelastic Collisions From 3-Dimensional Doppler Measurements

A. Introduction

Quenching collisions between molecules and electronically excited atoms are non-adiabatic processes of central importance in laser physics and atmospheric and combustion chemistry.[1-3] Despite this, experimental progress in understanding the dynamics of these collisions has been slow owing to the fact that the number of possible final states may be quite large and interference from ground state processes can be overwhelming. A large experimental effort has been devoted to these studies over the years, but until recently researchers had to content themselves with measurements of total cross sections or rate constants, while the detailed dynamics remained elusive.[4] Polanyi studied CO vibrational distributions from collisions with excited mercury atoms[5], and new insights became possible as laser and crossed beam techniques developed further. Quenching of $Na(3^2P)$ has been studied in some detail in crossed beams experiments involving a variety of molecular collision partners, and considerable insight has been obtained into the broad features of these processes.[6-10] Yet the difficulty in obtaining differential cross sections and the problems posed by near-resonant processes for conventional detection methods have hampered the full

exploitation of the power of crossed beams techniques in these studies. Following pioneering experiments in Kinsey's group[11,12] Doppler spectroscopy has proved to be a versatile tool in the study of atom-atom collisions[13-15], photodissociation[16], and even reactive scattering[17,18] and offers a means of circumventing background problems inherent in the study of inelastic collisions. But the application of Doppler techniques has generally been limited to situations in which only one final state is involved and the final translational energies are known by virtue of the state probed. In that case since the scattered species is confined to the surface of a sphere, the Doppler scan along the relative velocity vector can reveal the differential cross sections directly.[13] For the case in which numerous final states are involved and a range of product translational energies exist no such simple relation holds: a range of center-of-mass velocities and angles may simultaneously satisfy the Doppler resonance condition. We have successfully carried out investigation of such a case by taking Doppler scans over a range of probe laser angles and applying the "forward convolution" technique widely used in crossed beam studies of reactive scattering[19,20] to derive angular and translational energy distributions for systems in which the final translational energies are not known. We applied these methods to obtain complete contour maps of $Ba(^3P_2)$ flux from the inelastic processes $Ba(^1P_1) + O_2,N_2 \rightarrow Ba(^3P_2) + O_2,N_2 + 0.564$ eV. The contour map reveals near-resonant production of $Ba(^3P_2)$ in $Ba(^1P_1)$-O_2 collisions. In contrast, the contour map obtained for $Ba(^1P_1)$-N_2 collisions indicates that in this case

this process largely remains vibrationally adiabatic, although a near-resonant contribution is seen as a minor channel.

As mentioned above, much of the current experimental understanding of electronic-to-vibrational,rotational and translational energy transfer (E→VRT) derives from crossed beams studies of electronically excited sodium atom quenching,[6-10] and important parallels exist between the barium studies presented here and that previous work. The sodium experiments relied on translational energy analysis of superelastically scattered sodium, so that relatively low translational energy products could not be efficiently detected against the large elastically scattered background. Nevertheless, the general features of the inelastic process were usually apparent and in favorable cases, notably $Na(^3P)$-N_2 collision, the preponderance of superelastic scattering allowed for detailed insight into the quenching process. Extensive comparison with theoretical calculations showed the model of an intermediate Na^+-N_2^- ion pair state to be inaccurate, but revealed the importance of "prestretching" of the N-N bond on the adiabatic surface in the region of the crossing between the ground and excited state potential energy surfaces. Hertel described two basic quenching modes in the sodium studies: a non-resonant process such as that observed for N_2 and H_2, and a near-resonant process suggested in results for O_2,CO and N_2O. The sodium studies were performed only at a few laboratory scattering angles, so that contour maps were not obtained, indeed only the superelastic contribution could be accurately measured.

The barium studies presented here provide, to our knowledge, the first contour maps obtained for an electronically inelastic scattering process and clearly document a near-resonant quenching process both for O_2 and N_2. The results suggest a model for the $Ba(^1P_1) + M \rightarrow Ba(^3P_2) + M$ collisions which invokes the shape of the potential surfaces in the crossing regions to account for the observed $Ba(^3P_2)$ scattering distributions. Important differences in the behavior of barium and sodium are also apparent, particularly in the case of collision with O_2.

B. Experimental

The experimental apparatus[21-23] at Saclay features an effusive barium atomic beam crossed at 90° by a supersonic molecular beam under single collision conditions (Figure 1). The 554 nm $Ba(^1S_0\text{-}^1P_1)$ transition was pumped by a cw single frequency ring dye laser directed through an optic fiber, perpendicular to the collision plane, to the interaction region (Figure 2). Doppler scans of the collisionally populated $Ba(^3P_2)$ state were made by probing the $Ba(^3P_2 \rightarrow ^3S_1)$ transition at 790 nm while monitoring the $Ba(^3S_1 \rightarrow ^3P_1)$ fluorescence at 739 nm (Figure 3). The probe laser was introduced through the same optic fiber as the pump laser for perpendicular scans, or through a second optic fiber in the collision plane for other probe angles. The second fiber could be

rotated around the interaction region, allowing for Doppler scans from 18° to 50° from the molecular beam, schematically illustrated in Figure 4.

Fluorescence from the interaction region was dispersed by a 0.5 m monochromator coupled to a liquid nitrogen cooled RCA 31034 photomultiplier tube as shown in Figure 5. Filters were used to limit the contribution from $Ba(^1P_1)$ fluorescence (10^7-10^9 times more intense than the signal of interest) as well as the weaker $Ba(^3P_0)$-$Ba(^1S_0)$ line.

The molecular beam velocities were measured by time of flight using an electron bombardment ionizer-quadrupole mass spectrometer with a chopper wheel. The barium beam velocity distribution was determined by simulation of a Doppler scan on the $Ba(^1S_0)$-$Ba(^1P_1)$ transition. For the cross section measurements, the molecular beam flux was determined by means of the Pitot tube shown in Figure 1, as described in detail previously.

C. Simulation Program

In Kinsey's original description of a 3-dimensionsal Doppler technique, he advocated the use of a Fourier inversion method to obtain the contour map directly from the data.[11] Soon thereafter, his group published results[17] for the OH ($^2\Pi$ v=0, K=17, J=17.5) state from reactive scattering of H atoms with NO_2, but indicated that the data was not sufficiently smooth to justify the Fourier analysis. We chose to

approach the barium data with a forward-convolution method, both because noise in the data precludes the use of any direct inversion approach, and because forward convolution affords a number a benefits. For example, one may explore the influence of experimental parameters quite readily. Furthermore, the center of mass angular and translational energy distributions are quantities of interest, and they are obtained directly in the forward convolution approach. Finally, as will be seen in the treatment of these results, we may be guided by our knowledge of some features of the collision to obtain an appropriate form for the differential cross sections.

In the forward convolution approach, the Doppler spectra are simulated using a computer program[14,19,20] in which assumed forms of the translational energy and angular distributions are used to generate the contribution to the Doppler signal at a given laser angle and frequency offset. The program performs an integration over resonant velocities in the laser reference frame, in which the probe laser direction is taken to be the z axis. The Doppler signal is given by:[13,14,24-27]

$$I(\nu)d\nu = \iiint N(u,\theta_L,\phi_L)\ \delta(w - \vec{V}_{lab}\bullet \hat{n})\ u^2 \sin\theta_L\ du\ d\theta_L\ d\phi_L$$

where ν is the probe laser frequency, u is the center of mass speed of the detected particle, θ_L and ϕ_L are the center of mass polar and azimuthal angles in the laser reference frame, n is a unit vector in the probe laser direction, $N(u,\theta_L,\phi_L)$ is the number density distribution of detected particles and w is defined by the Doppler resonance condition:

$$\nu = \nu_o\ (1 \pm \frac{w}{c})$$

The component of the particle's velocity in the probe laser direction may be expressed in the center of mass frame:

$$\vec{V}_{lab}\bullet \hat{n} = u\cos\theta_L + \vec{V}_{cm}\bullet \hat{n}$$

The Doppler signal, expressed in terms of center of mass flux rather than number density,[17] is then given by:

$$I(\nu) = \iiint I(u,\theta_L,\phi_L)\ \delta(w - u\cos\theta_L - \vec{V}_{cm}\bullet \hat{n})\ u\sin\theta_L\ du\ \frac{d\theta_L}{d\nu}\ d\phi_L$$

This is the integral performed by the program. The laser reference frame differs from the conventional collision reference frame (in which the relative velocity vector is the z axis) only by a rotation, since they are both center of mass frames. The Jacobian for this transformation is thus unity, and we are free to substitute the flux in the collision reference frame, following the appropriate rotation, for that in the laser reference frame. But the flux in the collision reference frame is actually the differential cross section, so we have:

$$I(\nu) = \iiint \frac{d^3\sigma}{d^2\omega\, du}(u,\theta_L,\phi_L)\, \delta(w - u\cos\theta_L - \vec{V}_{cm}\bullet\hat{n})\, u \sin\theta_L\, du \frac{d\theta_L}{d\nu} d\phi_L$$

This integration is performed at each laser frequency for a given Newton diagram with a weighting determined by measured beam conditions. The process is then repeated for each successive Newton diagram.

The final result is then convoluted over a 50 MHz Lorentzian to account for power broadening.

The differential cross sections are generated from assumed forms of the translational energy and angular distributions. Independent translational energy and angular distributions were assumed for each final vibrational state of the molecular collision partner, with the contributions summed to give the simulated spectra. Although the data could be fit with a single separable angular and translational energy

distribution, the result was clearly artificial. The final vibrational states were thus fit separately in order to obtain physically reasonable distributions.

D. Results

1. $Ba(^1P_1) + N_2 \rightarrow Ba(^3P_2) + N_2$

Results for collision with N_2 at 0.21 eV are shown in Figure 6 along with the simulated spectra. The width of the peak in the perpendicular scan (Figure 6a) indicates substantial wide angle scattering. However, the velocity component of this distribution along the relative velocity vector cannot be determined unless the probe laser direction contains a component parallel to the relative velocity vector. The scan parallel to the relative velocity vector (Figure 6b) reveals that the $Ba(^3P_2)$ distribution is generally forward scattered with respect to the barium beam. Additional scans 35° and 50° from the N_2 beam are necessary to provide the redundant information from which final fits may be obtained. These fits were found to be very sensitive to the angular distributions but, owing to the spread in the Ba beam velocity, less so to the energy distributions. The simulations then allow quantitative interpretation of these observations, summarized in the flux-velocity contour map shown in figure 7. Resaonable fits to the data could be obtained with a single independent translational energy and angular distribution, without resolving the contributions representing final

N_2 vibrational states. Owing to the importance of the wide angle scattering and large translational energy release, however, this required constraining the relatively minor contribution from the sharp forward scattered peak to the same large translational energy release. It is difficult to conceive of any mechanism which could effectively couple electronic energy into translation, yet result in a sharp forward scattered peak. This, combined with the unambiguous results for O_2 below, argued for some coupling between the angular and translational energy distributions and the final N_2 vibrational states represent an obvious way in which they are likely to be coupled.

The contour map in Figure 7 shows important contributions from all possible final N_2 vibrational states. The sharp near-resonant v=2 peak is observed at the tip of the barium beam velocity vector. Both for N_2 and O_2 there exist near-resonant final vibrational states:

$$Ba(^1P_1) + O_2(v=0) \rightarrow Ba(^3P_2) + O_2(v=3) \quad \Delta E = 6.3 \text{ meV}$$

$$Ba(^1P_1) + N_2(v=0) \rightarrow Ba(^3P_2) + N_2(v=2) \quad \Delta E = 10.6 \text{ meV}$$

This near-resonant component can be seen in the raw data as the sharp spike in the center of the perpendicular scan (Figure 6a). Its contribution in the case of N_2 actually represents only a small fraction of the $Ba(^3P_2)$ flux when integrated over the entire scattering volume. The final fit consists of 80% v=0, 15% v=1 and 5% v=2. The simulations are quite sensitive to the contribution of the near-resonant v=2 channel. Clearly most of the $Ba(^3P_2)$ flux is forward-sideways scattered with substantial translational energy. The contour map suggests that for N_2, close

collisions dominate this process. Most of the distribution falls outside the limit for v=1 excitation: the production of the ground vibrational state of N_2 is strongly favored. N_2 (v=0) rotational excitation inferred from the contour map peaks at 0.1-0.15 eV, corresponding to j=20-25. This is consistent with the significant rotational excitation anticipated from a close collision.

2. $Ba(^1P_1) + O_2 \rightarrow Ba(^3P_2) + O_2$

The results for O_2, shown in Figure 8, represent a dramatic contrast to the N_2 results. The contour map obtained for $Ba(^1P_1)$-O_2 collision at 0.21 eV, shown in Figure 9, reveals the absence of the wide-angle scattering which dominates the N_2 result. The scattered $Ba(^3P_2)$ flux distribution is almost entirely composed of the near-resonant process: the peak is near the tip of the initial velocity vector of the barium beam. At that point all of the available electronic energy has become O_2 internal energy, and no momentum has been transferred in the collision. In addition, most of the $Ba(^3P_2)$ flux is confined to very small-angle scattering. The fit includes 80% v=3 and 20% v=2, with no contribution from v=0 or 1. Although our experiment does not directly address the distribution of internal energy between O_2 vibration and rotation, the small-angle scattering most likely implies large impact parameter collisions, hence

little rotational excitation. The O_2 final state distribution is thus dominated by low J, v=3.

3. Energy Dependence of the Cross Sections

Figure 10 shows the energy dependence of the absolute cross sections for $Ba(^1P_1) + X \rightarrow Ba(^3P_2) + X$, obtained for X = O_2, N_2, He and Ar. The indicated energies are "most probable" collision energies; no attempt has been made to deconvolute the spread resulting from the spreads in the beam velocities. The results for the rare gases reveal the presence of a small barrier to the curve crossing as has been discussed elsewhere.[15,28] The molecular collision partners both show substantially larger cross sections, reaching ~15 $Å^2$ for N_2 at the lowest collision energy measured. The steepness of the drop in the cross section with collision energy for N_2 is probably underestimated owing to the spread in the actual collision energies. O_2 shows the reverse trend in its energy dependence, still increasing substantially at the highest energy measured.

E. Discussion

Some insight into these results may be gained by comparison with the dynamics of related atom-atom collisions. Thermal energy collision of $Ba(^1P_1)$ with rare gases results in exclusive production of $Ba(^3P_2)$, and this was ascribed to inefficient or inaccessible crossings of the weakly attractive $Ba(^1P_1)$-RG ($^1\Pi$) and repulsive $Ba(^3P_{1,0})$-RG ($^3\Pi_{1,0}$) potential energy curves.[28] Crossed beam studies of the energy dependence of the cross section for $Ba(^3P_1)$ production in $Ba(^1P_1)$-Ar collisions have recently confirmed the existence of a barrier for this channel, a consequence of the location of the crossing on the repulsive wall of the $Ba(^1P_1)$-RG ($^1\Pi$) curve.[15] In the case of $Ba(^1P_1)$-N_2 collisions, the analogous repulsive triplet curves may now seen as three sets of repulsive triplet surfaces, each set corresponding to a given N_2 vibrational state. These surfaces are shown in Figure 11 for collinear $Ba(^1P_1)$-N_2, obtained by Mestdagh using the approach described by Hickman for alkali metal(np ^2P)-H_2, N_2 systems.[29] The curves corresponding to excited vibrational states of N_2 have been estimated simply by shifting the ground state curves by the 2360 cm^{-1} N_2 vibrational frequency. On approach, the first encountered crossing seam is with the $Ba(^3P_2)$-N_2(v=2) surface, which occurs at fairly large Ba-N_2 distance. The Franck-Condon factors for this transition are likely to be unfavorable, and this is consistent with the small fraction of scattered $Ba(^3P_2)$ flux we observe (5%) originating from this crossing. Furthermore, this crossing occurs in a relatively flat region of the surface, so little deflection is likely to result for these collisions. Again this is consistent with the sharply forward scattered, near-resonant $Ba(^3P_2)$ which we observe corresponding to N_2

(v=2). The next encountered crossing will be with the N_2 (v=1) surface, with perhaps more favorable Franck-Condon factors and substantially stronger deflection. The final crossing, with N_2 (v=0), occurs at close range with very favorable Franck-Condon factors. Much of the electronic energy may be released into translation through the long descent on this steeply repulsive region of the $Ba(^3P_2)$-N_2 (v=0) surface. The tendency to sideways scattering and large translational energy release thus reflects the strong coupling at this inner crossing.

The sodium studies revealed the importance of pre-stretching of the N_2 bond in the presence of the sodium atom in order to reach the crossing between the ground and excited state surfaces, and this was found to be most important for the large impact parameter collisions.[10] Others have shown the importance of prestretching in alkali metal - halogen molecule collisions[30], and again its importance for large impact parameter collisions is revealed in trajectory calculations. The curves in Figure 11 for the products $Ba(^3P_2)$ + N_2 (v=2) suggest the possible importance of prestretching here as well. The contour map indicates that this flux results mostly from large impact parameter collisions, and the anticipated small Franck-Condon factors are likely to be enhanced by this stretching of the N-N bond. The decrease in cross section with increasing collision energy is also expected for prestretching, and this has been shown in a number of studies.[30] Yet the relatively small contribution afforded by these near-resonant collisions suggest we look elsewhere for the large effect appearing in the energy dependence of the cross sections.

The barrier for formation of $Ba(^3P_1)$ from $Ba(^1P_1)$ collision with rare gases suggests an alternative explanation for the drop in cross section with collision energy for N_2. An analogous barrier is also likely to appear in the case of N_2, as can be seen in the potential curves of Figure 11. For collision energies in excess of this barrier, a significant fraction of the incoming flux may exit as $Ba(^3P_1)$ rather than $Ba(^3P_2)$, with a corresponding drop in the cross section. The absence of backscattered $Ba(^3P_2)$ in these collisions is also suggestive. If the crossing to the $Ba(^3P_1)$ surface is high on the inner wall, then it may be accessible to very low impact parameter collisions of sufficient kinetic energy, thus these low impact parameter collisions may favor the formation of $Ba(^3P_1)$ over $Ba(^3P_2)$. Further experiments are planned to explore these questions.

Important differences exist between the sodium experiments and the barium system presented here. The large exoergicity of the sodium quenching process (2.1 eV versus 0.56 eV for barium) implies much more energy available to N_2. Indeed, the peak of the N_2 vibrational distribution occurred at v=4, exceeding the total energy available in the barium collisions. Furthermore, the Na trajectory studies found up to 1 eV in N_2 rotational excitation, nearly twice the total electronic energy available in the barium studies. The possible existence of an analogous near-resonant process in the case of sodium is an interesting question, but the previous experiments can not address this question.

The O_2 results are completely dominated by a near-resonant mechanism in which most of the available electronic energy is efficiently coupled into O_2 vibration. Electron attachment to O_2 results in the formation of long-lived O_2^- compound states and concomitant stretching of the O-O bond.[31] The inelastic $Ba(^1P_1)$-O_2 collisions are thus likely to proceed via an ionic intermediate. For the Ba-O_2 system the potential curves will thus be well characterized by the multiple-curve-crossing model, in which a series of flat covalent surfaces representing the initial and final states are crossed by the strongly attractive Coulombic surfaces.[32,33] The sharp forward scattering again implies a transition at long range, in a flat region of the triplet surface. This near-resonant O_2 distribution illustrates the power of the Doppler technique: the inelastic process is readily apparent despite the fact that the peak of its distribution is superimposed on the barium beam, which is many orders of magnitude more intense.

The absence of the wide-angle non-resonant $Ba(^3P_2)$ from collision of $Ba(^1P_1)$ with O_2 is quite revealing. For collision of Ba with O_2, a reactive channel yielding BaO + O exists with a large cross section and it is seen for excited state as well as ground state barium.[17] No such reaction channel is available for N_2. The low impact parameter collisions which dominate the inelastic process for N_2 apparently lead to reaction in the case of O_2, with a corresponding "hole" in the angular distribution at wide scattering angles and the absence of O_2 (v=0,1) from this process. It appears that only a limited range of impact parameters may gain access to the crossing region while eluding the dominant reactive path in the O_2 case. In fact, the increasing cross

section with collision energy may come at the expense of the reactive cross section as more trajectories with access to the crossing region successfully elude complex formation.

This points to a number of crucial differences between the sodium and barium studies of quenching by O_2. For sodium, there was no reactive channel available, and the resulting Na superelastic scattering was well fit by a prior distribution which included the two electronically excited states of O_2 also accessible in that experiment.[3] Again the near-resonant process may exist hidden in the elastic scattering in the sodium results, but the statistical distribution implying an intimate collision is quite different from what is seen for barium.

Forward convolution analysis of 3-dimensional Doppler measurements can provide insight into inelastic collision processes which are otherwise experimentally inaccessible. The results presented document a near-resonant quenching mechanism for the first time. Because the technique does not discriminate against detection of low translational energy products, it allows for a comprehensive experimental understanding of electronically inelastic collisions.

References

1. W. H. Breckenridge and H. Umemoto, in **The Dynamics of the Excited State**, K. P. Lawley, ed., Adv. Chem. Phys. **50**, (Wiley, New York, 1982).
2. R. J. Donovan and G. Husain, in **Bimolecular Collisions**, M. N. R. Arnold and J. E. Baggott, eds., (Royal Society of Chemistry, London, 1989).
3. I. V. Hertel, Adv. Chem. Phys. **45**, 341 (1981).
4. L. Krause, Adv. Chem. Phys. **48**, 267 (1975).
5. G. Karl, P. Kruus, J. C. Polanyi and I. W. M. Smith, **46**, 244 (1967).
6. I. V. Hertel, H. Hoffmann, and K. A. Rost, Phys. Rev. Lett., **36**, 861 (1976).
7. I. V. Hertel, H. Hoffmann and K. A. Rost, J. Chem. Phys., **71**, 674 (1979).
8. I. V. Hertel, Adv. Chem. Phys. **50**, 456 (1982); E. E. B. Campbell, H. Schmidt and I. V. Hertel, Adv. Chem. Phys. **72**, 37 (1988).
9. P. Habitz, Chem. Phys., **54**, 131 (1980).
10. P. Achirel and P. Habitz, Chem. Phys., **78** 213 (1983).
11. J. L. Kinsey, J. Chem. Phys. **66**, 2560 (1976).
12. W. D. Phillips, J. A. serri, D. J. Ely, D. E. Pritchard, K. R. Way and J. L. Kinsey, Phys. Rev. Lett., **41**, 937 (1978).
13. J. A. Serri, J, L. Kinsey and D. E. Pritchard, J. Chem. Phys. **75**, 663 (1981).

14. J. M. Mestdagh, P. de Pujo, J. Pascale, J. Cuvellier, and J. Berlande, Phys. Rev. A, **35**, 1043 (1987).

15. J. P. Visticot, J. Berlande, J. Cuvellier, J.M. Mestdagh, P. Meynadier, P. de Pujo, O. Sublemontier, A. Bell and J. Frey, J. Chem. Phys. **93**, 5354 (1990).

16. E. F. Cromwell, D. J. Liu, M. J. J. Vrakking, A. H. Kung, and Y. T. Lee, J. Chem. Phys., **92**, 3230 (1990).

17. E. L. Murphy, J. H. Brophy, G. S. Arnold, W. L. Dimpfl and J. L. Kinsey, J. Chem. Phys. **70**, 5910 (1979).

18. B.Girard, N. Billy, G. Gouedard and J. Vigue, submitted to Europhysics Letters.

19. E. Entemann, J. Chem. Phys. **55**, 4872 (1971).

20. R. Buss, Ph. D. Thesis, Univ. of Calif., Berkeley, (1972).

21. J. Cuvellier, J. M. Mestdagh, J. Berlande, P. de Pujo, and A. Binet, Rev. Phys. Appl. **16**, 679, (1981).

22. J. Cuvellier, P. de Pujo, J. M. Mestdagh, J. P. Visticot, J. Berlande and A. Binet, J. Chem. Phys. **90**, 7050 (1989).

23. J. M. Mestdagh, J. Berlande, J. Cuvellier, P. de Pujo and A. Binet, J. Phys. B **15**, 439 (1982).

24. R. Schmiedl, H. Dugan, W. Meier and K. H. Welge, Z. Phys. A **304**, 137 (1982).

25. R. N. Dixon, J. Chem. Phys. **85**, 1866 (1986).

26. N. Kouchi, K. Ito, Y. Hatano and N. Oda, Chem. Phys. **70**, 105 (1982).

27. R. Vasudev, R. N. Zare and R. N. Dixon, J. Chem. Phys. **80**, 4863 (1984).

28. W. H. Breckenridge and C. N. Merrow, J. Chem. Phys. **88**, 2329 (1988).

29. A. P. Hickman, J. Phys. B **15**, 3005 (1982).

30. J. Los and A. W. Kleyn, in **Alkali Halide Vapors**, 189 (Academic Press, New York, 1979) and references.

31. G. J. Schulz, Rev. Mod. Phys., **45**, 423 (1973).

32. E. Bauer, E. R. Fisher and F. R. Gilmore, J. Chem. Phys. **51**, 4173 (1969).

33. D. Paillard, J. M. Mestdagh, J. Cuvellier, P. de Pujo and J. Berlande, J. Chem. Phys. **87**, 2084 (1987).

Chapter VI Figure Captions

Figure VI-1. Schematic view of Saclay crossed beams apparatus.

Figure VI-2. Schematic view of interaction region of crossed beams apparatus. A third optic fiber, not shown, allowed the second laser to be directed to the interaction region at various angles in the collision plane.

Figure VI-3. Summary of excitation and detection scheme for observing $Ba(^3P_2)$ produced in collisions of $Ba(^1P_1)$.

Figure VI-4. Illustration of 3-dimensional doppler technique. For scans in which the probe laser is in the plane of the beams, the angle Θ_L is defined with respect to the molecular beam. For the perpendicular probe direction, the laser is directed into the beam plane from above. The zero offset line is indicated for each probe laser angle, representing velocities which have no component in the probe laser direction.

Figure VI-5. Schematic view of fluorescence detection apparatus.

Figure VI-6. Doppler scans of $Ba(^3P_2)$ produced from collision of $Ba(^1P_1)$ with N_2 at 0.21 eV collision energy. The points are experimentally measured, the lines are best fit simulations. Probe laser direction is A) perpendicular to collision plane or in the collision plane and B) 21° C) 35° or D) 50° from the N_2 beam.

Figure VI-7. Velocity space $Ba(^3P_2)$ flux contour map obtained from the fit shown in Figure 1 for collision of $Ba(^1P_1)$ with N_2. The nominal Newton diagram is shown with limit circles corresponding to maximum $Ba(^3P_2)$ recoil velocity for indicated final N_2 vibrational state. The v=2 contribution has been reduced by a factor of four.

Figure VI-8. Doppler scans of $Ba(^3P_2)$ produced from collision of $Ba(^1P_1)$ with O_2 at 0.21 eV collision energy. For details refer to Figure 1.

Figure VI-9. Velocity space $Ba(^3P_2)$ flux contour map obtained from the fit shown in Figure 8 for collision of $Ba(^1P_1)$ with O_2. The v=3 contribution has been reduced by a factor of 4. For details refer to Figure 2.

Figure VI-10. Energy dependence of the cross section for $Ba(^3P_2)$ formation from collision of $Ba(^1P_1)$ with indicated collision partner.

Figure VI-11. Excited Ba-N_2 potential energy curves obtained as described.

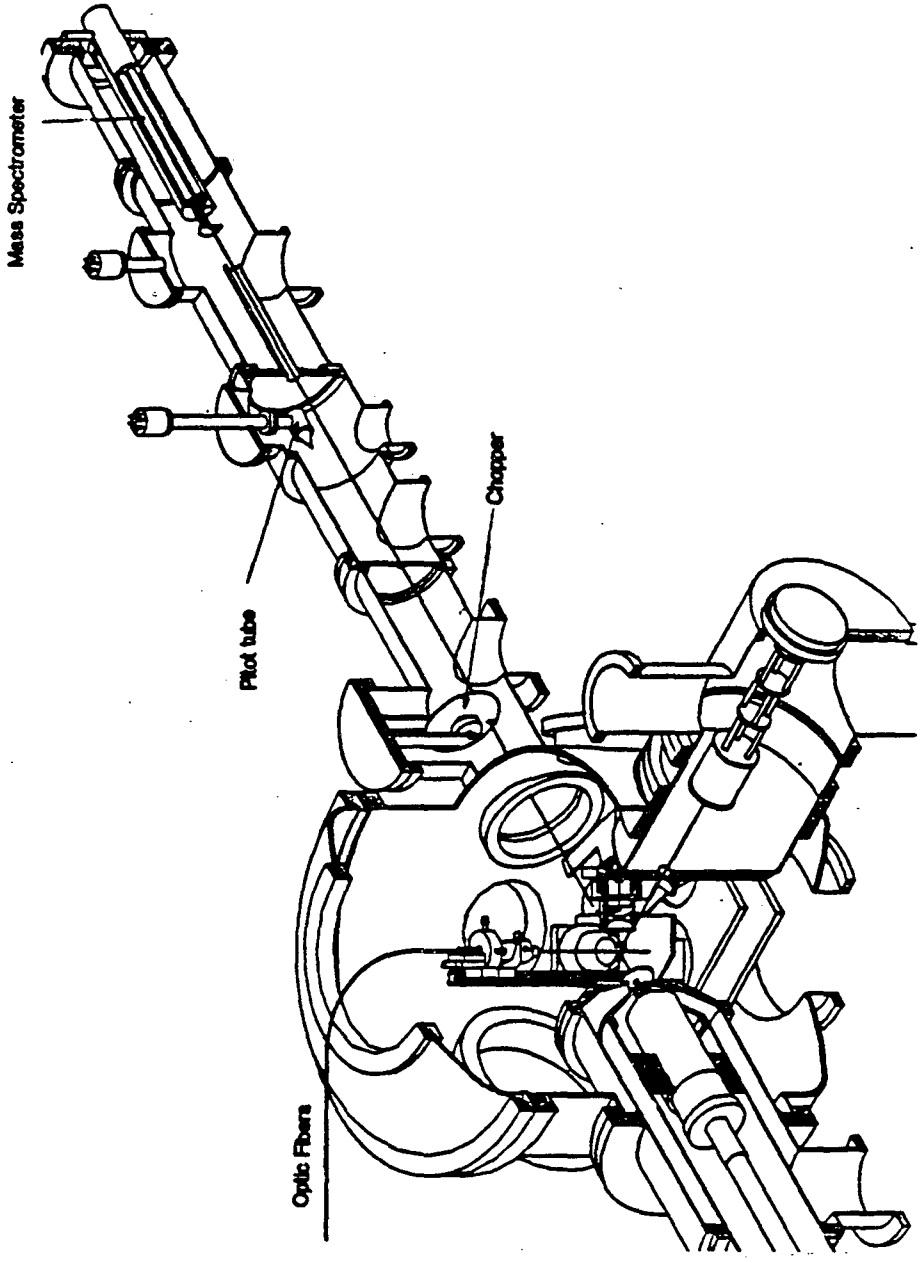

Figure VI-1

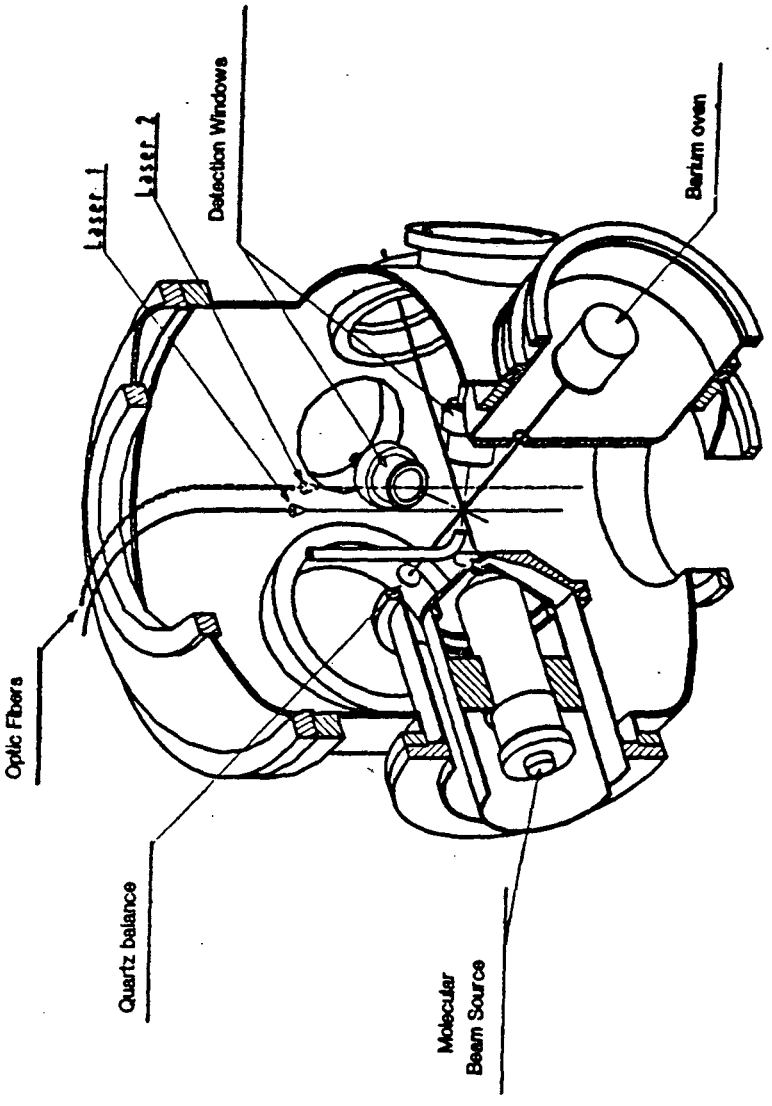
Laser 1
Laser 2
Detection Windows
Barium oven
Optic Fibers
Quartz balance
Molecular
Beam Source

Figure VI-2

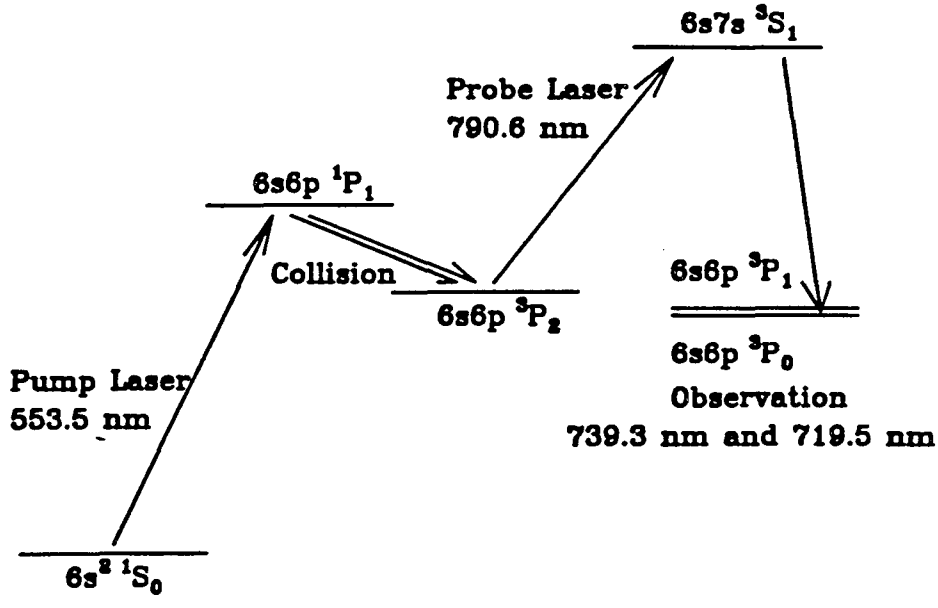
6s7s $^3S_1$
Probe Laser
790.6 nm
6s6p $^1P_1$
Collision
6s6p $^3P_2$
6s6p $^3P_1$
6s6p $^3P_0$
Observation
739.3 nm and 719.5 nm
Pump Laser
553.5 nm
$6s^2\ ^1S_0$

Figure VI-3

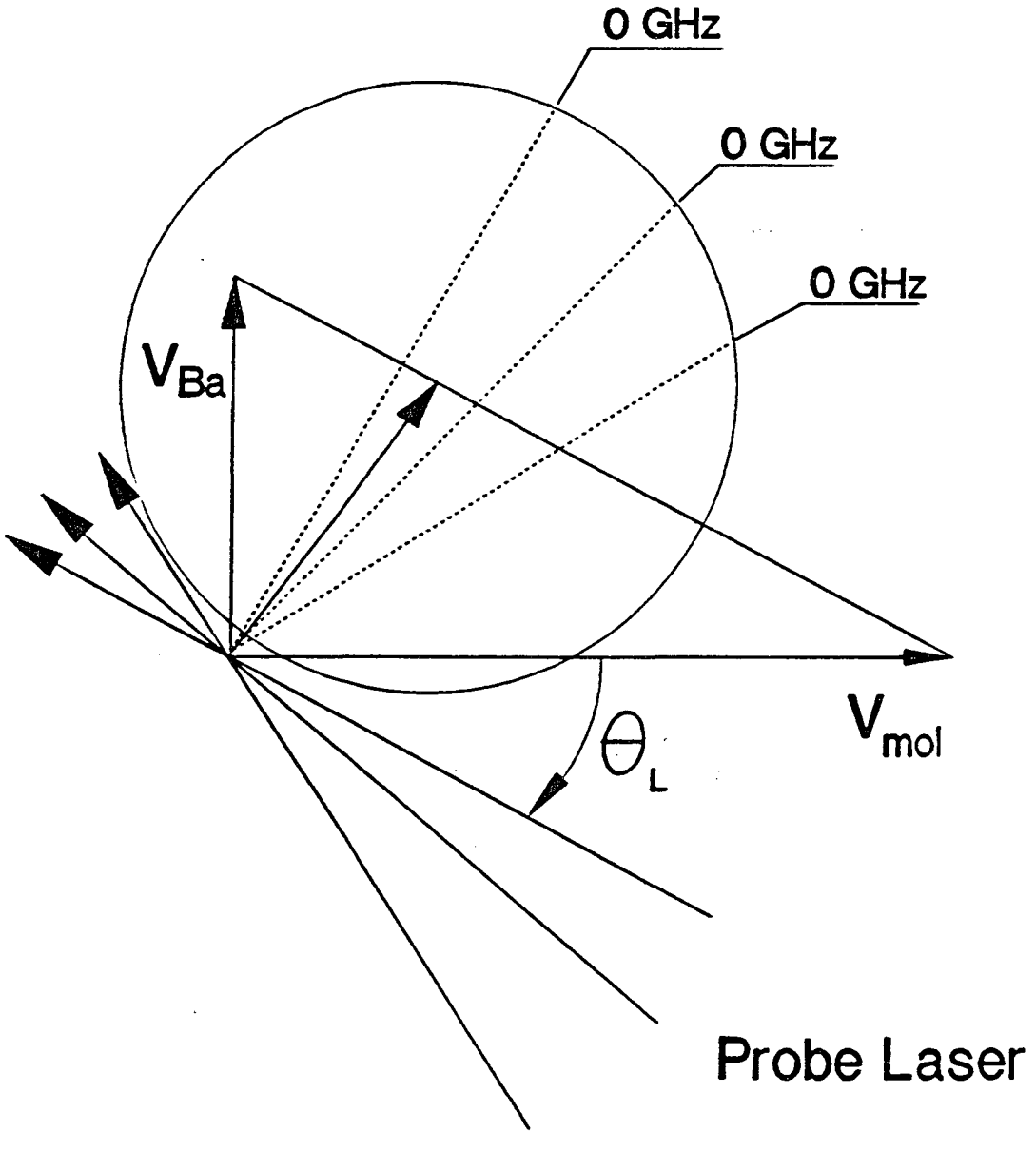

Figure VI-4

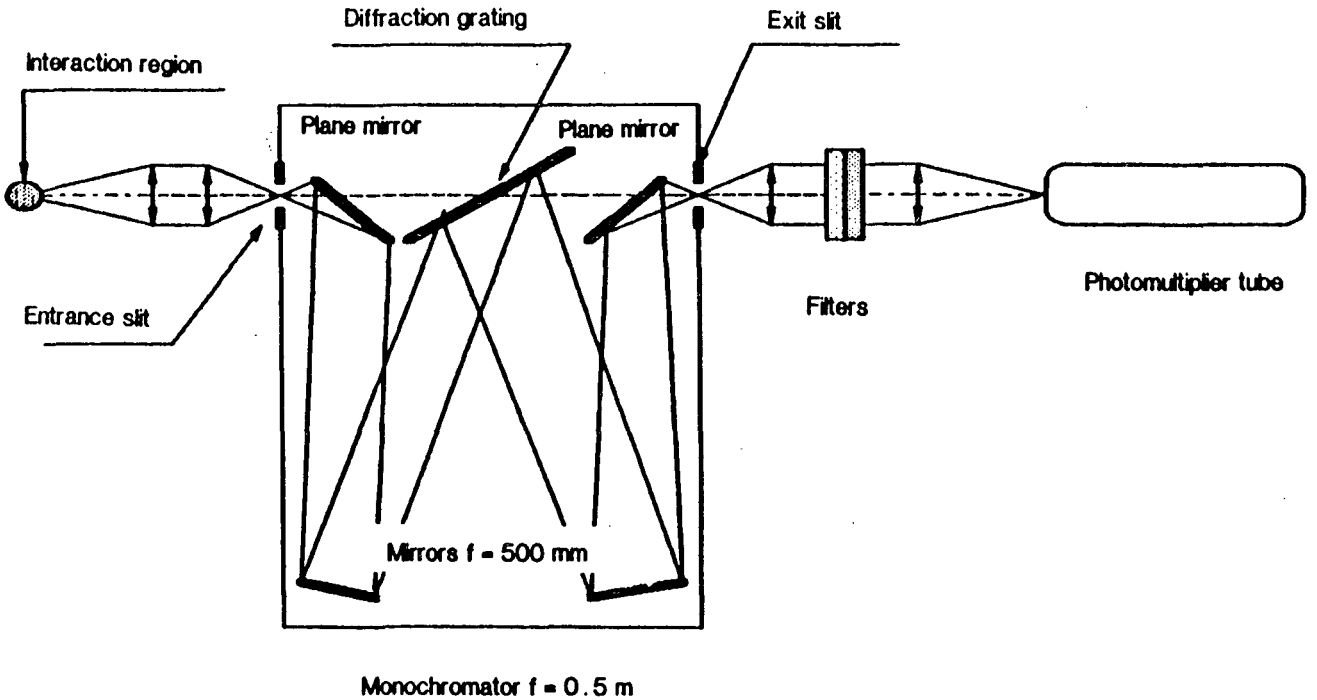
Diffraction grating
Exit slit
Interaction region
Plane mirror
Plane mirror
Photomultiplier tube
Filters
Entrance slit
Mirrors f = 500 mm
Monochromator f = 0.5 m

Figure VI-5

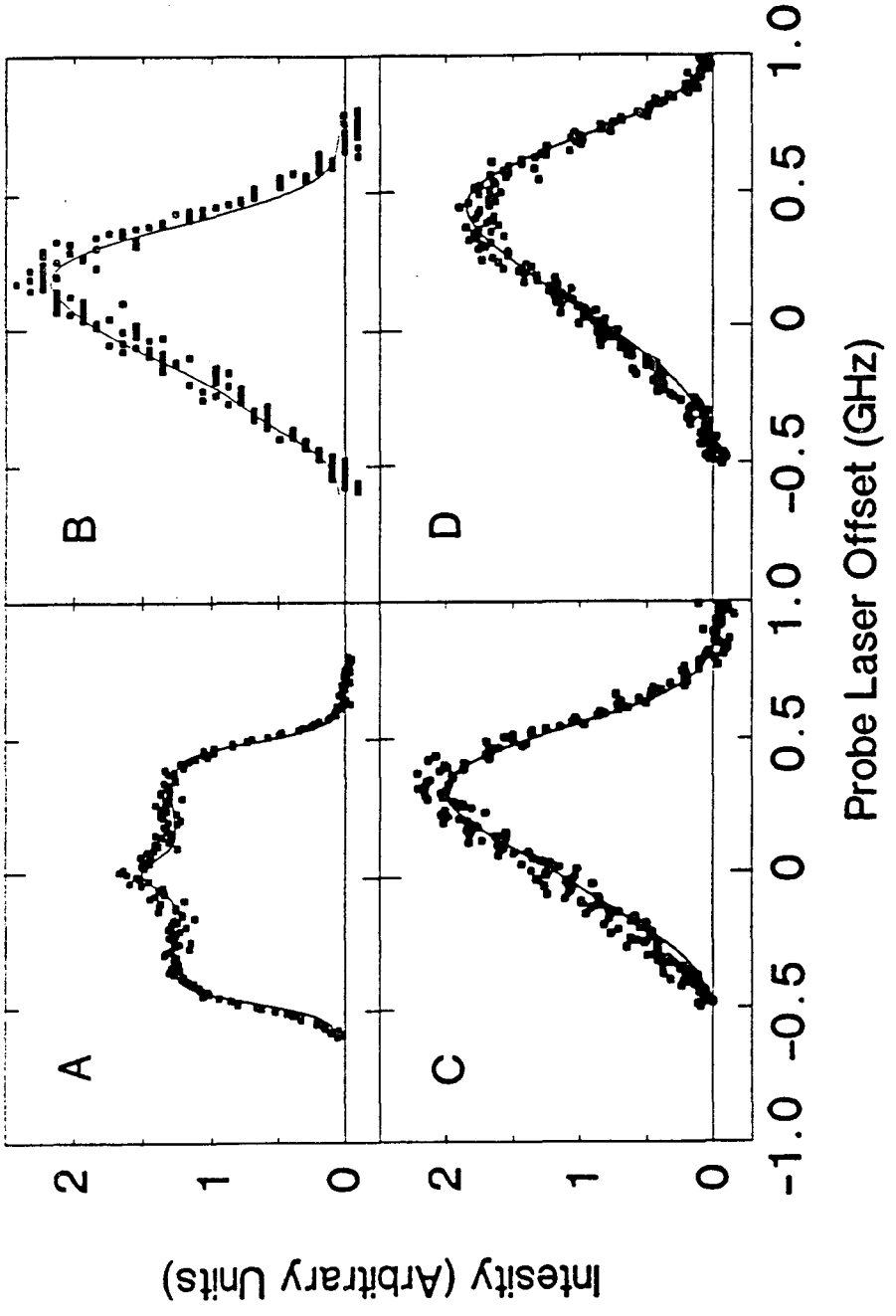
A
B
C
D
2
1
0
-1.0
-0.5
0
0.5
1.0
Intesity (Arbitrary Units)
Probe Laser Offset (GHz)

Figure VI-6

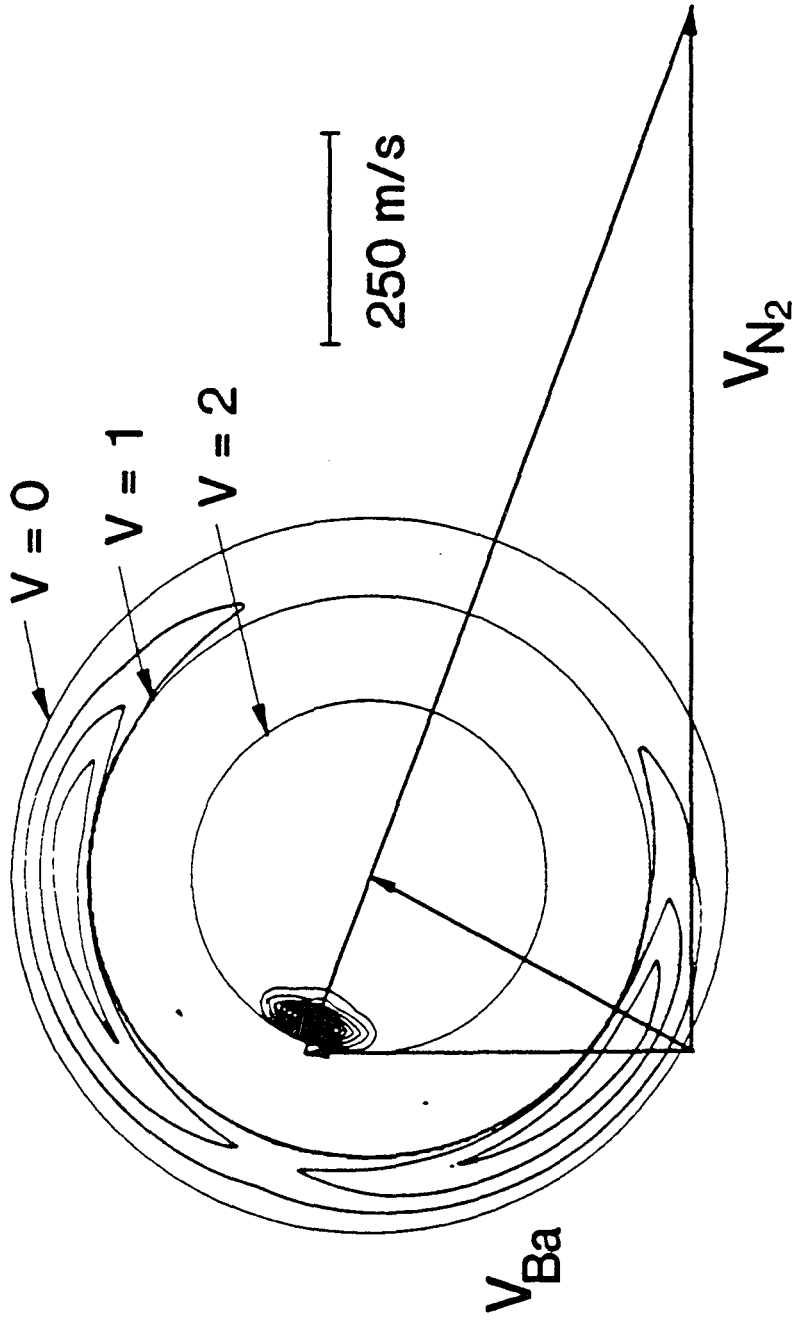

Figure VI-7

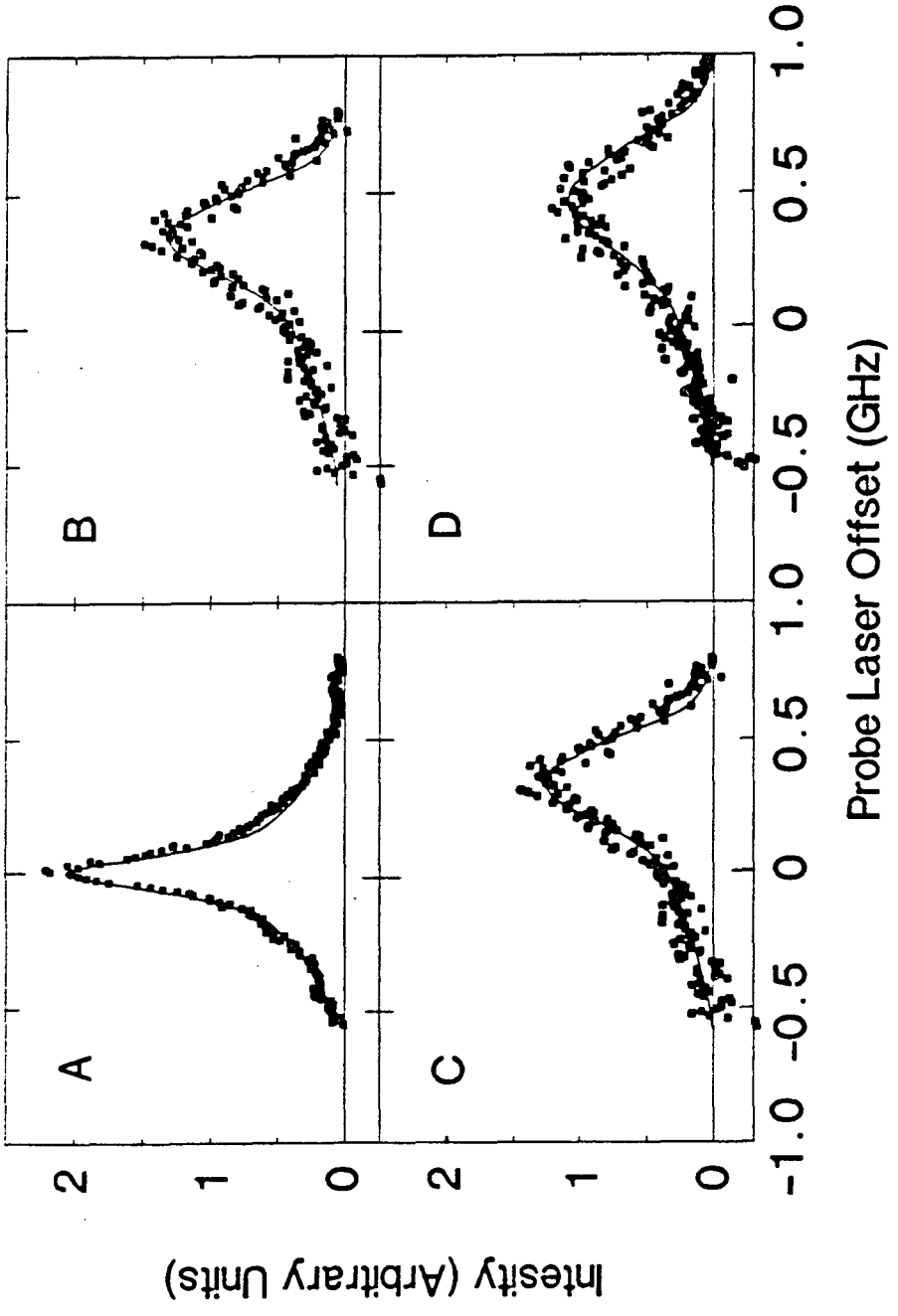
A
B
C
D
2
1
0
-1.0
-0.5
0
0.5
1.0
Intesity (Arbitrary Units)
Probe Laser Offset (GHz)

Figure VI-8

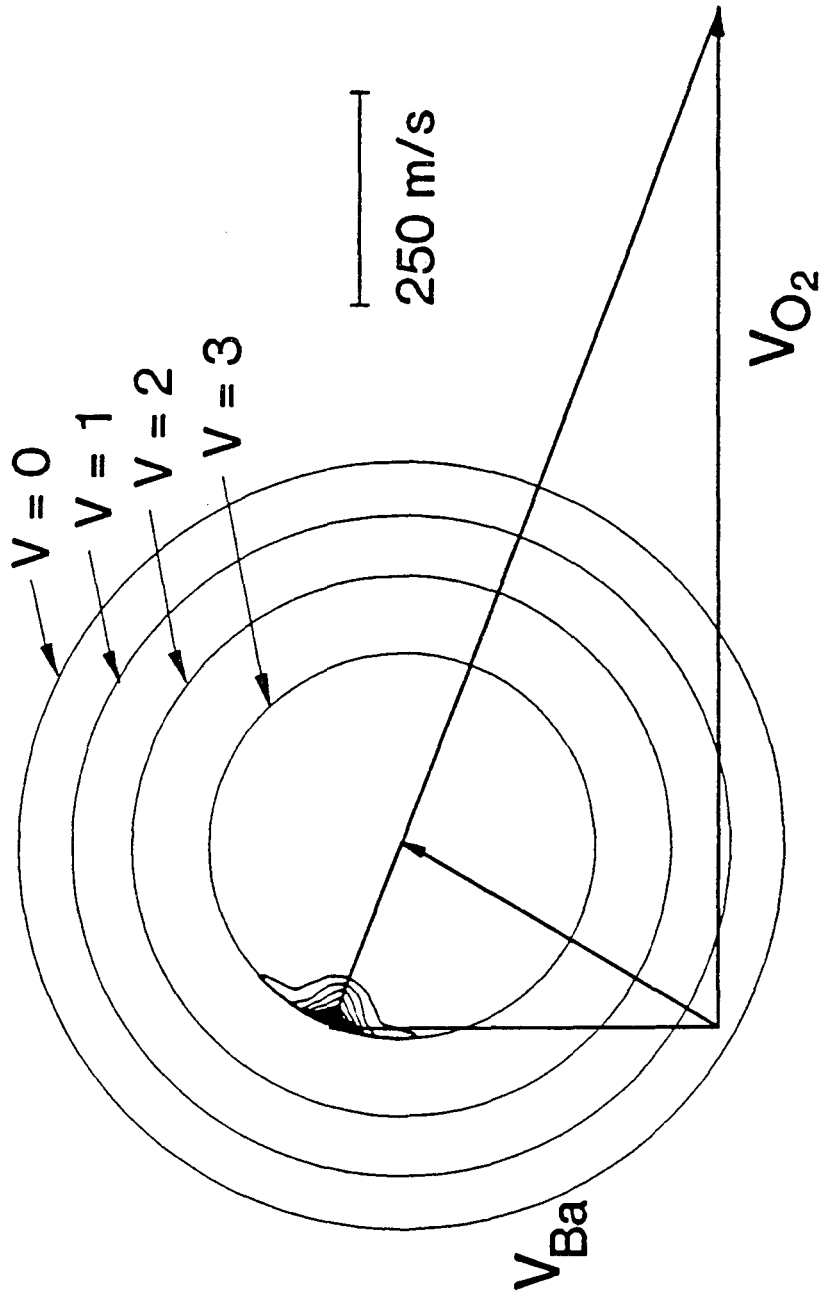

Figure VI-9

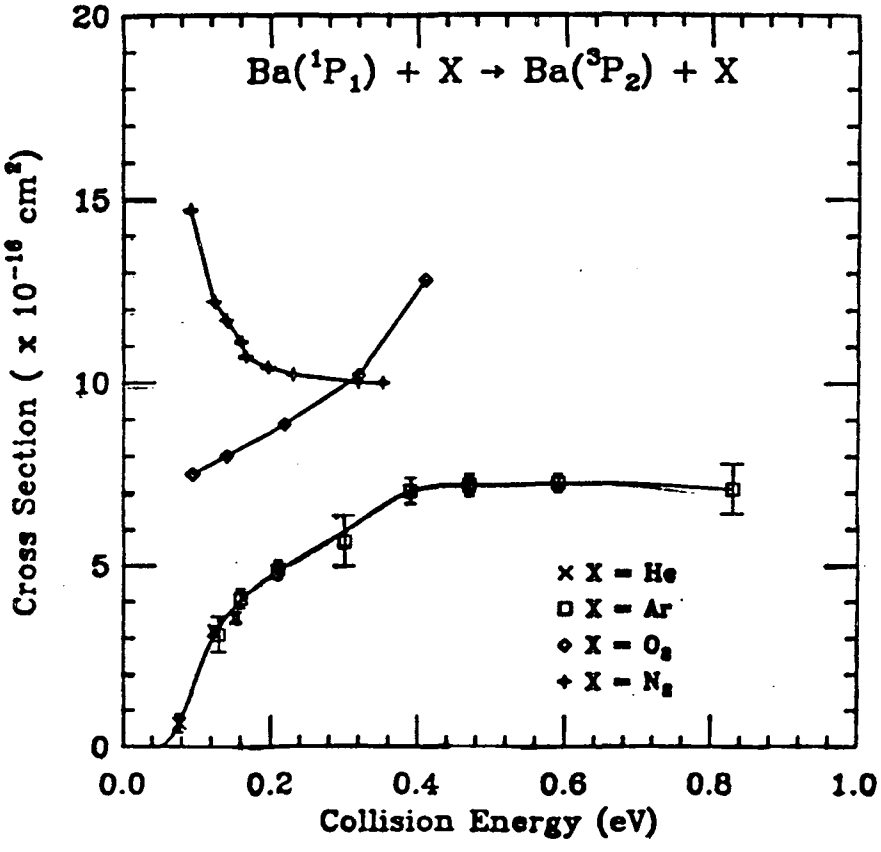
Ba(¹P₁) + X → Ba(³P₂) + X
Cross Section (x 10⁻¹⁶ cm²)
Collision Energy (eV)
0
5
10
15
20
0.0
0.2
0.4
0.6
0.8
1.0
× X = He
□ X = Ar
◇ X = O₂
+ X = N₂

Figure VI-10

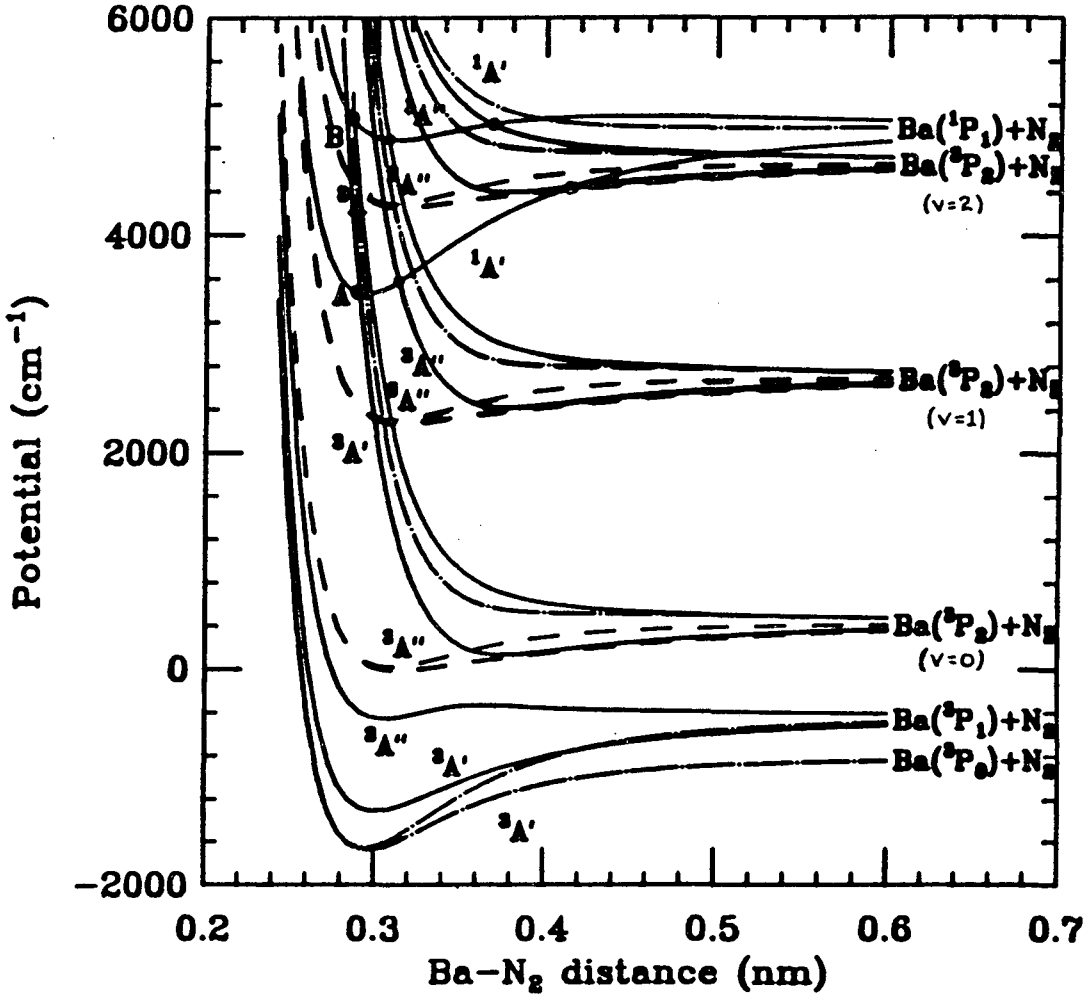
6000
4000
2000
0
−2000
Potential (cm⁻¹)
0.2
0.3
0.4
0.5
0.6
0.7
Ba−N₂ distance (nm)
¹A'
³A''
B
²A''
A
³A''
²A''
²A'
³A''
²A''
²A'
³A'
Ba(¹P₁)+N₂
Ba(³P₂)+N₂
(v=2)
Ba(³P₂)+N₂
(v=1)
Ba(³P₂)+N₂
(v=0)
Ba(³P₁)+N₂
Ba(³P₀)+N₂

Figure VI-11

LAWRENCE BERKELEY LABORATORY
UNIVERSITY OF CALIFORNIA
INFORMATION RESOURCES DEPARTMENT
BERKELEY, CALIFORNIA 94720